FINAL REPORT

Spectroscopic Studies of U(VI) Sorption at the Kaolinite-Water Interface

LANL Grant 9-X42-6947E-1

Hillary A. Thompson, George A. Parks, and Gordon E. Brown, Jr.

June 1, 1994

DISCLAIMER

Portions of this document may be illegible in electronic image products. Images are produced from the best available original document.

TABLE OF CONTENTS

LIST OF TABLES

LIST OF ILLUSTRATIONS

INTRODUCTION

The beneficial uses as well as harmful health effects associated with the element uranium (U) have drawn significant attention to the study of U chemistry. Uranium has two major uses: fuel for energy production and the primary reactant in the production of plutonium (Pu) for nuclear weapons. Uranium occurs naturally in the Earth's crust in concentrations that are neither a threat to human health nor economically useful (3 ppm; Krauskopf, 1992) and in ore bodies, which are local abundances of U in the Earth's crust. Mining and processing have increased the likelihood of dispersal of harmful amounts of U at the Earth's surface. Uranium-containing wastes resulting from such activities take various forms: open mine pits; waste chemicals that were utilized in the enrichment of U and consequently contain remnant amounts of U; expended U fuel; and the environmental media (water, soil, rocks, and air) that come into contact with each waste form.

Efficient use of U as a resource and safe handling, recycling and disposal of U-containing wastes require an understanding of the factors controlling the fate of U, where fate refers to the destination of U, typically expressed as an environmental medium or a process phase. Atomic-level environment largely governs elemental fate through the number and type of bonds to nearest neighbor atoms; these bonds constitute an energy barrier that must be overcome if the element is to be released from one environment to assume a different environment. Accurate description of a change in environment using a chemical reaction requires knowledge of the structure and identity of the reactants and products. Writing a chemical reaction is the first step in thermodynamic and kinetic modeling of a system, because the reactions provide the equilibrium and rate constants, respectively, that are required for modeling. The ability to accurately model a geochemical setting or process can provide information that would otherwise only be available through sample collection or may not be available at all if one is attempting to predict future fate.

The sorption process constitutes a change in elemental fate. Partitioning of an element from solution to a solid phase, or sorption, can be divided into three broad categories: adsorption, surface precipitation, and absorption. Adsorption involves partitioning to a solid surface, where the strength of partitioning can vary significantly from a tightly bound inner-sphere complex, in which up to two atoms in the solid surface have been found to bind to the element being sorbed (Chisholm-Brause, 1991; Manceau et al., 1992; O'Day, 1992), to a more weakly bound outer-sphere complex that maintains its hydration sheath but is electrostatically attracted to the surface. Surface precipitation may be a simple extension of inner-sphere complexation or elements dissolved from the

solid may be included to form a coprecipitate. Absorption is incorporation into the solid structure. Each type of sorption has very different implications for the fate of an element, corresponding to the different atomic-level environments surrounding the sorbed element.

Extended x-ray absorption fine structure (EXAFS), a type of x-ray absorption spectroscopy (XAS), offers the possibility for distinguishing among different modes of sorption by characterizing the atomic environment of the sorbing element. The use of EXAFS can provide quantitative estimates of coordination numbers and interatomic distances in solids, solutions, and mixed-phase (slurries) samples. In this study, we use EXAFS to determine the structure of U(VI) sorption complexes at the kaolinite-water interface.

In Chapter One, we present an overview of selected aspects of U structural chemistry as a basis for considering the structural environment of U at the solid-water interface. We limit our discussion to U(VI) because it is the dominant oxidation state under prevailing conditions in our study of sorption at the solid-water interface. In the solid state, we focus on the short- to intermediate-range (within 6 Å) structure around U, as this is the approximate range accessible using XAS. Aqueous U(VI) speciation is reviewed, with an emphasis on ligands that are present under the conditions of our sorption sample preparation. Knowledge of U(VI) aqueous speciation and of the local structures in which U(VI) is present in solids provides a starting point for speculation about structures that U(VI) sorption complexes might assume at the solid-water interface.

To evaluate the utility of XAS for characterization of the structural environment of U(VI) at the solid-water interface, we have carried out an in-depth analysis of XAS data from U(VI)-containing solid and solution model compounds, which we describe in Chapter Two. Through this study, we have established the ability of FEFF 5, an *ab initio* multiple-scattering EXAFS code, to calculate accurate phase shift parameters for U absorber atoms and accurate phase shift and effective scattering amplitude parameters for backscattering atoms in the U environment. We have also determined which neighboring atoms in the local environment around U can be detected using EXAFS for a variety of uranyl structures.

In Chapter Three, we consider sorption of U by kaolinite as a means of effecting the removal of U from surface collection pond waters on the Rocky Flats Plant site in northern Colorado. Using XAS, we characterize the structural environment of the sorbed U to verify that sorption has occurred and to identify the mode of sorption. We make use of our findings in Chapter Two to help interpret our EXAFS data. We observe the effect of varying key solution conditions on the structure of the resulting sorption complex(es).

CHAPTER ONE
Uranium(VI) Structural Chemistry

SOLID STATE STRUCTURAL CHEMISTRY

Solid U(VI) compounds stable at 20°C and 1 atm pressure fall into three groups by composition and structure: pure oxides, uranates, and uranyl salts. The only pure, stoichiometric U(VI) oxide stable under these conditions is γ-UO_3, however, the presence of water and other potential ligands destabilizes γ-UO_3. Uranates are composed of U, O, and one or more cations; most are exceedingly insoluble in water. Uranyl salts, broadly defined to include hydroxides, halides, nitrates, carbonates, silicates, phosphates, and arsenates, constitute the group most likely to be found in the presence of water. Given our interest in the solid-water interface, we focus on the uranyl salts.

Similarities among the uranyl salt structures are significant. The structural moiety that characterizes all uranyl salts is the very stable uranyl group, UO_2^{2+}, which consists of a central U atom bonded to two O atoms by relatively short, collinear bonds. Numerous studies have established the near linearity of the 3 constituent atoms and the covalency of the axial uranium-oxygen ($U\text{-}O_{ax}$) bonds (Weigel, 1986 and references therein). In uranyl salts, the $U\text{-}O_{ax}$ bond length ($R_{U\text{-}Oax}$) varies between 1.75 and 1.83 Å (Table 1).

The plane perpendicular to the axial bond axis is termed "equatorial," in which 4 to 6 atoms are arranged around the central U atom. The degree of puckering, i.e. location above or below the equatorial plane, is typically slight (Evans, 1963; $\leq$ 0.2 Å, Anderson et al., 1980). As the number of equatorial ligands increases from 4 to 6, some or all of the equatorial uranium-ligand bond lengths ($R_{U\text{-}Leq}$) increase. The amount of increase depends on the identity of the ligands. The increase in some, but not all, of the bond lengths results in increased static disorder among the equatorial ligands, where static disorder (σ_{stat}) is defined as the root-mean-square deviation from the mean interatomic distance for a single shell of atoms. Thus there exists a qualitative relationship between number of equatorial ligands and the mean $R_{U\text{-}Leq}$, as expected from the observed positive correlation between bond length and coordination number for most oxides (Shannon and Prewitt, 1969; Shannon, 1976).

In uranyl salts, the equatorial shell is occupied by 4 to 6 oxygen or halide atoms located 2.17 to 2.58 Å from the central U atom (Table 1). Several examples are shown in Figure 1. Equatorial oxygens are typically constituents of chemical functional groups that serve to distinguish among different oxygens, e.g. nitrate-O vs. hydroxide-O vs. mono- or bidentate silicate-O, thereby distinguishing among structure types (bidentate salt vs. hydroxide vs. 1:1 silicate). Bond lengths to equatorial oxygen atoms of a single type of

Distance	Compound	Method	Reference
U-O_{ax}			
1.749 (7) 1.770 (7)	$UO_2(NO_3)_2 \cdot 6H_2O$ (s) Uranyl nitrate hexahydrate	Neutron diffraction	Taylor and Mueller (1965)
1.752 (15) 1.821 (21)	$(UO_2)_2(OH)_2Cl_2(H_2O)_4$ (s)	XRD (powder and SC)	Aberg (1969)
1.76 (0.01) - 1.77 (0.02)	di-, tri-, and tetranuclear aqueous U(VI) species	X-ray scattering	Aberg (1970)
1.746 (4)	$RbUO_2(NO_3)_3$ (s) Rubidium uranyl nitrate	XRD (SC)	Zalkin et al. (1989)
1.823 ± 0.048	$UO_2(OH)_2$ (s)	XRD (SC)	Roof et al. (1964)
1.769 1.774	$NaUO_2(Ac)_3$ (s) Sodium uranyl triacetate	XRD (SC), thermally corrected	Templeton et al. (1985)
1.747 (25) 1.771 (26) 1.772 (27) 1.804 (30)	$(UO_2)_2(OH)_2(NO_3)_2(H_2O)_3$ (s)	XRD (SC)	Perrin (1976)
1.78 ± 0.05 1.82 ±0.05	$Ca(H_3O)_2(UO_2)_2(SiO_4)_2 \cdot 2H_2O$ (s) (α-) Uranophane	XRD (SC)	Stohl and Smith (1981)
1.798 (14) 1.808 (12) 1.818 (14) 1.829 (14)	$Ca(UO_2)_2(SiO_3OH)_2 \cdot 5H_2O$ (s) β-Uranophane	XRD (powder and SC) also XRF, IR, DTA	Viswanathan and Harneit (1986)
1.75 (1) 1.78 (1)	$HUO_2PO_4 \cdot 4H_2O$ (s) Hydrogen metaautunite	XRD (SC)	Morosin (1978)
1.801 (10) 1.808 (11)	$Ca(UO_2)_2(SiO_3OH)_2 \cdot 5H_2O$ (s) α-Uranophane	XRD (SC)	Ginderow (1988)
1.74 ± 0.08 1.85 ± 0.08	$K(H_3O)(UO_2)(SiO_4)$ Boltwoodite	XRD (powder and SC)	Stohl and Smith (1981)
1.76 1.78	$(UO_2^{2+})_2(OH)_2(NO_3)_4(Im)_2$ (s) Im=imidazole	XRD, IR, XPS	Perry (1982)
1.802 (5)	$K_4UO_2(CO_3)_3$ (s)	XRD	Anderson et al. (1980)

Table 1. Interatomic distance values (in Å) in uranyl compounds based on a variety of analytical methods, including powder and single crystal (SC) x-ray diffraction (XRD), neutron diffraction, x-ray scattering, x-ray fluorescence (XRF), infrared spectroscopy (IR), differential thermal analysis (DTA), and x-ray photoelectron spectroscopy (XPS). Numbers in parentheses are standard deviations of the last digit(s), as reported by the authors. Neighboring atoms addressed include axial oxygen (O_{ax}), equatorial oxygen (O_{eq}), nitrate-N, Si, P, and U.

Distance	Compound	Method	Reference
U-O_{eq}			
2.397 (3) *part of nitrate:* 2.504 (5) 2.547 (6)	$UO_2(NO_3)_2 \cdot 6H_2O$ (s) Uranyl nitrate hexahydrate	Neutron diffraction	Taylor and Mueller (1965)
2.321 (23) 2.366 (21) 2.396 (19) 2.533 (21)	$(UO_2)_2(OH)_2Cl_2(H_2O)_4$ (s)	XRD (powder and SC)	Aberg (1969)
2.39 - 2.50 (0.01)	di-, tri-, and tetranuclear aqueous U(VI) species	X-ray scattering	Aberg (1970)
2.17 2.24 2.26 2.39 2.41 2.44 2.49	$(UO_2)_4O_2(OH)_2Cl_2(H_2O)_6 \cdot xH_2O$ (s)	XRD (SC)	Aberg (1971)
part of nitrate: 2.474 (3)	$RbUO_2(NO_3)_3$ (s) Rubidium uranyl nitrate	XRD (SC)	Zalkin et al. (1989)
2.237 ± 0.059 2.434 ± 0.057	$UO_2(OH)_2$ (s)	XRD (SC)	Roof et al. (1964)
part of acetate: 2.469 2.475	$NaUO_2(Ac)_3$ (s) Sodium uranyl triacetate	XRD (SC), thermally corrected	Templeton et al. (1985)
2.343 (28) 2.370 (16) 2.388 (19) 2.407 (23) 2.429 (29) 2.432 (25) 2.435 (31) *part of nitrate:* 2.516 (20) 2.520 (22) 2.549 (35) 2.577 (22)	$(UO_2)_2(OH)_2(NO_3)_2(H_2O)_3$ (s)	XRD (SC)	Perrin (1976)
2.21 ± 0.06 2.26 ± 0.05 2.34 ± 0.06 *shared w/ Si:* 2.43 ± 0.06 2.46 ± 0.06	$Ca(H_3O)_2(UO_2)_2(SiO_4)_2 \cdot 2H_2O$ (s) (α-) Uranophane	XRD (SC)	Stohl and Smith (1981)

Table 1. (continued)

Distance	Compound	Method	Reference
U-O_{eq} (cont.)			
2.216 (17) 2.277 (17) *shared w/ Si:* 2.250 (16) 2.316 (18) 2.337 (14) 2.390 (14) 2.445 (15) 2.460 (19) 2.485 (14) 2.528 (17)	$Ca(UO_2)_2(SiO_3OH)_2 \cdot 5H_2O$ (s) β-Uranophane	XRD (powder and SC) also XRF, IR, DTA	Viswanathan and Harneit (1986)
2.307 (8)	$HUO_2PO_4 \cdot 4H_2O$ (s) Hydrogen metaautunite	XRD (SC)	Morosin (1978)
2.241 (8) 2.294 (10) 2.296 (9) 2.437 (10) 2.463 (9)	$Ca(UO_2)_2(SiO_3OH)_2 \cdot 5H_2O$ (s) α-Uranophane	XRD (SC)	Ginderow (1988)
2.23 ± 0.08 *shared w/ Si:* 2.35 ± 0.12 2.45 ± 0.10	$K(H_3O)(UO_2)(SiO_4)$ Boltwoodite	XRD (powder and SC)	Stohl and Smith (1981)
2.35 *part of nitrate:* 2.52 2.54 2.55 2.59	$(UO_2^{2+})_2(OH)_2(NO_3)_4(Im)_2$ (s) Im=imidazole	XRD, IR, XPS	Perry (1982)
part of carb.: 2.425 (6) 2.432 (6) 2.434 (6)	$K_4UO_2(CO_3)_3$ (s)	XRD	Anderson et al. (1980)

Table 1. (continued)

Distance	Compound	Method	Reference
U-nitrate N			
2.950 2.984	$UO_2(NO_3)_2 \cdot 6H_2O$ (s) Uranyl nitrate hexahydrate	Neutron diffraction	Taylor and Mueller (1965)
2.912	$RbUO_2(NO_3)_3$ (s) Rubidium uranyl nitrate	XRD (SC)	Zalkin et al. (1989)
U-Si or U-P			
3.12 ± 0.02 3.64 ± 0.02	$Ca(H_3O)_2(UO_2)_2(SiO_4)_2 \cdot 2H_2O$ (s) α-Uranophane	XRD (SC)	Stohl and Smith (1981)
3.602	$HUO_2PO_4 \cdot 4H_2O$ (s) Hydrogen metaautunite	XRD (SC)	Morosin (1978)
3.144 3.631 3.750 3.783	$Ca(UO_2)_2(SiO_3OH)_2 \cdot 5H_2O$ (s) α-Uranophane	XRD (SC)	Ginderow (1988)
3.20 ± 0.03 3.54 ± 0.03	$K(H_3O)(UO_2)(SiO_4)$ Boltwoodite	XRD (powder and SC)	Stohl and Smith (1981)
U-U			
3.944 (1)	$(UO_2)_2(OH)_2Cl_2(H_2O)_4$ (s)	XRD (powder and SC)	Aberg (1969)
3.84 - 3.88 (0.01)	di-, tri-, and tetranuclear aqueous U(VI) species	X-ray scattering	Aberg (1970)
3.69 3.78 4.04	$(UO_2)_4O_2(OH)_2Cl_2(H_2O)_6$ $\cdot xH_2O$ (s)	XRD (SC)	Aberg (1971)
3.939 (1)	$(UO_2)_2(OH)_2(NO_3)_2(H_2O)_3$ (s)	XRD (SC)	Perrin (1976)
3.916 ± 0.004;	$Ca(H_3O)_2(UO_2)_2(SiO_4)_2 \cdot 2H_2O$ (s) α-Uranophane	XRD (SC)	Stohl and Smith (1981)
3.944 ± 0.005;	$K(H_3O)(UO_2)(SiO_4)$ Boltwoodite	XRD (powder and SC)	Stohl and Smith (1981)
3.93	$(UO_2^{2+})_2(OH)_2(NO_3)_4(Im)_2$ (s) Im=imidazole	XRD, IR, XPS	Perry (1982)

Table 1. (continued)

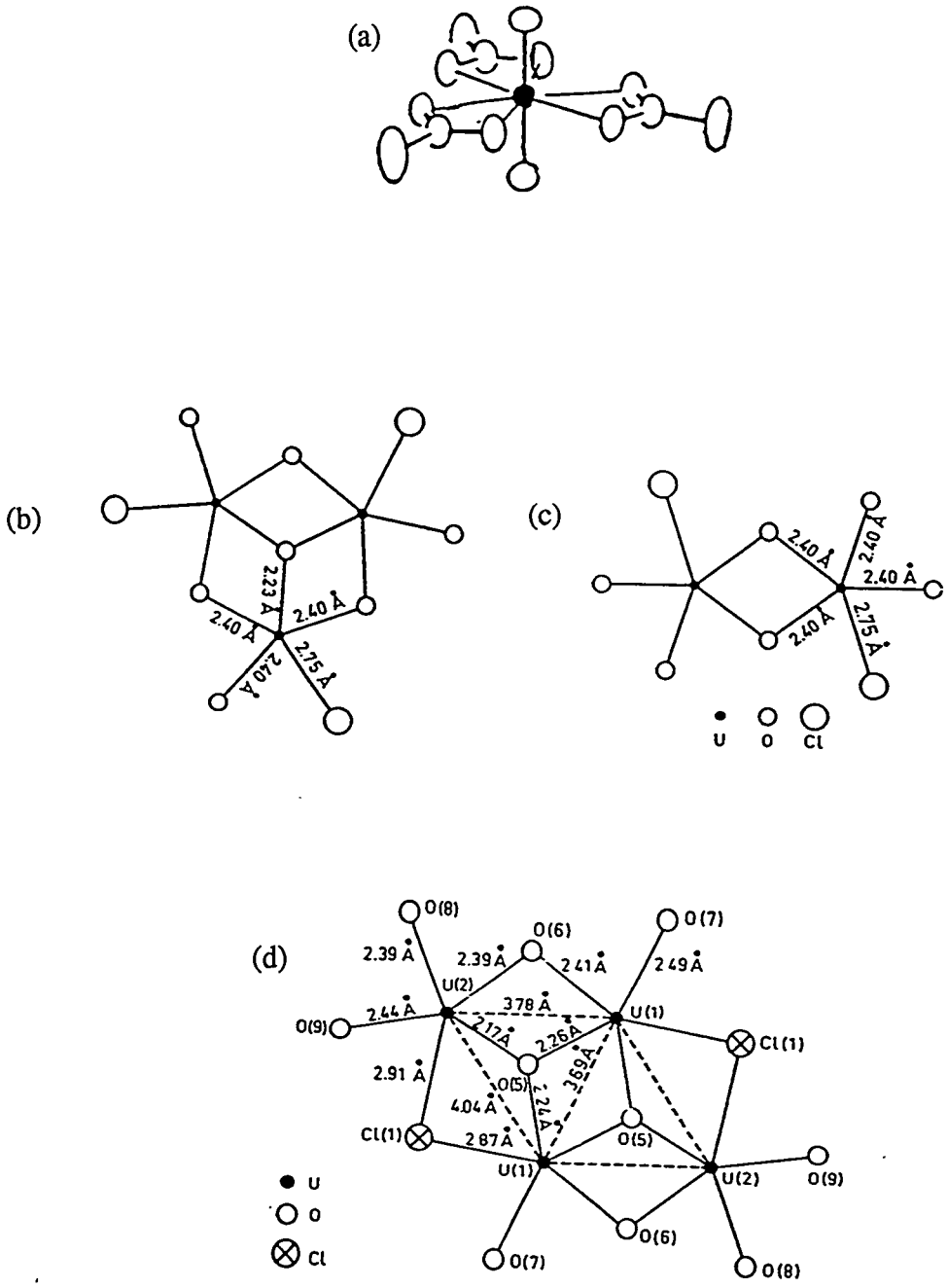

Figure 1. Short to intermediate range structures of some uranyl salts and aqueous uranyl complexes. In all structures, U atoms are shaded. (a) Rubidium uranyl (tri)nitrate (s), not showing Rb atoms (Zalkin et al., 1989). (b) Trinuclear uranyl hydroxo complex, $[(UO_2)_3(OH)_4Cl_3(H_2O)_3]$ (aq) (Åberg, 1970). Uranyl bonds are perpendicular to the plane of the page in this and the following two structures. (c) A uranyl dimer solid or aqueous complex, $[(UO_2)_2(OH)_2Cl_2(H_2O)_4]$ (Åberg, 1969; Åberg, 1970). (d) Tetranuclear uranyl hydroxide, $(UO_2)_4O_2(OH)_2Cl_2(H_2O)_6$ (s) (Åberg, 1971).

functional group typically vary significantly less than do bond lengths to different types of functional groups. For example, the central U atom in rubidium uranyl nitrate (Zalkin et al., 1989) is surrounded in the equatorial plane by three identical functional groups (nitrate), and the six U-O_{eq} bonds are the same length (2.47 Å). In uranyl nitrate hexahydrate, the six equatorial oxygen atoms fall into two groups. Four of the oxygen atoms are constituents of two nitrate groups, and the corresponding $R_{U\text{-}Oeq}$ are 2.50 to 2.54 Å. Water molecules provide the remaining two O_{eq} atoms, whose $R_{U\text{-}Oeq}$ is equal to 2.40 Å. Similarly in the uranyl hydroxide nitrate $(UO_2)_2(OH)_2(NO_3)_2(H_2O)_3$ (Perrin, 1976), hydroxide and bridging (between two U atoms) equatorial oxygens are located 2.34 to 2.43 Å from U, whereas nitrate equatorial oxygens are located 2.52 to 2.58 Å from U. These examples provide some basis for distinguishing among equatorial ligands based solely on $R_{U\text{-}Oeq}$. Bidentate groups such as nitrate, carbonate, and silicate, have $R_{U\text{-}Oeq}$ typically $\geq$ 2.45 Å. Monodentate and bridging O_{eq} are most often $\leq$ 2.45 Å from U.

Even larger amounts of static disorder are associated with many of the atoms more distant than equatorial oxygens. Nearest nitrate-N and carbonate-C are located 2.86 to 2.98 Å from the central U atom. The number of N or C atoms varies between 1 and 3. Shortest $R_{U\text{-}Si}$ (in uranyl silicates) and $R_{U\text{-}P}$ (in uranyl phosphates) range from 3.1 to 3.8 Å, with 2 to 4 Si or P neighbors. Among uranyl hydroxides, carbonates, and silicates, the shortest U-U distance varies from 3.69 to 4.30 Å.

Bonding to form an extended U(VI) structure occurs through the equatorial, rather than axial, ligands (Weigel, 1986). Resultant structures tend to be layered (Smith, 1984); each layer has a thickness approximately equal to the distance between the two uranyl O atoms (Fig. 2). Multiple layers are held together by hydrogen bonding between axial O atoms and interlayer water molecules - either individual water molecules as in the case of hydrogen meta-autunite or water molecules in the hydration sheath of an interlayer cation, as in meta-ankoleite. Interlayer spacing tends to be greater in the latter case.

Consistency in local structure among different U(VI) solids is significant enough to suggest that these solids might serve as good model structures for U(VI) species at the solid-water interface. Although solution speciation might be expected to provide an equally good model, it is less well understood, as is discussed in the next section. Furthermore, some have postulated that the surface complex is a precursor to heterogeneous precipitation (Muto et al., 1965; Healy et al., 1968; Bleam and McBride, 1985). If this is the case, then the local environment of U in solids that form as heterogeneous precipitates might be expected to serve as an excellent model for surface species.

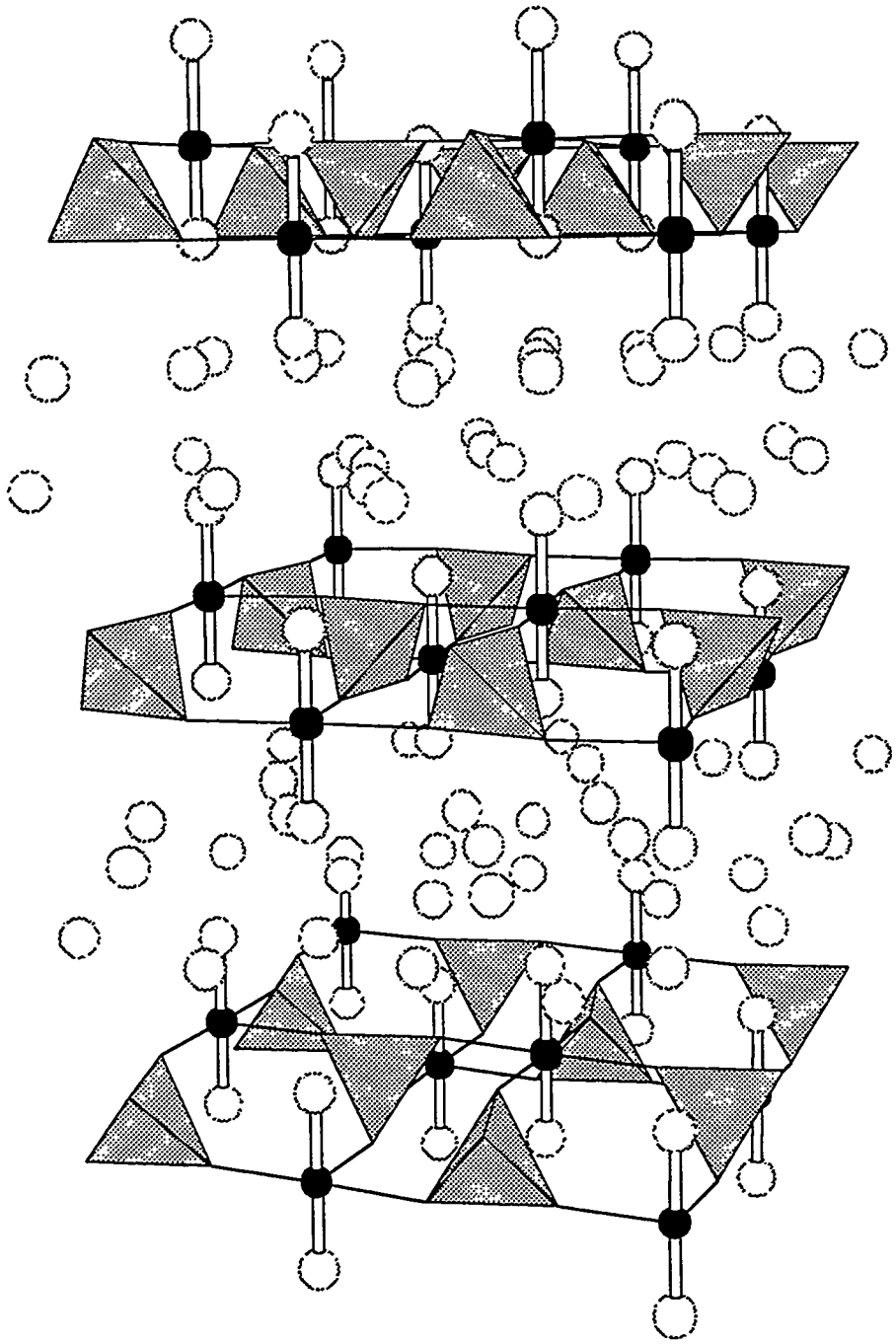

Figure 2. Extended structure of meta-autunite (Morosin, 1978). Uranyl phosphate layers are parallel to (001). U atoms are black, uranyl bonds are denoted with double lines, PO_4^{3-} groups are denoted by tetrahedra, and interlayer atoms represent water molecules.

AQUEOUS SOLUTION CHEMISTRY

One cannot consider uranium solution speciation without addressing the conditions that dictate speciation, including oxidation potential (Eh), pH, total carbonate content of the system (ΣCO_2), total U content of the system (ΣU), ionic strength, and abundance of other complexing ligands in solution. Their individual effects on U speciation are discussed below.

Because uranium has several oxidation states (IV, V, and VI), oxidation potential (Eh) plays an important role in determining uranium speciation. Uranium (VI) is dominant at the earth's surface in the form of solid oxides and as dissolved or colloidal species in water. Uranium (VI) solubility in water is relatively high owing to its ability to form complexes with a variety of common solution constituents. The presence of sulfides or certain organics in solution can reduce U(VI) to U(V) or U(IV) (Andreyev and Chumachenko, 1964). Uranium(V) is uncommon, while U(IV) is found primarily in minerals such as uraninite and pitchblende and is highly insoluble in water when protected from oxidation and high concentrations of complexing ligands (e.g., fluoride or carbonate (Langmuir, 1978)).

Uranium(VI) forms complexes with hydroxo and other pH-sensitive ligands; thus, its aqueous speciation is governed by pH. In simple, ligand-free solutions not exposed to CO_2, U(VI) forms hydroxo complexes of the form $[UO_2]_p[OH]_q^{2p-q}$ (aq). Upon addition of CO_2 to the system, hydroxo, carbonato, and mixed hydroxy-carbonato U(VI) complexes of the form $[UO_2]_p[OH]_q[CO_3]_r^{2p-q-2r}$(aq) are predicted, where p, q, and r are nonnegative integers. Polynuclear species are indicated by $p \geq 2$. In solutions undersaturated with respect to all solid U phases, an increase in ΣU is expected to increase the concentration of polymeric relative to monomeric species. The relative stabilities of these complexes have been reviewed extensively (Baes and Mesmer, 1976; Langmuir, 1978; Sylva and Davidson, 1979; Maya, 1982a; Tripathi, 1984; Grenthe et al., 1992; and references therein). The distribution of U species as a function of pH for $\Sigma U = 10^{-1.7}$ mol·m^{-3} in CO_2-free and atmospheric CO_2-equilibrated systems as calculated with the Grenthe data set is shown in Figure 3. Details of calculations are in Appendix 1.

As in U(VI) solids, the basic structural moiety of aqueous U(VI) is uranyl (Karim et al., 1980; Charpin et al., 1985; Chisholm-Brause et al., 1992; Dent et al., 1992). Four to six ligands are arranged in a planar equatorial fashion around the uranium atom (Görller-Walrand and Colen, 1982; Charpin et al., 1985). In low ionic strength aqueous solution under oxidizing conditions, O atoms tend to occupy the equatorial positions immediately adjacent to U.

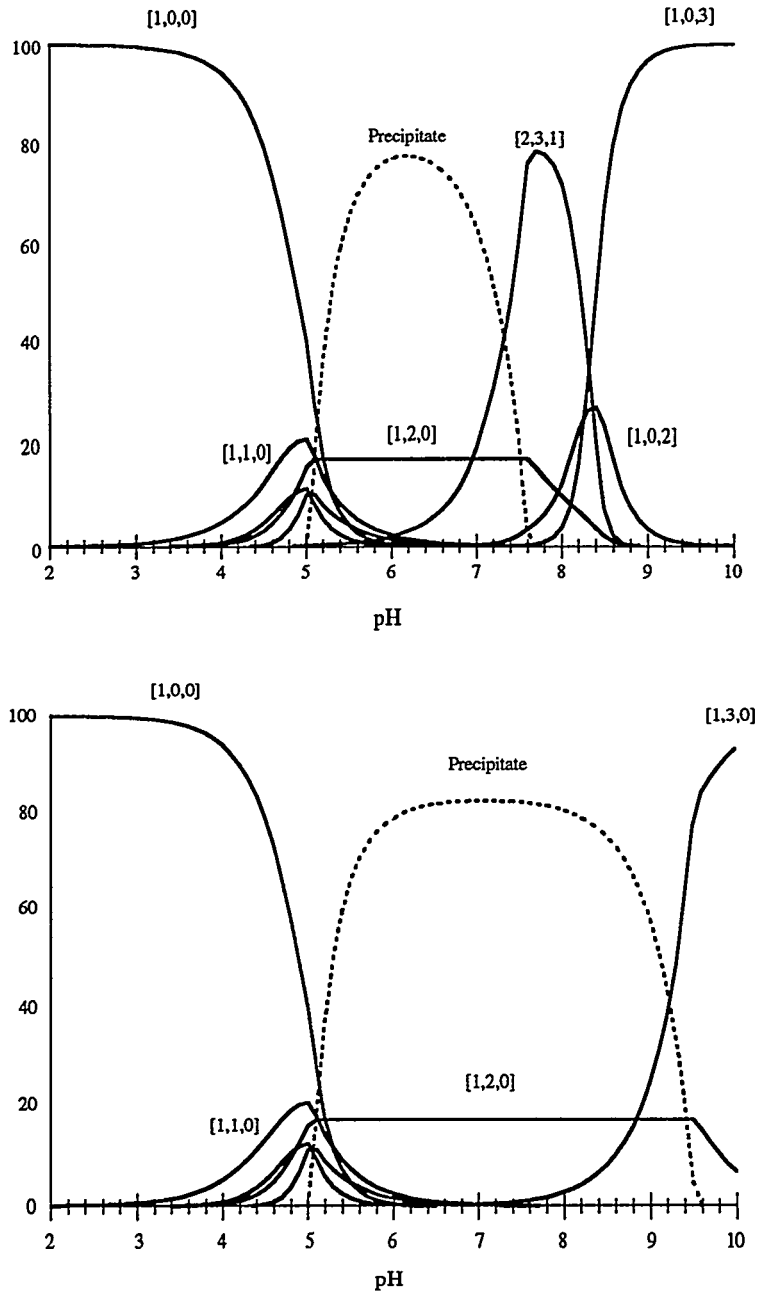

Figure 3. Equilibrium aqueous U(VI) speciation diagrams for $\Sigma U = 10^{-1.7}$ mol·m^{-3} (ionic strength = 1 mol·m^{-3} $NaNO_3$) in the presence (top) and absence (bottom) of atmospheric CO_2. Aqueous complex designations are of the form [p,q,r] for $(UO_2)_p(OH)_q(CO_3)_r$. In both diagrams, [2,2,0] and [3,5,0] peaks are buried under the [1,1,0] peak. Both solutions are supersaturated with respect to $UO_3 \cdot 2H_2O$ and β-$UO_2(OH)_2$ precipitation in the mid-pH range, shown with dashed lines.

In polynuclear complexes, U atoms are joined through their equatorial ligands. As a general model for polynuclear structures, Sillén (1954) proposed the "core link" model, in which each U atom is bonded by a pair of hydroxo groups (or O) to the nearest U atom along the line joining all U atoms already part of the polynuclear species. Åberg has confirmed the core link model for a uranyl dimer (Åberg, 1969; Åberg, 1970), but she has refuted it for complexes with p>2. Her X-ray scattering studies of concentrated uranyl solutions ($3 \cdot 10^3$ mol·m^{-3}) have identified a triangular trimer (Åberg, 1970; Åberg et al., 1983) and a quadrilateral tetramer (Åberg, 1971) (Fig. 1). X-ray absorption studies of aqueous uranyl solutions under moderate pH conditions show the presence of a neighboring atom 3.9 Å from U, the number of which grows at higher pH and higher ΣU(VI) (Chisholm-Brause et al., 1992). The solution behavior is consistent with polynuclear complex formation, and the location of the (presumably) U neighbor is consistent with Åberg's trimer structure.

Uranium(VI) forms relatively strong complexes with other common ligands, including but not limited to fluoride, phosphate, and organic ligands including natural colloidal materials like fulvic and humic acids (Langmuir, 1978; Tripathi, 1984; Hsi and Langmuir, 1985; Ho and Miller, 1986; Dent et al., 1992). Because we do not expect to find these potential ligands in concentrations that will pose significant competition for hydroxo and carbonato ligands in our sorption experiments, we will not address them further. Other dissolved inorganic anionic species do not strongly complex U(VI) relative to hydroxo and carbonato ligands. Cations that are likely to be present in the sorption experiments may undergo ion exchange with U(VI) on a solid surface, as do, e.g., Ca^{2+} and Mg^{2+} on bentonite (Borovec, 1981).

SUMMARY

The composition and structure of the atomic environment that U(VI) assumes in the solid state are well known for a large number of crystalline materials. For a variety of compositions, the uranyl moiety surrounded by four to six O_{eq} atoms forms the compositional and structural basis of the solid. There are a limited number of structure types (e.g., bidentate salts, 1:1 silicates, 3:2 phosphates, and 1:1 phosphates) that dictate the number and length of equatorial bonds, and location of the next nearest neighbor (e.g., N, C, Si, or P) and nearest U atom.

Compositional variety within structural guidelines is also characteristic of the short- to intermediate-range U(VI) environment in aqueous solution. While the qualitative compositions of aqueous U(VI) complexes have been well studied (i.e., which ligands complex U(VI)), the stoichiometries and structures are known for only a small number of

complexes. The uranyl moiety is known to be preserved in aqueous solution under oxidizing conditions. In ligand-free (with the exception of hydroxo and carbonato ligands) solutions, bonding to form polynuclear species is very similar to compositionally similar structures in the solid phase. Relying on these known structural similarities, it seems reasonable to use the substantial database of U(VI) solid state structures to understand the structure of aqueous U(VI) complexes.

In systems that are more representative of geologic settings, such as a solid in contact with aqueous solution, the structure and composition of the U environment can be even more complex. In addition to the possibilities of finding U in the bulk solid phase and in solution complexes, U may be present at the solid-water interface as sorption complexes. The structure of U(VI) sorption complexes at the kaolinite-water interface is the topic of Chapter Three. In combination with what is known about the U(VI) environment in bulk solid and solution phases, we have employed X-ray absorption spectroscopy (XAS) to elucidate U(VI) sorption complex structures. Chapter Two presents an XAS sensitivity study in which we have applied the technique to U solid and solution phases of known structure and composition (model compounds) to determine the extent to which the technique can provide information on the structural environment of uranium.

CHAPTER TWO
XAS Analysis of Uranium(VI) Model Compounds

INTRODUCTION

To evaluate the utility of X-ray absorption spectroscopy (XAS) for characterization of the structural environment of U(VI) at the solid-water interface, we have carried out an in-depth analysis of XAS data from U(VI) model compounds.[1] Model compounds are substances characterized by the presence of the atom of interest (in sorption samples, typically the sorbing metal atom) in a limited number of uniform sites for which the structure and composition are known. Too little is known about the structure of any solid-water interface complex to use it as a model compound for interpreting structural data for unknowns. Instead, we use single-phase model compounds for analysis of sorption sample structural data. In the solid phase, the best model compounds tend to be highly crystalline materials. In solutions, because numerous species can be present simultaneously, solution conditions must be carefully selected such that a single species dominates the composition; that species constitutes a suitable solution model compound. Regardless of the phase, independent confirmation of the structure and identity of model compounds is imperative.

The use of model compounds to analyze data for an unknown assumes short- to intermediate-range compositional and structural similarity between the model compound and the unknown structure. Long-range structural similarity is much less important because the parameters that are extracted from model compound data to fit unknown data depend on the electronic structure of each absorber-scatterer pair, which is not significantly affected by long-range structure. Careful selection of model compounds is therefore imperative; one must have some knowledge or at least ideas about the composition and structure of the unknown to select appropriate model compounds. We have already discussed similarities in local structure around U in solids and aqueous solution in Chapter One. We will discuss our expectations regarding the local structure of U sorption complexes at the kaolinite-water interface in Chapter Three. With this in mind, we have selected seven solids and one aqueous solution species, all of which contain the uranyl moiety, as model compounds. Each one, in its pure form, fulfills the model compound criteria stated above.

---

[1]Hereafter, as we only address U(VI) in this study, we will use the symbol U to represent U(VI).

BACKGROUND

X-Ray Absorption Spectroscopy

Technique Description

X-ray absorption spectroscopy (XAS) probes the local atomic environment (≤ 6 Å) of an absorbing atom (consult Brown et al., 1988 and references therein for a review of the technique). In the case of U L_{III}-edge XAS, incident x-rays with energies at and above the electron binding energy of the U L_{III} edge (17166 eV) are absorbed by U atoms in the sample. Photoelectrons emitted by the absorption process are scattered by neighboring atoms. The resulting interference between outgoing and incoming photoelectric waves is observed in the oscillatory structure beginning 20 to 50 eV above the edge, known as the EXAFS (extended x-ray absorption fine structure), represented by the variable $\chi(k)$ (Fig. 1). The EXAFS spectrum is typically plotted against k, the photoelectron wave vector, where k is related to the kinetic energy (E) of the outgoing photoelectron by

$$k = \left[\frac{2m}{\hbar^2}(E-E_0)\right]^{1/2} \quad (1)$$

in which E_0 is the threshold energy of the photoelectron at k=0 and m is the electron mass. The EXAFS region contains information that is sensitive to the identity (Z), number (N), and distance (R) of neighbors, summed over all local environments of the absorber and can be expressed by

$$\chi(k) = \sum_R N_R S_0^2 \frac{|f_{eff}(\pi,k,R)|}{kR^2} \sin\left(2kR + 2\delta^c + \Phi\right) e^{-2\sigma^2 k^2} e^{-2R/\lambda} \quad (2)$$

where S_0^2 is a many-body amplitude reduction factor, $|f_{eff}(\pi, k, R)|$ is the effective amplitude function of the scatterer, $2\delta^c$ and Φ are phase shifts for the absorber and backscatterer, respectively, σ^2 is a Debye-Waller factor, and λ is the mean free path of the electron. Identity of a neighboring atom is reflected in the corresponding amplitude and phase shift (Φ) functions.

The Debye-Waller factor, σ^2, is a parameter that accounts for static and vibrational disorder according to the equation

$$\sigma^2 = \sigma^2_{stat} + \sigma^2_{vib} \quad (3)$$

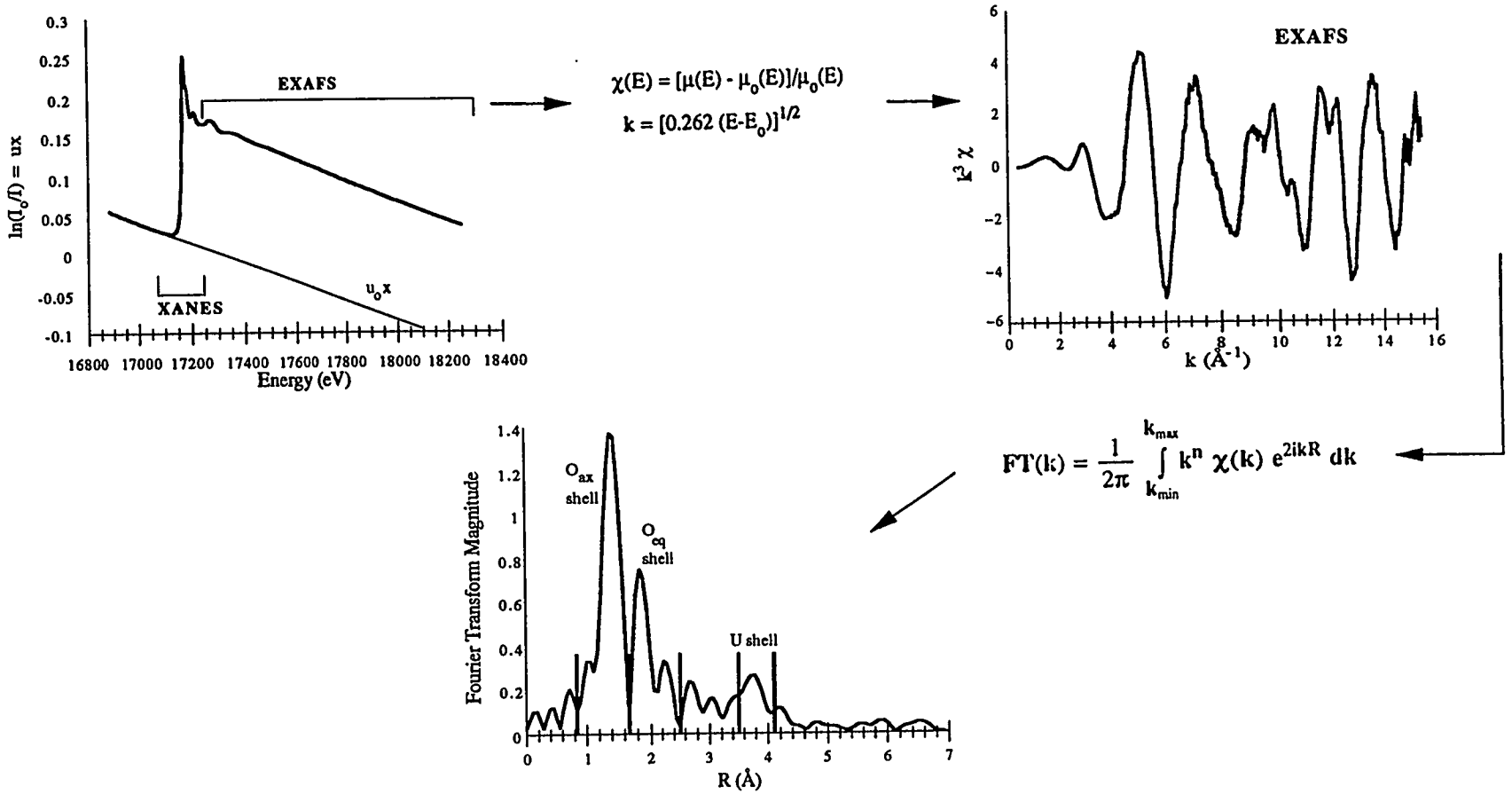

Figure 1. Illustration of XAS data analysis for uranophane, $Ca(UO_2)_2(SiO_3OH)_2 \cdot 5H_2O$. *Top left* Raw XAS data plotted as a function of energy, showing approximate locations of the XANES and EXAFS regions, as well as the background (μ_0x). *Top right* The EXAFS function, $\chi(k)$, is calculated as shown and plotted against k. *Lower half* Fourier transform of $\chi(k)$ is calculated and plotted against R, uncorrected for phase shift. Note the significant overlap of FT features at all R values.

The Debye-Waller factor is a measure of mean-square deviation of bond lengths from their average lengths, caused by multiple bonds of a single type (e.g., U-O_{ax}) that have different lengths (static), variation in bond length from one site to another in a structure (static), and atomic vibrations (vibrational).

Fourier transformation of $\chi(k)$ produces a type of radial distribution function which displays peaks at the approximate R (not corrected for phase shifts of the backscattering atoms (sin Φ)) of atoms in the local environment around the element of interest (Fig. 1). The Fourier transform (FT) presents a more readily understandable picture of the atomic environment around the absorbing atom than the $\chi(k)$ function.

The region of the absorption spectrum that lies between the absorption edge and the EXAFS region is the X-ray Absorption Near Edge Structure (XANES) region. The XANES region can contain features indicative of multiple scattering (i.e., scattering involving more than a two leg path between the absorber and one scattering atom) and particular site geometries (Bianconi et al., 1985). The U(VI) L_{III}-edge XANES region contains at least two distinct features, denoted A and B, that are indicative of the hexavalent oxidation state (Fig. 2) (Petiau et al., 1986). Feature A, which typically occurs 10 to 15 eV above the absorption edge, has been attributed to multiple scattering among atoms of the uranyl moiety. Feature B is found 30 to 50 eV above the absorption edge, the distance from the edge being inversely proportional to the length of the equatorial bonds ($R_{U\text{-}Leq}$) in U(VI) salts. In this and the following chapter, XANES information has been used only to confirm information extracted from the EXAFS region for each sample.

Data Analysis

EXAFS data can be analyzed both qualitatively and quantitatively. Qualitatively, one can roughly correlate peak positions in the Fourier transform (FT) of $\chi(k)$ data with absorber-scattering atom interatomic distances. Knowledge of a sample's elemental composition combined with the shape (as a function of k) of each element's amplitude function can narrow the possibilities of which FT peaks correspond to which backscattering atoms. In less disordered structures than uranyl, qualitative analysis can provide a significant amount of information about the structural environment around the absorbing atom (see examples given in Sayers and Bunker, 1988). The broad range of equatorial bond lengths around a single uranyl moiety, already described in Chapter One, produces FT features that are slightly shifted in R relative to each other and therefore overlap, resulting in broadened, less readily interpretable, features. Furthermore in natural systems, in which a variety of potential uranyl ligands may be present, the certainty with which one can interpret the FT for compositional information is poor.

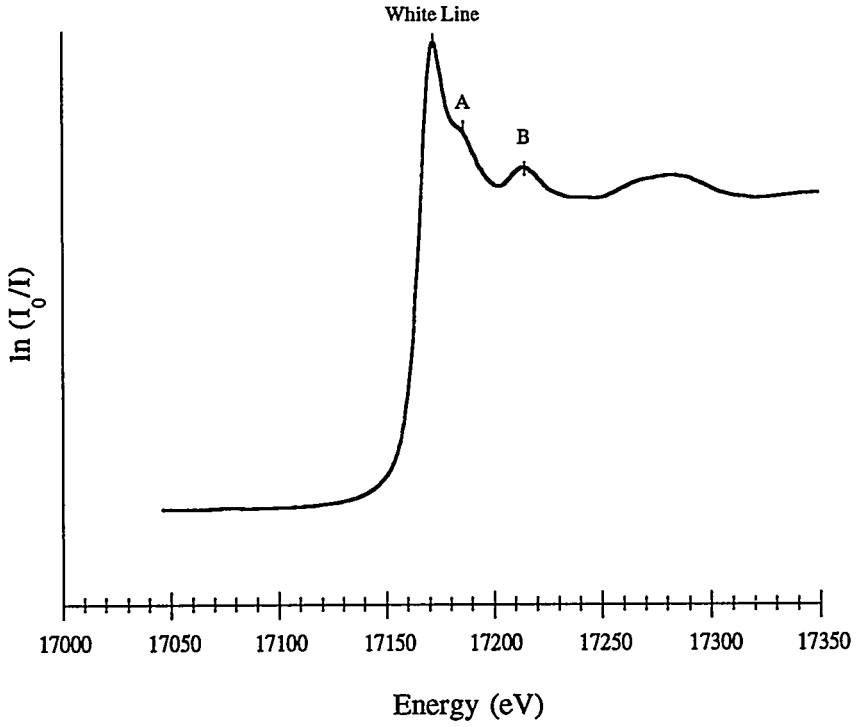

Figure 2. Uranium(VI) L_{III}-edge XANES region. Positions of the white line and features A and B were measured as described in the experimental section of the text. There is an inverse relationship between the distance from the white line to A (B) and the U-O_{ax} (U-O_{eq}) bond length.

Given our objectives with respect to U at the solid-water interface, quantitative analysis of EXAFS data is a necessary component of this study. Quantitative interpretation of EXAFS data for a sample of unknown structure and/or composition relies on experimental data or theoretical calculations for model compounds, for which N, R, and σ^2 are known or estimated. Using fixed values of these parameters, all other parameters in Equation 2 are extracted by fitting the experimental or theoretical data using a least-squares algorithm. The resulting values of $|f_{eff}(\pi, k, R)|$, $2\delta^c$, Φ, and λ are used to enable extraction of N, R, and σ^2 from the EXAFS spectra of unknown samples.

FEFF

In this study, we utilize theoretical calculations of model compound EXAFS spectra to generate reference phase shift and amplitude parameters for quantitative interpretation of EXAFS spectra of unknown samples. Theoretical calculations were made using the computer code FEFF 5 (v. 5.03) developed by Rehr et al. (1991). FEFF 5 is an *ab initio* multiple-scattering EXAFS code (details of FEFF 5 theory and computation are given by Mustre de Leon et al., 1991 and Rehr et al., 1991). Running FEFF 5 in a minimalist mode (i.e., without taking advantage of its advanced modules), the user provides atomic coordinates and a value for S_0^2 for a cluster of atoms in the known compound. Debye-Waller factors (σ^2) can be set to zero (no disorder), set to a global value that affects all paths equally, or individually adjusted for each path based on structural and vibrational data. A path describes the n-leg journey among cluster atoms that an electron travels. All possible single (n=2) and multiple scattering ($n \geq 3$) paths are determined from the input cluster by FEFF 5. Using the input, FEFF 5 calculates wave phase shifts ($2\delta^c$ and Φ), effective scattering amplitudes ($|f_{eff}(\pi, k, R)|$), and electron mean free paths (λ) for each path. Path significance is calculated several times during the FEFF calculation based on increasingly accurate estimates of path amplitude. FEFF 5 then uses a form of Equation 2 to calculate $\chi(k)$ for a single path or any combination of paths, as specified by the user or left to FEFF's determination of path significance.

Uranium XAS Studies

Among past U XAS studies, a variety of approaches has been applied to quantitatively interpret the data. Despite their differences, all of the studies have produced a consistent amount of information about the U environment, namely, numbers and distances of axial and first shell equatorial neighbors. Notably, accuracy of the resulting information (as measured by comparison with independent structural determinations) varies with the data analysis method.

In one of the first U EXAFS studies, Karim et al. (1980) modeled experimental EXAFS data for UO_2F_2(s) and aqueous U(VI) complexes using central atom phase shift and backscattering atom phase shift and amplitude parameters from Teo and Lee's (1979) tabulations (based on first principles calculations). Because the tabulations only extended to Z=82 (Pb), they extrapolated the central atom phase shift parameter from Pb to U. Their simulations of experimental data for both solid and solution models included two axial oxygen atoms (O_{ax}) and first equatorial shell atoms (O_{eq} or F). Although major features in the experimental FT were reproduced by the simulation, there was noticeable disagreement in relative peak size and exact position. In the case of UO_2F_2 (s), the simulation overestimated the U-O_{ax} bond length ($R_{U\text{-}Oax}$) by 0.04 Å and underestimated $R_{U\text{-}Oeq}$ by 0.08 Å.

In 1985, Charpin et al. reported experimental EXAFS data for several uranyl-containing solids and aqueous solutions obtained from two different quantitative analysis techniques. Their preferred method of analysis involved extraction of phase shift and amplitude parameters from the O_{ax} contribution to the experimental EXAFS spectrum for a solid, e.g., uranyl triacetate tetraphenylphosphonium. These parameters were then used in the simulation of O_{eq} shell data for the same compound, as well as both O_{ax} and O_{eq} contributions in aqueous uranyl solutions. Compared with crystallographic data, EXAFS-derived values of $R_{U\text{-}Oeq}$ in the solid were overestimated by as much as 0.1 Å.

Barrett et al. (1988) calculated *ab initio* backscattering atom phase shift parameters for O and U, which they refined using experimental data for solid model compounds, $^{VI}UO_2F_2$ (U-O) and U metal (U-U). The accuracy of the resulting parameters was tested on experimental data for $^{IV}UO_2$, from which $R_{U\text{-}O}$ was 0.06 Å longer than that predicted by crystallographic data. It is likely that the use of U(VI) parameters (from O_{ax}) to fit U(IV) EXAFS may account for some or all of the distance discrepancy.

In each of the quantitative data analyses described above, no distinction was made between axial and non-axial (i.e. equatorial or U(IV) neighbors) phase shift and amplitude parameters, other than an accounting for differences in distance from the central U atom. In each case, the studies demonstrated poorer agreement with crystallographic parameters than has been shown for typical EXAFS analysis ($\Delta R \leq 0.02$Å) (Scott, 1984; Rehr et al., 1991). Indeed, the axial bond has been demonstrated to be significantly more covalent than the equatorial bond (McGlynn et al., 1961; Hoekstra, 1963), a factor which is relevant to the analysis of EXAFS data through the use of phase shift and amplitude parameters. Others have realized the significance of bond type and conducted their qualitative analyses accordingly.

Farges et al. (1992) extracted separate O_{ax} and O_{eq} phase shift and amplitude parameters from experimental EXAFS data for sodium uranyl triacetate. Prior to using these parameters to analyze data for a U-doped silicate glass in which the U environment was unknown, they tested the parameters on experimental data for other uranyl solids of known composition and structure, from which they obtained agreement with crystallographic interatomic distances within ±0.03 Å.

Chisholm-Brause et al. (1992) similarly realized the importance of distinguishing between O_{ax} and O_{eq} parameters. They extracted O_{ax} parameters from experimental EXAFS data for uranyl solids and used FEFF 5 to calculate O_{eq} parameters, which were then calibrated using experimental data for model compounds. Although they apparently found the parameters suitable for use in fitting data from U sorption on montmorillonite experiments, they do not report a comparison with crystallographic values for the calibration model compounds.

While the recognition of the importance of individually determining O_{ax} and O_{eq} phase shift and amplitude parameters constitutes a major milestone in U EXAFS data analysis, other advances could make the technique much more valuable to the study of U sorption at the solid-water interface. With very few exceptions, U EXAFS data analysis has not proceeded beyond the O_{eq} shell. For solid-water interface studies, one would like to be able to observe a contribution to the $\chi(k)$ spectrum from an atom unique to the sorbent. Typically, the nearest neighbor to a sorbed U atom that satisfies this criterion is a metal atom in the surface layer of the metal oxide solid that is bonded directly to an equatorial O atom. Both Combes (1988) and Manceau et al. (1992) have observed contributions from Fe atoms in U EXAFS spectra of U sorbed to iron oxide solids. Based on the U-Fe distance, the Fe atom must be bonded to 2 O atoms that lie in the equatorial plane around U. XAS studies of U sorption on lower atomic number oxides ($Z<26$), however, have failed to demonstrate the presence of a metal atom unique to the sorbent (e.g. Si or Al in montmorillonite (Chisholm-Brause et al., 1992) or Si in silica colloids (Dent et al., 1992)) in the atomic environment of U.

Furthermore, few studies have reported polynuclear complex formation based on U EXAFS data (implied by the presence of a U backscatterer contribution in the $\chi(k)$ spectrum of U). Both in aqueous solution and at the solid-water interface, the formation of polynuclear complexes is of interest as a precursor to solid phase formation. In U(VI)-containing solids, nearest U neighbors are typically found 3.7 to 4.3 Å from the central U atom. This is expected to be within the capability limits of the technique, especially for U, because it is such a strong scattering atom.

Objectives of this Study

With the ultimate objective of using XAS to determine the structure and composition of U complexes sorbed at the solid-water interface, our specific objectives for this study are as follows:

- test the ability of FEFF 5 to calculate phase shift parameters for U absorber atoms and phase shift and effective scattering amplitude parameters for backscattering atoms in the U environment
- determine which backscattering atoms in the local atomic environment around U can be detected using EXAFS
- establish reasonable ranges for σ^2 values for each shell of backscattering atoms in the U environment
- provide reference phase shift and amplitude parameters for quantitative analysis of U sorption sample EXAFS data

EXPERIMENTAL

Materials

Solid Model Compounds

The solid uranium compounds used as model compounds are from a variety of sources. Uranyl nitrate hexahydrate and uranyl (di)acetate are reagent grade chemicals from J.T. Baker Chemical Co. The uranyl carbonate is of unknown origin, but was identified as rutherfordine based on its XRD powder pattern. Rubidium uranyl nitrate was synthesized by I. Pickering of SSRL by combining stoichiometric amounts of uranyl nitrate and rubidium nitrate, as described in Zalkin et al. (1989). The uranyl phosphate/silicate minerals selected as model compounds include meta-autunite, meta-ankoleite, and uranophane. Meta-autunite came from the Smithsonian collection, #112882-1. Meta-ankoleite was synthesized by M. Barr of Los Alamos National Laboratory (LANL) by stepwise addition of KOH to a uranyl phosphate solution. Uranophane came from a private collection. The boron nitride (BN) used in preparation of solid model compounds is from Aldrich Chemical Company.

X-ray diffraction (XRD) powder spectra were collected for all of the solid model compounds to confirm their identity and crystallinity. Spectra for the nitrate, (di)acetate, and carbonate compounds were produced using copper K_α radiation (λ = 1.5418 Å) on the Stanford University Geological and Environmental Sciences Department Rigaku Powder X-ray Diffractometer. Diffraction data for phosphate and silicate minerals were collected at LANL on a Phillips XRG3100 instrument using copper K_α radiation. Reference spectra

were obtained from the JCPDS database.[2] Model compound spectra overlain by JCPDS reference spectra are included in Appendix 2 and are discussed in the results section.

For XAS sample preparation, solid model compounds were ground in an agate mortar and pestle and mixed with solid boron nitride (BN) in a proportion to yield 30% absorption of the incoming beam, or $\mu\rho x = 1$, where μ is the mass absorption coefficient of the sample ($cm^2 \cdot g^{-1}$), ρ is the density of the sample ($g \cdot cm^{-3}$), and x is the thickness of the sample (cm). Mass absorption coefficients are tabulated in McMaster et al. (1969). The mixture was then pressed into an 0.5 mm thick aluminum sample holder and the sample was enclosed between Mylar windows.

Solution Model Compound

The solution model compound consisted of 50 mM uranyl nitrate (J.T. Baker Chemical Co. reagent grade) in doubly deionized water, with sufficient reagent grade nitric acid to reduce the pH of the solution to <1.0. Dissolution of the starting solid was visibly complete. These conditions should ensure predominance of the monomeric $UO_2^{2+}(aq)$ ion, based on species distributions calculated using the computer code HYDRAQL (Papelis et al., 1988) and the thermodynamic data provided in Appendix 1. Species identification has not been independently verified, however. Just prior to XAS data collection, an aliquot of solution was loaded into a 1.5 mm thick Teflon solution cell with Mylar windows using a Becton-Dickinson Plastipak® syringe.

Methods

XAS Data Collection

Uranium L_{III}-edge XAS spectra (~17 - 18 keV; edge inflection 17166 eV) were collected at the Stanford Synchrotron Radiation Laboratory (SSRL) during dedicated beam conditions (~3 GeV and 40-90 mA), using high flux wiggler beam line IV-2 (18 kG wiggler field). The x-ray beam was unfocused on a Si(220) monochromator crystal, cut #2 (ϕ=90°). Spectra were collected in transmission mode for the solid and liquid model compounds using Ar-filled ionization chambers. Harmonic rejection was effected by 40-80% detuning of the incident beam. Three to four scans were collected for each sample. A reference "foil" was mounted between two ionization chambers downstream from the sample to provide a continuous energy calibration reference.[3]

---

[2]Available from the International Center for Diffraction Data, 12 Campus Blvd., Newton Square, PA, 19073.

[3]Typically metal foils of the element of interest are used as energy calibration references. In this case, the "foil" was U metal that has been oxidized to U(VI).

XAS Data Analysis

A brief description of the XAS data analysis procedure, focusing on details specific to this study, is provided here for model compounds. Numerous review articles provide more complete accounts (see, for example, Cramer and Hodgson, 1979; Scott, 1984; Sayers and Bunker, 1988). Unless otherwise stated, all of the programs mentioned were written by G. George of SSRL.

Raw data files for each scan collected were calibrated individually using the programs CALIB and AVEX by setting the position of the first inflection point of the calibration "foil" absorption edge equal to 17166 eV, the nominal L_{III}-edge energy for elemental uranium (Vaughan, 1986). The position of the first inflection varied by less than 2.5 eV among scans for a single sample, presumably due to beam movement on the monochromator crystals. Although all of the uranium in this study is expected to be in the +VI oxidation state, not elemental, consistency rather than absolute calibration is the objective. A weighted average of all calibrated files for each sample calculated in AVEX produced a single averaged spectrum for each sample. Weighting was proportional to the square of signal-to-noise, where the signal is defined as the magnitude of the edge jump and the noise level is determined by application of a high pass filter to the data (George and Pickering, 1993).

The program PROCESS was used to accomplish background subtraction and Fourier transform calculation. Polynomials of order -1 were fit to pre-edge spectra and subtracted. (At this point the XANES region (17050 to 17350 eV) was extracted; its analysis is discussed at the end of this section.) Splines consisting of 3 or 4 regions of fourth order polynomials, the number of regions depending primarily upon the data range, were fit to the EXAFS regions of the pre-edge background-subtracted data and subtracted. Resulting spectra were normalized by the absorption cross-section for uranium, measured at 17200 eV, which was extrapolated through the EXAFS region using the Victoreen equation (Scott, 1984). The resulting EXAFS spectrum was transformed over the range k = 3 to 14 $Å^{-1}$. This k-range was used for all samples and theoretical spectra, unless precluded by data quality, to allow comparison of resulting Fourier transforms.

Reference phase shift ($2\delta^c$ and Φ) and effective scattering amplitude ($|f_{eff}(\pi, k, R)|$) parameters were calculated using FEFF 5 for each model compound. Atomic cluster input consisted of model compound atomic positions, determined independently by XRD (see Table 1 for XRD references). The value of S_0^2 was set to 1.0 for all model compounds; this falls within a range (0.8 to 1.0) that is typical for metals and has been used for oxides and salts (Mustre de Leon et al., 1991). Although σ^2 values are known to be path-dependent, we chose an initial global σ^2 value of 0.003 $Å^2$ for all paths to enable

Model Compound	FEFF Reference	XRD Reference
Uranyl (di)acetate	none	JCPDS#14-972, contributed by E. Lanterman, Ingersoll Research Center JCPDS#32-1405, NBS Monogr. **25** 18 76 (1981).
Uranyl nitrate hexahydrate	Taylor and Mueller (1965)	JCPDS#31-1436; Taylor and Mueller (1965)
Rutherfordine	Cromer and Harper (1955)	JCPDS#11-263; Clark and Christ (1957)
Rubidium uranyl nitrate	Zalkin et al. (1989)	Zalkin et al. (1989)
Uranophane	Ginderow (1988)	JCPDS#39-1360; Ginderow (1988)
Meta-autunite	Morosin (1978)	JCPDS#39-1351, Grant-in-Aid Report
Meta-ankoleite	none	JCPDS#29-1061; Weigel and Hoffmann (1976)

Table 1. Structural references for FEFF 5 calculations and XRD reference spectra.

approximate scaling of multiple paths as a function of k, which allows qualitative comparison of theoretical with experimental EXAFS spectra. The theoretical spectra included all paths predicted to be significant by FEFF 5, using a conservative low amplitude cutoff value. Where qualitative agreement was good, theoretical $\chi(k)$ was calculated for individual paths. The global σ^2 value was effectively reset to zero for each path's spectrum prior to extraction of individual path phase shift and amplitude parameters.

All experimental data were fit without further refinement (e.g. deglitching) using the program OPT. Individual backscattering shells were fit to filtered data to establish values of S_0^2, R, and σ^2, to be used as starting values in a multi-shell fit of the unfiltered data. The energy shift term, ΔE_0, which accounts for the difference between the threshold Fermi level of an electron gas (FEFF's energy reference) and the actual threshold energy associated with the atom cluster being studied and is highly correlated with R, was allowed to adjust freely in the single shell fits provided R did not deviate significantly from crystallographic values. Data for individual shells were extracted by applying a Gaussian window to FT features that could be isolated (those corresponding to O_{ax}, O_{eq}, and U backscatterers, where present), then back transforming the windowed data. Due to the significant overlap of U-L_{eq} distances, FT features between and sometimes including O_{eq} and U could not be isolated. For model compounds, values of N for all shells were fixed to known crystallographic values because of their high degree of correlation with S_0^2 and σ^2.

In the multi-shell fit of unfiltered spectra, S_0^2 was fixed to the average of values obtained in single shell fits (1.0). The value of ΔE_0 was adjusted but forced to the same value for all coordination shells, in accordance with the findings of O'Day et al. (1994) that ΔE_0 is primarily a function of the absorbing atom. Values of N remained fixed to their crystallographic values, while R and σ^2 values for each shell were allowed to adjust to arrive at a best fit of the data.

XANES

Positions of features in the XANES region were measured at their zero points on the first derivative of the pre-edge background-subtracted spectra. Because the first feature (denoted A) occurs in a region of the spectrum in which the overall trend is sloping, its derivative never reaches zero and therefore was measured as the local maximum of the first derivative. Peak positions relative to the absorption edge maximum (white line) were calculated by subtraction; relative positions are compared with literature values and among the samples.

RESULTS

X-ray Diffraction

Model compound spectra overlain by JCPDS reference spectra are included in Appendix 2; Table 1 lists pertinent information for the compounds used to produce reference spectra. A match of peak position within ± 0.3° 2θ and relative peak intensity within ± 10% was obtained for uranyl nitrate hexahydrate, suggesting that our specimen is very pure. All other spectra showed some discrepancy relative to their respective reference spectra. Discrepancies and their implications for the use of these solids as EXAFS model compounds are discussed below.

The uranyl (di)acetate XRD spectrum matches equally well to two JCPDS spectra. Reference peak positions are well reproduced by our spectrum; however, relative intensities of several lines are underestimated in our spectrum by as much as 30%. Because all of the reference peaks are present in our spectrum, with no extra peaks, the intensity mismatch is not likely caused by any impurity. As is known to be true for uranyl nitrate, it is quite likely that the number of water molecules in the uranyl (di)acetate structure varies. A difference in hydration state between the reference compound and our model compound could produce the observed discrepancy in relative line intensities, without affecting peak positions. Such a difference would not be expected to affect the atomic environment around U, at least as far as the distant acetate-O atoms (approximately 4.5 Å). We therefore conclude that our uranyl (di)acetate specimen is suitable for use as an EXAFS model compound.

Peak positions in the rutherfordine XRD spectrum match within ±0.3° 2θ with those in the reference spectrum, with the following exceptions. Peaks are present at 2θ values of 12°, 25°, 29°, and 30° in our spectrum that are not indicated by the reference spectrum. The 12° peak is outside of the scan range for the reference spectrum, and therefore is not necessarily extraneous. The 25°, 29°, and 30° peaks may be indicative of an impurity, however. The greyish-yellow color of our sample (as opposed to white to pale yellow as reported by Clark and Christ, 1957) further suggests the presence of an impurity. Assuming the presence of an impurity, we have been unable to match the positions of the "impurity peaks" to any spectrum included in the JCPDS database. All of the impurity peaks are of low relative intensity, suggesting that any impurities that are present constitute a small fraction of the specimen (<20%). Intensities of our 19° (020), 39° (040), and 60° (060) peaks match those of the reference spectrum within 10% relative intensity, whereas all other relative peak intensities exceed those in the reference spectrum but are proportionally correct relative to each other. Given rutherfordine's perfect (010) cleavage, we suspect that the reference spectrum suffered from preferred orientation,

resulting in enhanced intensities for peaks corresponding to parallel planes ((020), (040), (060)). Correcting for preferred orientation in the reference spectrum would result in a much better match of relative peak intensity between our spectrum and the reference spectrum. We therefore proceed with the use of our rutherfordine specimen as an XAS model compound, recalling that it may not be pure.

Because a reference spectrum for rubidium uranyl (tri)nitrate is not present in the JCPDS database, we generated a spectrum for matching purposes based on the structural refinement of Zalkin et al. (1989) using the program LAZY (Yvon et al., 1977). All peaks in the resulting reference spectrum are accounted for in our powder pattern, with good relative intensity agreement. There are a significant number of additional peaks in our spectrum, however. All of the additional peaks are accounted for by a combination of the reference spectra for the tetranitrate, $Rb_2UO_2(NO_3)_4$, and uranyl nitrate hexahydrate, $UO_2(NO_3)_2 \cdot 6H_2O$; the former is a plausible product given the synthetic route, the latter is a reactant. Peaks corresponding to these two additional compounds are too small and overlapping to estimate whether relative peak intensities are in agreement with reference spectra. Based on fitting the intensity of the most intense reference peak for each compound to our spectrum, we estimate that the three compounds are present in our specimen in a ratio of approximately 1 $Rb_2UO_2(NO_3)_4$: 1 $UO_2(NO_3)_2 \cdot 6H_2O$: 3 $RbUO_2(NO_3)_3$. Given its mixed composition, this specimen is not useful as an EXAFS model compound, but it may provide some insight into the XAS spectra of mixed sites.

The uranophane XRD spectrum displays only minor discrepancies with the reference spectrum. All reference spectrum peaks are present in our spectrum, with no additional peaks. Below 2θ of 50°, peaks in our spectrum are very sharp, suggesting a high degree of crystallinity. Peak intensity discrepancies are associated with low intensity peaks in our spectrum that correspond to diffraction planes parallel to the (100) basal plane ((200)-11.2°, (400)-22.5°, 34.0° is probably incorrectly indexed as (711), and the peak at 45.9° is not indexed) (Frondel et al., 1956). This would suggest that relative to our spectrum, the reference spectrum suffers from preferred orientation along (100). We conclude that our uranophane specimen is of very high purity and crystallinity and therefore potentially an excellent EXAFS model compound.

Our meta-autunite XRD spectrum contains all reference spectrum peaks, with one small extra peak at 11° 2θ. Peaks in our spectrum are fairly sharp, indicating a high degree of crystallinity. Relative peak intensities show several discrepancies with those in the reference spectrum. Assuming agreement for the most intense peak ($2\theta \approx 10°$), peaks located at 16°, 24°, 34°, and 57° in our spectrum are short by as much as 40%. There is no obvious explanation such as preferred orientation to account for different peak intensities

because the corresponding planes are not parallel. The discrepancy may be due to a difference in interlayer cation identity or hydration state between the two specimens. The autunite family of minerals shares a common sheet structure and composition, and differs solely in the identity of interlayer cations. For each autunite mineral, the number of water molecules incorporated in the structure can vary. In the worst case, this might suggest that the reference sample and our specimen are two different minerals. Nonetheless, they are both autunite minerals, for which the local structure around U (at least as far as the nearest phosphate-P) is constant. Our specimen of meta-autunite should be a good EXAFS model compound for this range of distances.

Our meta-ankoleite spectrum is in generally good agreement with the corresponding reference spectrum. All reference spectrum peaks are present in our spectrum within ±0.3° 2θ of their reference spectrum positions, with one small extra peak in our spectrum at 11° 2θ. The sharpness of the peaks in our spectrum is indicative of a high degree of crystallinity. Reference spectrum relative peak intensities are well reproduced in our spectrum, with the exception of peaks at 9.7° and 32.6°, both of which are significantly smaller in our spectrum. As in meta-autunite, we conclude that our specimen is a good EXAFS model compound for neighboring atoms at least as far as the phosphate-P.

Although we have selected these solids for their suitability as XAS model compounds, it is apparent that our particular specimens are not all suitable. As we have found, this problem is endemic to U(VI) minerals by their very nature of formation, which involves a progressive change in mineral identity with distance from an ore body. It is consequently difficult to obtain pure specimens of uranium minerals. Uranium(VI) solids also have a tendency to absorb water, the amount depending upon the humidity of the environment and exposure time. Rather than search indefinitely for a larger suite of perfect model compound specimens, we have proceeded with XAS data collection and analysis for these compounds, cognizant of their shortcomings.

X-ray Absorption - Qualitative Analysis

As a precursor to quantitative fitting of our model compound EXAFS data, we have conducted a qualitative comparison of FEFF and experimental spectra. The comparison serves two purposes. In part, it serves as an indicator of FEFF's ability to calculate spectra (and therefore phase shift and amplitude parameters for quantitative analysis) that closely resemble those collected experimentally. This has been tested previously for lower atomic number absorbers (Co - O'Day et al., 1994), but not for U, for which it has been postulated that relativistic effects might alter experimental spectra in an unknown way. If FEFF does appear to perform well, then we should be able to use paths that FEFF predicts

to be significant (but might not otherwise be considered, e.g., multiple-scattering paths) to interpret unexplained features in experimental spectra. We will make use of the second point in our quantitative analysis section.

In our comparison, we consider only five of the eight model compounds, because structural refinements that report atomic coordinates have not been found for uranyl (di)acetate, meta-ankoleite (although meta-ankoleite is isostructural with meta-autunite), and the aqueous uranyl monomer, UO_2^{2+}(aq). FEFF-calculated spectra superimposed on experimental spectra for uranyl nitrate hexahydrate (UNS), uranophane (URAN), meta-autunite (AUT), rubidium uranyl nitrate (RBUNS), and rutherfordine (RUTH) are included in Appendix 3. The extent of agreement between FEFF and experimental spectra varies considerably. Whereas all major and most minor oscillations are reproduced by FEFF for UNS, fewer of the minor features coincide for URAN and AUT, only major oscillations coincide for RBUNS, and there is very little agreement for RUTH.

Several expected sources of discrepancies should be considered before questioning the ability of FEFF 5 to calculate EXAFS spectra for U compounds. The value of ΔE_o, discussed in the experimental section, has not been accounted for in superimposing the spectra. Based on values determined while fitting the data, ΔE_o could be as high as 6 eV, which would shift the EXAFS spectrum by approximately 1 $Å^{-1}$. This does not appear to cause any significant discrepancies, with the possible exception of RUTH, however.

The use of a global Debye-Waller factor (σ^2=0.003 $Å^2$) in FEFF is certainly responsible for some of the observed discrepancy. It results in incorrect relative path amplitudes, such that the wrong paths dominate the FEFF spectrum. Furthermore, the shape of the $\chi(k)$ amplitude envelope for each individual path may be altered; because of the k^3 weighting of $\chi(k)$, this could significantly affect the appearance of the multi-path spectrum. Eliminating this source of discrepancy would require assignment of realistic, path-dependent σ^2 values to each path (25 to 60 paths for the spectra in Appendix 3). While we can ascertain path-dependent σ^2 values by fitting experimental data for model compounds, this is only possible for FT features that can be isolated, typically limiting σ^2 determination to single-scattering paths corresponding to the nearest few neighbors. Although these constitute a significant part of the EXAFS signal, other contributions are clearly significant, as will be demonstrated.

An additional factor that is difficult to quantify and will affect spectra to varying degrees is sample impurity. Whereas FEFF spectra are calculated based on ideal structures, experimental sample impurities that are not detectable by XRD may affect experimental spectra. Similarly, the quality of the structural refinement on which FEFF calculations are based can affect FEFF spectra dramatically. The poor agreement between

FEFF and empirical RUTH spectra is most likely due to the imprecision of the structural refinement. Very large tolerances in interatomic distances (±0.09 Å on the $R_{U\text{-}Oax}$ value alone) are reported in the rutherfordine structure refinement (Cromer and Harper, 1955). We suspect the Cromer and Harper structure of being inaccurate as well as imprecise based on refinements of similar uranyl carbonate structures, such as potassium uranyl carbonate (Anderson et al., 1980), in which the U-O_{ax} distance is 1.80 Å, and aqueous triuranylhexacarbonate ion (Åberg et al., 1983), in which the U-O_{ax} distance is 1.80 Å, to Cromer and Harper's 1.67 Å. Poor structure refinements are not uncommon for U-containing crystalline materials, because the most commonly used tool is XRD, and U absorbs x-rays very effectively, leaving limited intensity for diffraction. Such absorption is often difficult to account for.

While we could repeat this qualitative comparison, accounting for ΔE_0 and estimating path-dependent σ^2 values, we feel that the excellent potential of FEFF for calculating EXAFS spectra (and therefore phase shift and amplitude parameters) of U compounds is demonstrated in the UNS spectra. Instead, we have extracted single-scattering path phase shift and amplitude parameters from each of these five FEFF calculations for use in quantitative analysis of our data. In fitting the data, we treat both ΔE_0 and σ^2 as adjustable parameters to address the issues raised above. Quantitative analysis of experimental data will serve as a further test of FEFF's ability to model U EXAFS.

X-ray Absorption - Quantitative Analysis

Using FEFF-calculated phase shift and amplitude parameters, we have been able to account for most of the features in our experimental EXAFS data that are discernible above background noise. Stack plots of empirical EXAFS spectra and FTs for all of the model compounds are included in Figures 3 and 4. Data fits are included in Appendix 4. Because we are working with model compounds, we can evaluate our ability to model the data by comparing resulting interatomic distance (R) values with crystallographic (XRD) data (Table 2). In the following, we address the fit to experimental data for each model compound individually. Fourier transform features are reported uncorrected for phase shifts.

Unhydrolyzed monomeric aqueous uranyl ion

The unhydrolyzed monomeric uranyl ion (UNL - $UO_2^{2+}{\cdot}5H_2O$) that is expected under conditions of preparation of this solution sample consists of a uranyl moiety surrounded by five equatorial water molecules (Görller-Walrand and Colen, 1982). In the

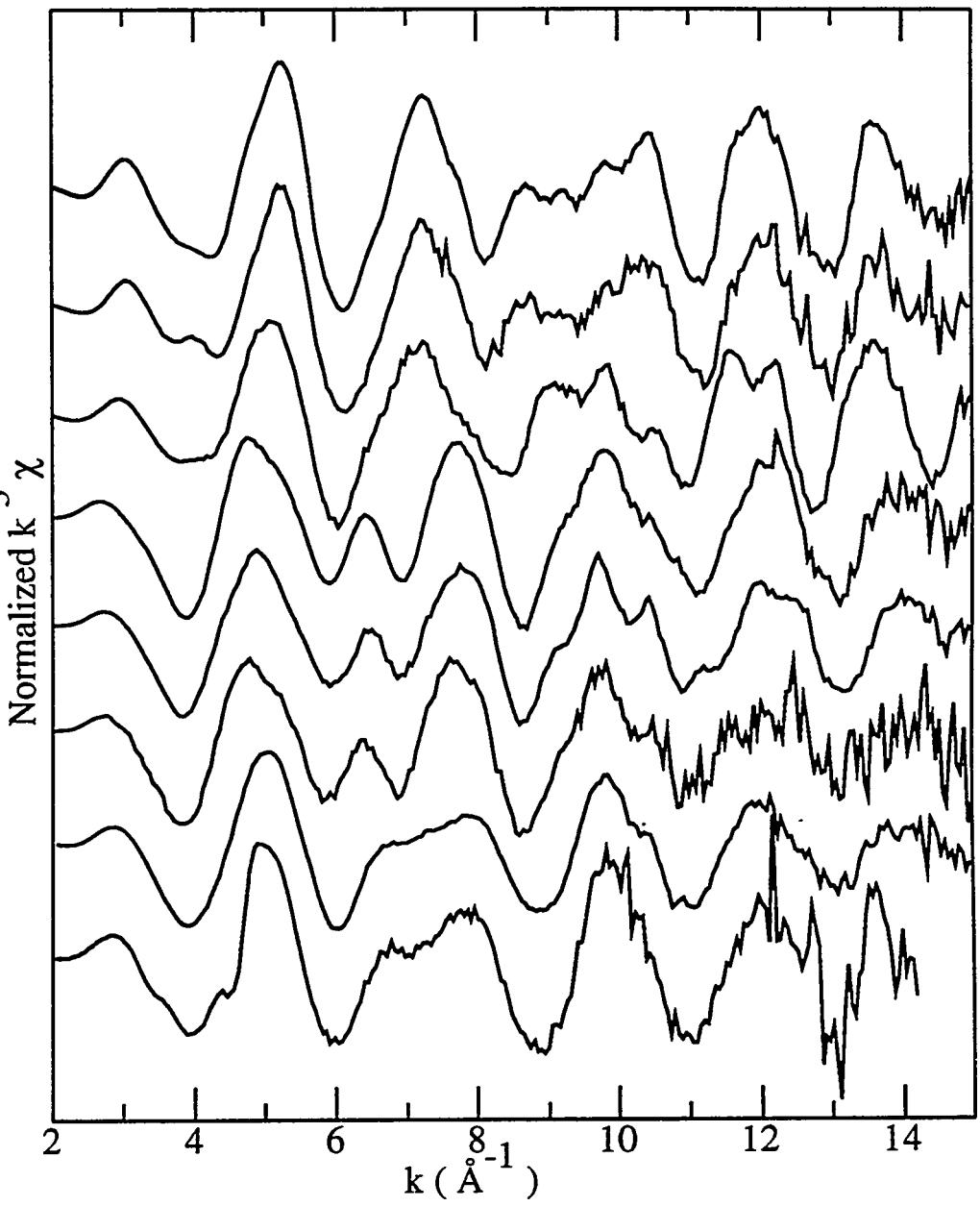

Figure 3. EXAFS spectra for model compounds. From bottom to top, spectra are for unhydrolyzed monomeric aqueous uranyl ion, uranyl (di)acetate, uranyl nitrate hexahydrate, rutherfordine, rubidium uranyl nitrate, uranophane, meta-autunite, and meta-ankoleite.

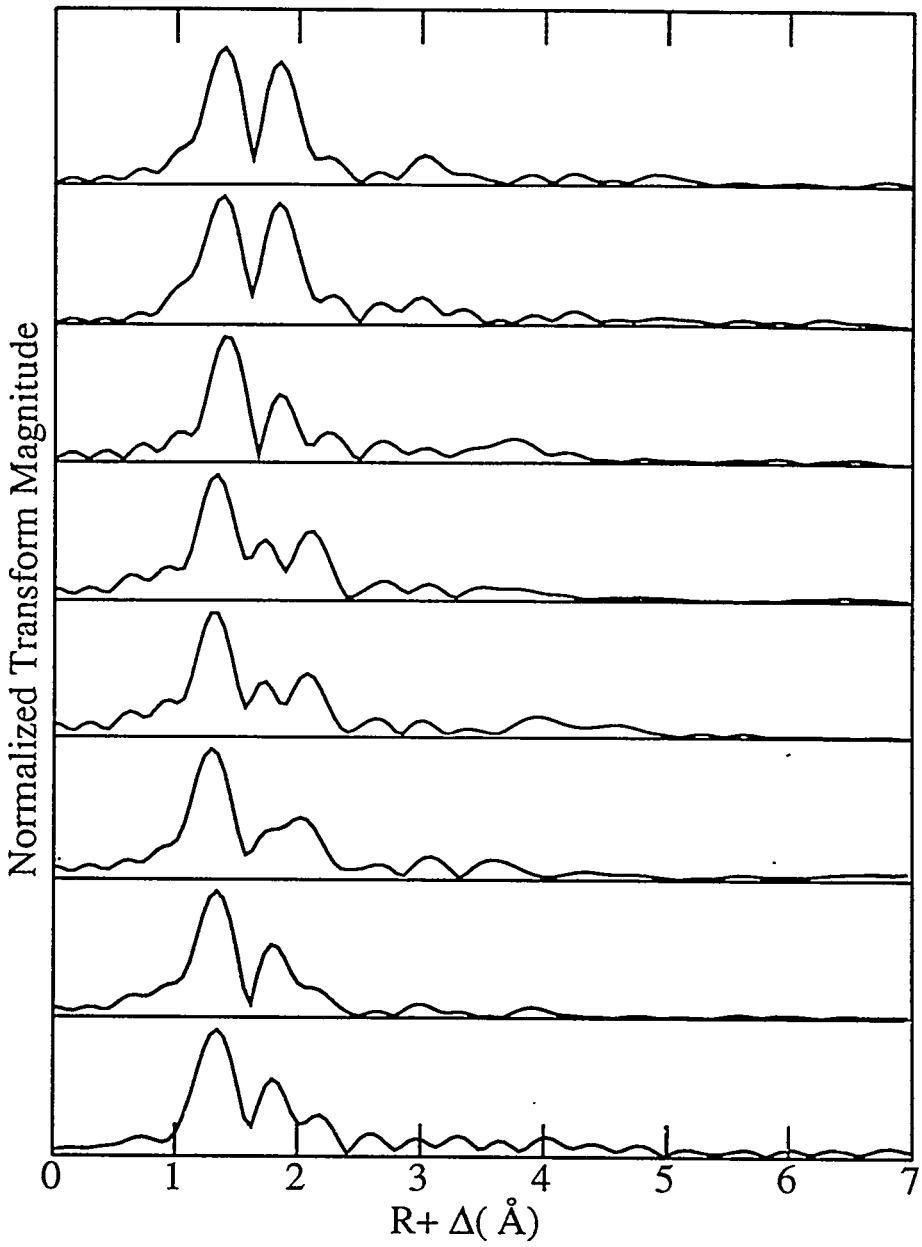

Figure 4. Fourier transforms of EXAFS spectra for model compounds. From bottom to top, spectra are for unhydrolyzed monomeric aqueous uranyl ion, uranyl (di)acetate, uranyl nitrate hexahydrate, rutherfordine, rubidium uranyl nitrate, uranophane, meta-autunite, and meta-ankoleite.

COMPOUND	LIGAND	*EXAFS* N	R (Å)	σ^2 (Å^2)	*XRD* N	R (Å)
Unhydrolyzed monomeric aqueous uranyl ion	O_{ax}	2.0	1.76	0.0011		
$UO_2^{2+}\cdot 5H_2O$ (aq)	O_{eq}	5	2.41	0.0083		
Uranyl (di)acetate	O_{ax}	2	1.77	0.0024		
$UO_2(CH_3CO_2)_2 \cdot nH_2O$ (s)	O_{eq}	6	2.41	0.0120		
Uranyl nitrate hexahydrate	O_{ax}	2	1.75	0.0025	2	1.76
$UO_2(NO_3)_2 \cdot 6H_2O$ (s)	O_{eq}	6	2.46	0.0097	6	2.48
	N	2	2.93	0.0068	2	2.96
Rutherfordine	O_{ax}	2	1.76	0.0019	2	1.68
UO_2CO_3 (s)	O_{eq}	6	2.45	0.0108	6	2.48
	C	2	2.93	0.0036	2	2.86
	O_{dist}	8	4.26	0.0099	8	4.37
	U	2	4.31	0.0055	2	4.30
Rubidium uranyl nitrate	O_{ax}	2	1.76	0.0011	2	1.75
$RbUO_2(NO_3)_3$ (s)	O_{eq}	6	2.49	0.0081	6	2.47
	N	3	2.93	0.0121	3	2.91
Uranophane	O_{ax}	2	1.82	0.0016	2	1.80, 1.82
$Ca(UO_2)_2(SiO_3OH)_2 \cdot 5H_2O$ (s)	$O_{eq(1)}$	3	2.32	0.0022	3	2.28, 2.30
	$O_{eq(2)}$	2	2.50	0.0017	2	2.45, 2.48
	U	2	3.97	0.0054	2	3.92
Meta-autunite	O_{ax}	2	1.77	0.0037	2	1.77
$Ca(UO_2)_2(PO_4)_2 \cdot 6H_2O$ (s)	O_{eq}	4	2.29	0.0035	4	2.31
Meta-ankoleite	O_{ax}	2	1.78	0.0028		
$K_2(UO_2)_2(PO_4)_2 \cdot 6H_2O$ (s)	O_{eq}	4	2.29	0.0030		

Table 2. Results of model compound EXAFS analysis. XRD reference values are taken from references stated in Table 1. Where multiple bond lengths are reported in the reference, an arithmetic mean was taken. The second set of distance values reported for uranophane come from Viswanathan and Harneit (1986).

absence of a structure determination that reports atomic coordinates, we have relied on FEFF phase shift and amplitude parameters derived from the solid uranyl nitrate hexahydrate (UNS) structure in fitting UNL EXAFS data. Of the five compounds for which FEFF spectra were calculated, UNS is structurally most similar to UNL.

All of the major oscillations and FT features are accounted for by a fit that consists of O_{ax} and O_{eq} contributions. We were unable to account for the peak shoulder at 4.4 $Å^{-1}$ in the EXAFS spectrum by deglitching, which we thought its most likely cause given its shape. All of the FT features beyond 2.3 Å are believed to be artifacts of the transform function or noise.

Agreement between our EXAFS-derived R values and those of Chisholm-Brause et al. (1992; also an EXAFS study) seems reasonable given the fact that they did not fix their N values. If x-ray spectra include contributions from neighboring atoms that have not been accounted for in the fit, then allowing too many variables to adjust can result in incorrect values that attempt to account for atoms missing from the fit. On this basis we fix coordination number values in fits wherever they are reasonably well known.

Uranyl (di)acetate

Uranyl (di)acetate (URAC - $UO_2(CH_3CO_2)_2 \cdot nH_2O$) consists of a uranyl moiety with six O_{eq} atoms, four of which belong to two bidentate acetate groups and two of which are part of two water molecules. No extended structure has been reported for URAC. Mentzen and Giorgio (1970) report interatomic distances of 1.72 Å ($R_{U\text{-}Oax}$), 2.50 Å ($R_{U\text{-}Oeq,\ acetate}$), and 3.0 Å ($R_{U\text{-}Oeq,\ water}$). The first value is so much shorter and the last one so much longer than similar distances in other compounds that we doubt their validity. In the absence of a structure refinement that reports atomic coordinates for URAC, we used FEFF phase shift and amplitude parameters for solid UNS to fit URAC EXAFS data on the basis that the UNS and URAC structures are quite similar. Furthermore, the significant similarities between EXAFS spectra for UNL and URAC suggest that it should be reasonable to expect to use the same parameters for fitting both.

As in UNL, most of the major URAC EXAFS features are accounted for by a two-shell (O_{ax} and O_{eq}) fit. Unlike UNL, however, the structure between 6 and 8 $Å^{-1}$ is poorly fit for URAC. Fourier transform peaks at 3.0 and 3.9 Å are also unaccounted for by the two-shell fit. URAC is expected to have structure beyond the O_{eq} atoms that might contribute to the EXAFS spectrum, including two C atoms approximately 2.85 Å from U (based on the structure of sodium uranyl triacetate, Templeton et al., 1985), but these do not correspond to FT peak positions, nor does their inclusion improve the fit. In the

absence of a complete structural refinement, we are unable to discern what is lacking in our fit of the experimental spectrum.

To the extent that the URAC spectrum has been fit, the $R_{U\text{-}Oax}$ value is in good agreement with that for sodium uranyl triacetate (1.758 (3) Å), but the URAC $R_{U\text{-}Oeq}$ value is significantly shorter than the 2.464 (2) Å in sodium uranyl triacetate. This is not unreasonable, given that two of the equatorial ligands in URAC are water molecules, which tend to have significantly shorter U-O_{eq} distances (closer to 2.30 Å) than acetate. Grouped with U-Oeq bond lengths for acetate, the water ligands would cause a shorter average $R_{U\text{-}Oeq}$ value for URAC than that found for sodium uranyl acetate.

Uranyl nitrate hexahydrate

Uranyl nitrate hexahydrate (UNS - $UO_2(NO_3)_2{\cdot}6H_2O$) consists of a uranyl moiety surrounded by six O_{eq} atoms, four of which belong to two bidentate nitrate groups and two of which are part of two water molecules. Dik et al. (1988) proposed an extended structure for anhydrous uranyl nitrate in which the two water molecules were replaced by the distant O in nitrate groups bound in a bidentate fashion to two other uranyl moieties, but no extended structure has been proposed for the hydrated species.

All major and most minor UNS EXAFS oscillations are accounted for by a three-shell (O_{ax}, O_{eq}, and N) fit. The amplitude of the 6.3 $Å^{-1}$ peak is underestimated, as is the dip at 6.8 $Å^{-1}$. Some fine structure between 11.5 and 12.5 $Å^{-1}$ that may not be real is not accounted for by the three-shell fit. Structure in the EXAFS spectrum that is not accounted for by the three-shell fit probably corresponds to FT features that have not been fit, notably peaks at 3.1 and 3.6 Å. Atoms in the UNS structure beyond N include O atoms at a variety of distances starting with 4.16 Å, none of which coincide with the two FT peaks, nor would they be expected to contribute much amplitude due to their weak scattering at relatively long distances. This suggests that these peaks, and perhaps the unfit EXAFS structure, are due to multiple scattering.

To evaluate multiple scattering (MS) in the UNS structure, we return to the FEFF calculation that included all paths deemed significant by FEFF. Despite the use of a global σ^2 value, the calculation did predict FT peaks at 3.1 and 3.6 Å, albeit with incorrect magnitudes. Of the 22 MS paths with effective distances between 3.3 and 3.7 Å, linear three and four leg paths between U and one or both of its axial O atoms are predicted to have the largest amplitudes, but the corresponding FT features peak at 2.9 Å. The next strongest contributions are predicted to arise from linear scattering among the U, N, and distant nitrate-O atoms; the corresponding FT feature peaks at 3.7 Å, thereby contributing amplitude to one of the two unfit peaks. Nine different types of MS paths have effective

distances between the two just described, each with similar order-of-magnitude amplitudes. Adding only those paths with the highest amplitudes to the existing three-shell fit does not account for the FT feature at 3.1 Å. Adding all of them and individually adjusting all of their N and σ^2 values would be a monumental task, as we have found that fixing their σ^2 values to a common value does not produce the proper ratio of peak heights. We conclude that the FT peaks at 3.1 and 3.6 Å result from complex interference among a number of MS paths. The possible absence of MS paths from the three-shell fit has apparently not affected the values of parameters resulting from the fit; values of R are within 0.02 Å of crystallographic values for O_{ax} and O_{eq} shells and within 0.03 Å for the N shell.

Rutherfordine

The rutherfordine structure (RUTH - UO_2CO_3), as determined by Cromer and Harper, consists of uranyl moieties surrounded by six O_{eq} atoms, four of which belong to bidentate carbonate groups and two of which belong to monodentate carbonate groups. Each carbonate O atom is shared by two uranyl groups, which forms the basis for a sheet-like structure. Stacking of the layers is believed to occur with some disorder, such that interatomic distances may be somewhat affected (Christ et al., 1955).

All major and minor RUTH EXAFS oscillations are reproduced by a fit consisting of contributions from O_{ax}, O_{eq}, C, U, and distant O atoms. Contributions from O_{eq}, C, and distant O shells produce the EXAFS oscillation that peaks at 6.3 $Å^{-1}$. Typically, distant O atoms would not be expected to contribute significant amplitude due to their weak scattering potential, but excluding the distant O contribution from this fit results in a much poorer fit of the EXAFS spectrum in the 5.5 to 7.5 $Å^{-1}$ region. These distant O atoms behave differently because they are axial to neighboring U atoms, therefore their positions are stabilized by the strong U-O_{ax} bond. Furthermore, eight atoms coincide to contribute significant amplitude. The only obviously unfit feature is a FT peak centered at 4.6 Å.

EXAFS-derived R values are in relatively poor agreement with XRD values, but as discussed earlier, the accuracy of the XRD values is suspect, and stacking differences may account for some R differences. Without a high quality structural refinement, it is not possible to determine the source of the 4.6 Å peak.

Rubidium uranyl nitrate

We recall from our XRD results that our rubidium uranyl nitrate specimen is a mixture of rubidium uranyl nitrate (approximately 60%), uranyl nitrate hexahydrate (20%), and rubidium nitrate (20%). Because we are working at the U L_{III} edge, we do not expect the $RbNO_3$ to contribute to the EXAFS spectrum. Rubidium uranyl nitrate should

definitely contribute, whereas the presence of uranyl nitrate may or may not be identifiable in the spectrum on the basis of its small mole fraction.

Rubidium uranyl nitrate (RBUNS - $RbUO_2(NO_3)_3$) consists of a uranyl moiety with six O_{eq} atoms, all of which belong to bidentate nitrate groups. No extended structure has been reported for RBUNS. We have previously discussed the UNS structure, which is quite similar to that of RBUNS, with the substitution of two water ligands for one bidentate nitrate ligand. Given the grouping of UNS O_{eq} into a single FT peak, we expect O_{eq} bond lengths derived from EXAFS analysis of pure UNS and pure RBUNS to be indistinguishable, whereas $R_{U\text{-}N}$ might be slightly longer for UNS (2.96 Å) than RBUNS (2.91 Å). Because distinguishing between EXAFS spectra for RBUNS and UNS rests on a slight R value difference for a second shell neighbor that is not extremely strongly bound (U-N $\sigma^2 \approx 0.007$ Å^2 for 2 N in UNS), we do not expect to discern two distinct compounds (RBUNS and UNS) in our empirical spectrum, to the extent that scattering is dominated by single-scattering paths.

As in UNS, oscillations in the RBUNS EXAFS spectrum are reasonably well accounted for by a three-shell (O_{ax}, O_{eq}, and N) fit. The 6.3 Å^{-1} peak and following dip (6.9 Å^{-1} in RBUNS) are similarly underestimated, and FT peaks at 3.1 and 3.5 Å (compared with 3.1 and 3.6 Å in UNS) are not predicted by the fit. Despite the grouping of distant O atoms in the RBUNS structure, their inclusion in the fit does not improve the fit of the 6.3 Å^{-1} peak, as occurred for RUTH. The distant O atoms that group in RBUNS are equatorial to other U atoms, and therefore have higher associated disorder than those that can be seen in the RUTH spectrum.

Although agreement between the complete FEFF spectrum and the experimental spectrum is not as good for RBUNS as UNS, we observe in the resulting FTs that the unfit RBUNS peaks are predicted by FEFF. Multiple-scattering paths in this distance range and beyond that are linear and involve the tightly bound axial oxygen atoms or the nitrate-N and distant nitrate-O are predicted by FEFF to have significant amplitudes. Furthermore, we would expect MS to be even more important in RBUNS than UNS due to the higher symmetry of RBUNS, which results in greater numbers of each path type. Judging from our difficulties in attempting to fit UNS FT peaks with individual MS parameters, and knowing that our RBUNS specimen is a mixture, we have not further pursued fitting the outstanding features. Nonetheless, agreement with crystallographic R values is within ±0.02 Å for each of the three single-scattering shells, from which we conclude that the potential absence of MS paths from the fit does not alter resulting R values.

Uranophane

Uranophane (URAN - $Ca(UO_2)_2(SiO_3OH)_2 \cdot 5H_2O$) is a 1:1 uranyl silicate mineral which consists of uranyl moieties in fivefold equatorial coordination. Uranyl pentagons form a continuous edge-sharing chain; chains are linked to form sheets by silicate tetrahedra (Fig. 5). Uranyl silicate sheets lie parallel in the uranophane structure, with Ca^{2+} ions between the layers. The uranophane structure can take on slightly different crystallographic parameters, depending upon the number of water molecules that are associated with the structure in the interlayer. Two refinements of one of the structures have been reported recently (Viswanathan and Harneit, 1986; Ginderow, 1988). We used the former in calculating FEFF phase shift and amplitude parameters for fitting URAN empirical EXAFS data.

A four-shell (O_{ax}, O_{eq1}, O_{eq2}, and U) fit of URAN EXAFS data results in an excellent reproduction of virtually all oscillatory features. Resulting interatomic distances agree within ±0.05 Å for all four shells with both reported structures. Unlike spectra discussed thus far, the URAN O_{eq} shell clearly splits into two subshells (Fig. 6). This is apparent in the FT, and is suggested by the multitude of U-O_{eq} distances in structures reported by both Ginderow (1988) and Viswanathan and Harneit (1986). While the crystallographic distances do not clearly separate into two groups by distance, they do span the range from 2.22 to 2.53 Å, which is a large enough ΔR value to be discerned as two separate peaks in an EXAFS spectrum for which the Δk is 11 $Å^{-1}$ (or greater), according to

$$\Delta R \geq \frac{\pi}{2\Delta k} \tag{4}$$

As can be seen in Figure 7, the U shell makes a considerable difference in the quality of the fit to both the EXAFS spectrum and its FT.

Despite the high quality of the fit, a distinct feature at 12 $Å^{-1}$ is not accounted for, and FT features between 2.5 and 3.5 Å are not properly fit. The fit does not include atoms located between O_{eq} and U, namely Si, as attempts to include one or more Si atoms did not significantly improve the fit. The four nearest Si atoms are extremely variable in distance from U (3.14, 3.63, 3.75, and 3.78 Å), and therein may lie the difficulty in trying to fit them. Furthermore, according to FEFF calculations, several significant MS paths have total path lengths that are interspersed with single scattering to Si atoms. The "complete" FEFF calculation, which includes significant Si atom contributions as well as some significant MS paths, does reproduce the feature at 12 $Å^{-1}$ and its FT matches that of the experimental data remarkably well.

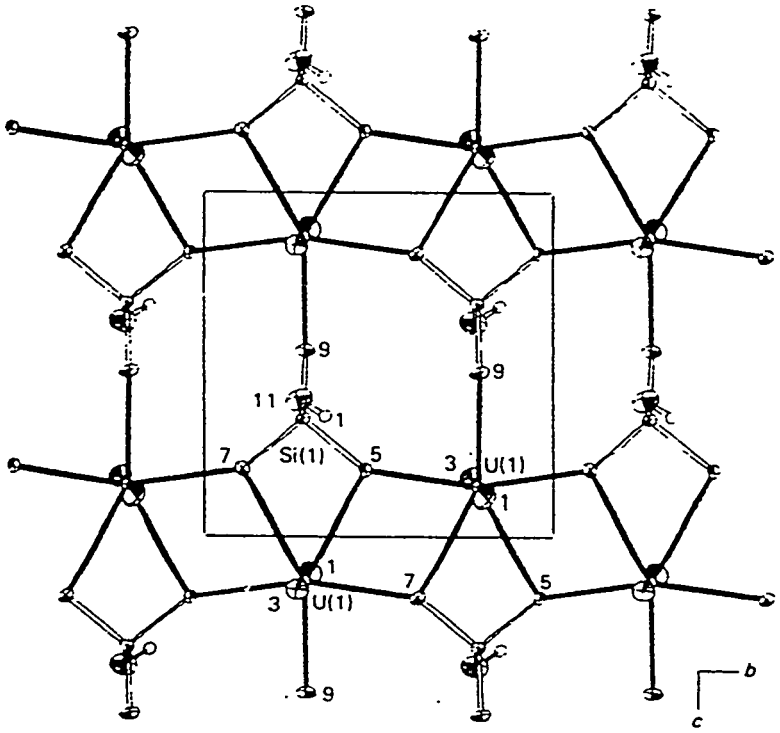

Figure 5. Extended structure of the uranophane (010) plane, after Ginderow (1988). Uranyl bonds are roughly perpendicular to the page. U and Si atoms lie approximately in the plane of the page. Si atoms bond to U through O_{eq} atoms in bidentate and monodentate fashion. Uranyl silicate layers such as this stack in the direction perpendicular to the plane of the page.

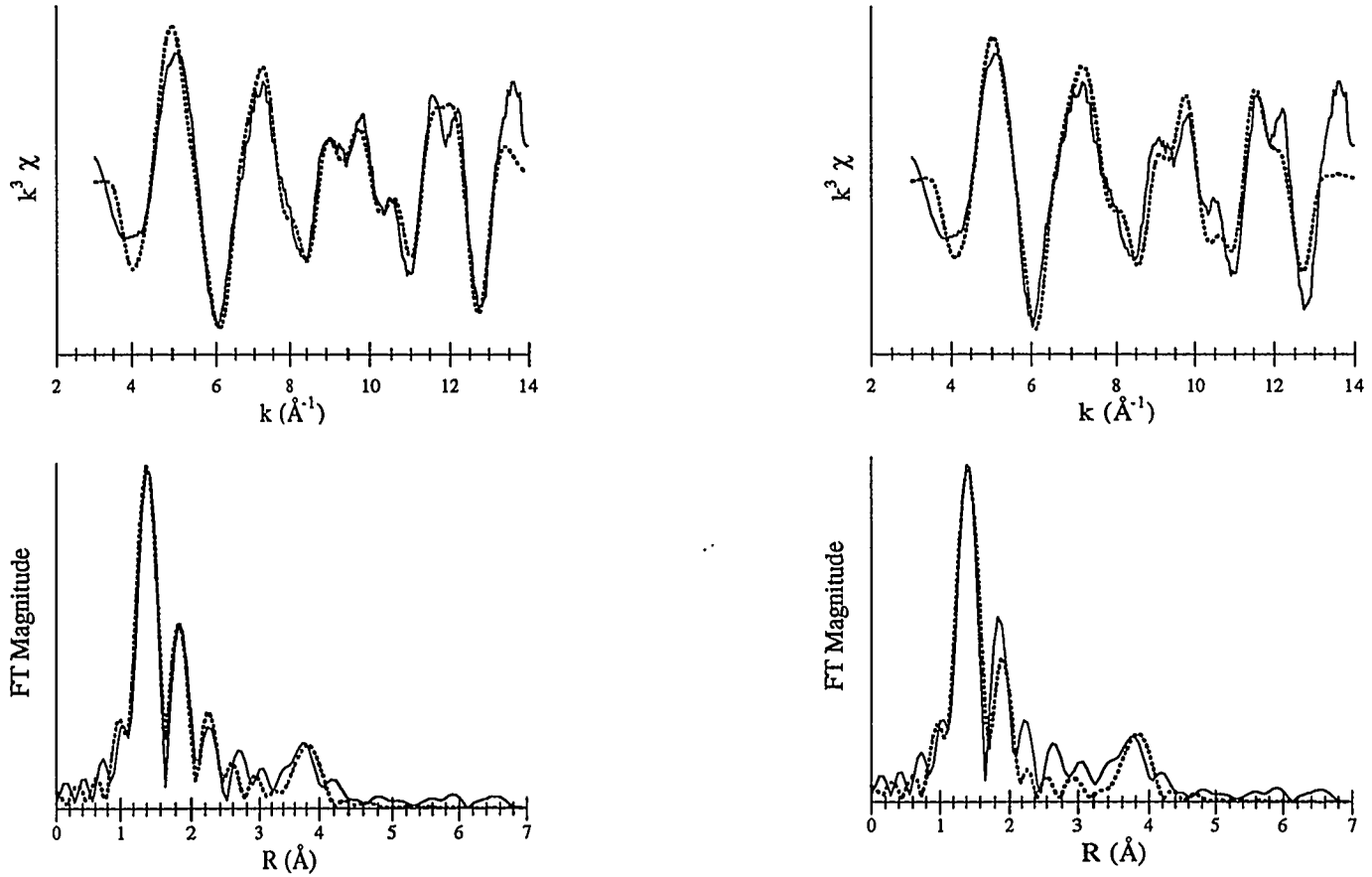

Figure 6. Fits of uranophane spectra comparing one and two equatorial oxygen shells. Fourier transform spectra are uncorrected for phase shift. Solid lines are experimental spectra; dotted lines are fits. Fit in left pair of spectra contains two O_{eq} subshells; fit in right pair of spectra contains single O_{eq} shell. Note the improved fit of the 2.2 Å FT peak in the two subshell fit.

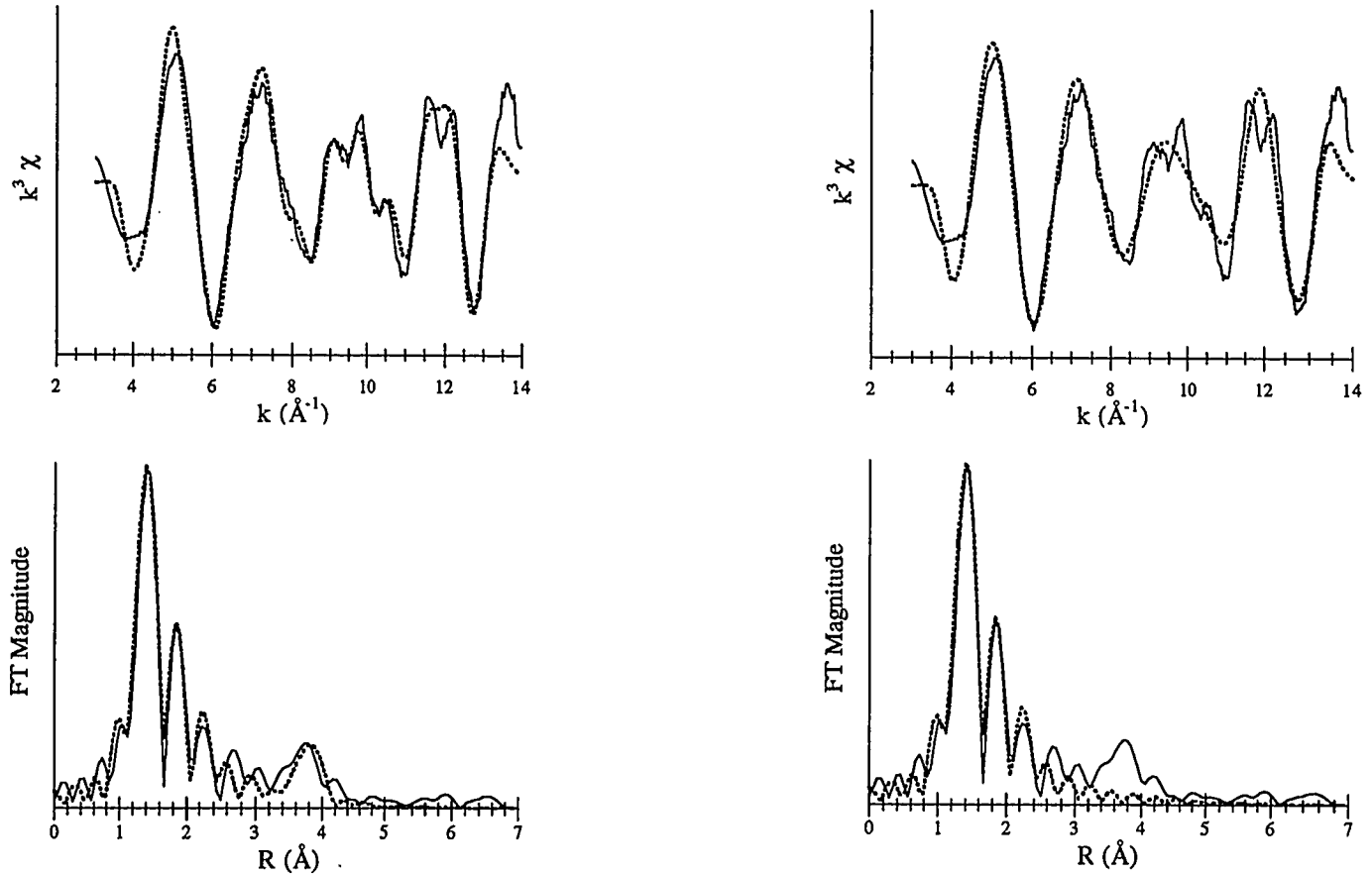

Figure 7. Fits of uranophane spectra with and without a shell of U neighbors at 3.92 Å. Fourier transform spectra are uncorrected for phase shift. Solid lines are experimental spectra; dotted lines are fits. In all fits, two equatorial oxygen subshells were included. Fit in left pair of spectra contains a U shell; fit in right pair of spectra does not. Note the improved fit of the 3.8 Å FT peak and the k = 8 to 11 $Å^{-1}$ region of the EXAFS spectrum in the fit that includes U neighbors.

Meta-autunite

Meta-autunite [AUT - $Ca(UO_2)_2(PO_4)_2 \cdot 6H_2O$] is a 1:1 uranyl phosphate mineral in which each uranyl moiety is surrounded by four O_{eq} atoms, each of which occupies one corner of a phosphate tetrahedron (Smith, 1984). The uranyl phosphate network extends to form sheets, between which Ca^{2+} ions are located. In the absence of a meta-autunite structure refinement that reports atomic coordinates, we have used the structure of hydrogen uranyl phosphate, which is isostructural with meta-autunite, to calculate FEFF phase shift and amplitude parameters for fitting AUT EXAFS spectra.

A two-shell (O_{ax} and O_{eq}) fit accounts for all of the major EXAFS oscillations, but only the obvious O_{ax} and O_{eq} FT peaks. There appears to be fine structure between 8.5 and 10.5 $Å^{-1}$ which is reproduced by FEFF, but the noise level in the data largely obscures the features. Fourier transform peaks between 2.5 and 3.5 Å appear to stand above the noise level but are not accounted for by the fit; FEFF predicts the dominant peak at 3.1 Å. In addition to O_{ax} and O_{eq} paths, the FEFF calculation predicts significant amplitude for P (4 at 3.60 Å), distant O (4 at 3.88 Å and 4 at 4.11 Å), and several MS paths. Although we have been unsuccessful in fitting the unfit features by including additional shells for P, distant O, and significant MS paths in the fit, we again conclude that a combination of these shells accounts for the observed experimental spectrum.

Meta-ankoleite

Meta-ankoleite [ANK - $K_2(UO_2)_2(PO_4)_2 \cdot 6H_2O$] is isostructural with meta-autunite, with K^+, rather than Ca^{2+}, ions occupying the interlayer region. In the absence of a structural refinement that provides atomic coordinates, we have used FEFF phase shift and amplitude parameters for AUT to fit our ANK data. All of the features described for AUT are present in the ANK spectra, although with a higher signal-to-noise ratio. A two-shell (O_{ax} and O_{eq}) simulation of ANK data is very similar to the one for AUT in its ability to fit spectral features, but the fit's shortcomings are more apparent for ANK due to the higher quality data. As with AUT, we must attribute unfit features in the ANK spectrum to the possible combination of P, distant O, and MS.

Disorder Parameters

Agreement among adjusted σ^2 values for similar backscattering shells among the eight model compounds is good; trends within each shell are consistent with expectation. Values of σ^2 for the U-O_{ax} bond lie between 0.0011 and 0.0037 $Å^2$. The larger σ^2 values are found for those compounds (AUT, ANK) in which the relevant static disorder (difference between the two U-O_{ax} bond lengths) is larger. For compounds in which the

equatorial O atoms were fit as a single shell (all except uranophane), U-O_{eq} σ^2 values lie between 0.0030 and 0.0120 Å^2. While this range is relatively large, the lower values are for AUT and ANK, for which lower σ^2 values would be expected because they have only 4 O_{eq} atoms, all located the same distance from U. Without AUT and ANK, the lower limit for U-O_{eq} σ^2 values increases to 0.0081 Å^2. The new low σ^2 values belong to UNL and RBUNS, in which 5 and 6 O_{eq} atoms, respectively, are equidistant from U. More static disorder is characteristic of the O_{eq} shell of the other model compounds, hence the higher σ^2 values. For uranophane, splitting the O_{eq} shell into two subshells results in σ^2 values of approximately 0.002 Å^2 for each subshell. For the two compounds in which a U backscattering shell was fit (RUTH and URAN), σ^2 values for 2 U neighbors were consistent at 0.0055 Å^2.

While σ^2 values have been derived by fitting EXAFS spectra for similar systems by other authors, these have generally been determined relative to a non-zero reference σ^2, whereas we have removed the σ^2 component from our reference phase shift and amplitude parameters. They are therefore not suitable for comparison. Disorder parameters can be estimated using different formulae (Scott, 1984), but the theory is not well developed, especially for complicated systems such as uranyl.

Comparison of our EXAFS-derived σ^2 values with mean-square atomic displacements determined by XRD would be meaningless for several reasons. The EXAFS value represents a mean-square deviation of a bond from the average bond length, whereas XRD mean-square displacements (MSDs) typically measure radial displacement of individual atoms. Depending upon whether the direction of maximum atomic displacement coincides with the bond axis of interest, MSDs could be expected to under or overestimate EXAFS σ^2 values. Whereas an EXAFS σ^2 value for U-O_{eq} bonds fit as a single shell accounts for all of their static disorder, XRD MSD values that are measured individually for each O_{eq} atom (as is often the case) do not incorporate the static disorder arising from the variable U-O_{eq} bond lengths. On this basis alone, XRD MSD values would be expected to underestimate EXAFS σ^2 values. Finally, several authors report XRD MSD values for O_{ax} that are larger than those for O_{eq} (Taylor and Mueller, 1965; Anderson et al., 1980; Templeton et al., 1985; Viswanathan and Harneit, 1986). In contrast, there is significant evidence for the low disorder associated with U-O_{ax} bonds relative to U-O_{eq} bonds in the form of XRD data. The shorter length of the O_{ax} bond suggests that it is a stronger bond and therefore undergoes less vibrational disorder, in accordance with bond length-bond strength arguments put forth originally by Zachariasen (1954). In addition, U-O_{ax} bond lengths tend to be more uniform than U-O_{eq} bond lengths, hence the lower static disorder associated with U-O_{ax}. These observations have been confirmed by the relative sizes of

our $U\text{-}O_{ax}$ and $U\text{-}O_{eq}$ σ^2 values. We do not understand the origin of this last discrepancy and cannot reconcile XRD MSD values with our and others' findings.

Uranium XANES

Focusing on relative rather than absolute energies, there appears to be a correlation between the positions of near edge features in the XAS data and bond lengths determined from EXAFS spectra analysis, as discussed in Petiau et al. (1986). These XANES features are present in all experimental spectra collected in this study. Following the approximation

$$\Delta \cdot R^2 \approx \text{constant}, \tag{5}$$

in which Δ is the energy difference between positions of a XANES feature and the white line and R is the interatomic distance of the atom pair to which the XANES feature corresponds, one would expect to observe a decrease in R with increasing Δ, or vice versa. Interatomic distances were selected for comparison based on the correlations drawn by Petiau et al., namely Δ_2 with $R(U\text{-}O_{eq})$ and Δ_1 with $R(U\text{-}O_{ax})$ (Table 3).

Comparing Δ_2 with $R(U\text{-}O_{eq})$, the approximation clearly applies. As Δ_2 increases from 33 to 42 eV, $R(U\text{-}O_{eq})$ decreases from 2.5 Å > $R(U\text{-}O_{eq})$ > 2.45 Å (UNS, RBUNS, RUTH) to 2.45 Å > $R(U\text{-}O_{eq})$ > 2.35 Å (UNL, URAC) to 2.35 Å > $R(U\text{-}O_{eq})$ > 2.25 Å (AUT, ANK). It is difficult to fit URAN into the trend because its equatorial ligands clearly split into two shells, but in keeping with the dominance of the lower R shell (stronger scattering at shorter distance), its XANES Δ_2 appears to be consistent with the trend. Although Δ_1 and $R(U\text{-}O_{ax})$ do not violate the correlation expressed in Equation 5, Δ_1 values are too small to substantiate it.

Consistency in edge position, within experimental limitations, confirms that all model compounds are in the same oxidation state (VI). The presence of XANES A and B features further indicates the uranyl moiety in all of the samples. Changes in Δ_2 with $R(U\text{-}O_{eq})$ are consistent with theory.

COMPOUND	White Line (eV)	A (eV)	Δ_1[1] (eV)	$R_{U\text{-}Oax}$ (Å)	B (eV)	Δ_2[2] (eV)	$R_{U\text{-}Oeq}$ (Å)
Uranyl nitrate hexahydrate	17173	17187	14	1.75	17205	32	2.46
Rubidium uranyl nitrate	17171	17184	13	1.76	17205	34	2.49
Rutherfordine	17171	17184	13	1.76	17207	36	2.45
Unhydrolyzed monomeric aqueous uranyl ion	17171	17181	10	1.76	17208	37	2.41
Uranyl (di)acetate	17171	17182	11	1.76	17209	38	2.39
Uranophane	17172	17182	11	1.82	17212	40	2.32, 2.50[3]
Meta-autunite	17172	17184	12	1.77	17214	42	2.29
Meta-ankoleite	17172	17183	11	1.78	17214	42	2.29

[1]Energy difference between peak of white line (first derivative = 0) and maximum slope of A feature (first derivative = local maximum)
[2]Energy difference between peak of white line (first derivative = 0) and peak of B feature (first derivative = 0)
[3]Equatorial oxygens are best fit in uranophane using two separate shells.

Table 3. Comparison of relative energy positions of model compound XANES features with interatomic distances. Feature designations correspond to Figure 2.

CONCLUSIONS

Through qualitative comparison of theoretical and experimental EXAFS spectra and use of theoretical parameters to fit experimental spectra, we have confirmed the ability of FEFF 5 to accurately calculate single-scattering phase shift and amplitude parameters for U L_{III}-edge EXAFS spectra. Although no experimental FT features have been explicitly fit using multiple-scattering (MS) path parameters, FEFF demonstrates the significance of MS paths in some uranyl structures and its ability to estimate their relative significance.

We have learned a significant amount about the capabilities and limitations of EXAFS analysis with respect to U structure determination. Contributions from O_{ax} and O_{eq} dominate the EXAFS spectrum. Although their FTs are qualitatively similar at low R, different uranyl compounds can produce very different EXAFS oscillations depending on the number and arrangement of O_{eq} atoms. For the FT range used for all of the model compounds (3 to 14 $Å^{-1}$), the equatorial oxygen shell splits into two distinct FT peaks only for uranophane, which is the only model compound in which the difference between longest and shortest $R_{U\text{-}Oeq}$ is > 0.15 Å, the threshold for discerning two peaks for Δk = 11 $Å^{-1}$, according to Equation 4. A broader FT range would be expected to allow the O_{eq} contribution in uranyl nitrate hexahydrate ($\Delta R_{U\text{-}Oeq}$ = 0.15 Å) to separate into two distinct peaks. Thus we can use Equation 4 in conjunction with the observation of shell splitting for a given k range to provide supplemental interatomic distance information.

More distant atoms are discernible in the spectra in one of two ways: through additional oscillations superimposed on the O_{ax} + O_{eq} EXAFS spectrum (or in the FT) or through unfit amplitude in an oscillation partially fit by O_{ax} + O_{eq}. In these ways we have observed contributions to uranyl spectra by N (2.9 Å), C (2.9 Å), U (3.9 and 4.3 Å), and distant O (4.2 Å) atoms. The distant O contribution is the most surprising, but its significance can be explained by the coincidence at a single distance from the central U atoms of multiple O atoms that are axial to other U atoms. We have not succeeded in explicitly fitting contributions from Si or P (3.1 to 3.8 Å). Because the former was in a highly (static) disordered site whereas the latter was not, our inability to fit them was not simply the result of large amounts of disorder. For both Si and P, features were present in the FT in the general vicinity expected based on known interatomic distances, but the overlap of several single and multiple-scattering path lengths resulted in our inability to explicitly fit the features. This overlap is a recurring complication in attempting to fit U EXAFS data beyond the axial O shell. From this we conclude that scattering from Si and P at distances greater than 3.0 Å in uranyl structures is difficult, though not necessarily impossible (depending on the structure), to detect using EXAFS spectroscopy.

Because unfit amplitude in an EXAFS oscillation may be indicative of an additional shell of neighbors or low disorder relative to reference compounds, rather than simply a greater number of the neighbors that are already accounted for, it is important to be able to set limits for N, R, and σ^2 values. In part, limits can be based on structural chemistry of the element of interest, e.g., U(VI) virtually always has exactly two O_{ax} neighbors. The values of N and σ^2 are highly correlated, however, which necessitates that σ^2 must also be constrained. Our model compound study has shown that this can be done. For each similar backscattering shell, values of σ^2 resulting from least-squares fits of eight model compounds fall into narrow ranges. In fitting EXAFS spectra for unknowns, these ranges can be used to constrain parameters in the fit.

CHAPTER THREE
Uranium(VI) Sorption on Kaolinite

BACKGROUND

Rocky Flats Plant

Uranium contamination of surface pond waters at the Rocky Flats Plant (RFP) in northern Colorado is one of the environmental legacies of uranium processing in the United States. While RFP was operational, radionuclides (predominantly ^{238}U, ^{239}Pu, and ^{241}Am) were released to the air as a result of uranium processing (Triay, 1992). Over time, part of the resulting airborne contaminant plume settled to the ground. Impoundments were constructed on the site to prevent the uncontrolled release of these contaminants to downstream water supplies by collecting storm water runoff, treated sanitary effluent (B-series ponds), and ground water return flows, each of which might have contacted the contaminated ground surface. The ponds now contain ^{238}U, ^{239}Pu, and ^{241}Am in concentrations of 10^{-7} to 10^{-5} mol·m^{-3}. Aqueous Pu(VI) is believed to be in colloidal form. Aqueous U(VI) is expected to be dissolved. We do not know what form aqueous Am adopts in the ponds.

The RFP pond waters constitute a hazardous waste stream by virtue of the presence of radionuclides at levels above those determined to be suitable for public consumption. The waters cannot be discharged to a municipal water treatment plant because the radionuclides would either remain in the aqueous phase or partition with other waste constituents, both of which would result in further dispersal of the radionuclides. Consequently, further treatment of pond waters prior to discharge to a public facility is required.

Sorption of uranium and other radionuclides on a high surface area solid followed by flocculation and removal of the solid has been proposed to remove radionuclides from pond waters (Triay, 1992). Kaolinite and other clay minerals are theoretically good candidates for the sorbing solid owing to their relatively high surface areas (Van Olphen and Fripiat, 1979), negative surface charge and hence propensity for surface interaction with cations, relative abundance, and low cost. For the smectite family of clay minerals, possibility for interlayer sorption provides an additional mechanism of uptake. In preliminary experiments, researchers at Los Alamos National Laboratory (LANL) have shown that Pu(IV) and Pu(VI) are removed to varying degrees from RFP pond waters by Ca-montmorillonite, halloysite, and kaolinite under limited experimental conditions (e.g., pH was not controlled) (Triay, 1992). Kaolinite showed the most promise as a Pu sorbent in the absence of flocculants. This was surprising because montmorillonite would be

expected to have a higher sorption capacity on the sole basis of structure. They have also demonstrated U(VI) removal from deionized water solutions by montmorillonite and other clay minerals.

These results confirm the ability of clay minerals to remove different amounts of select radionuclides from deionized and RFP pond water solutions. The resulting U-clay complexes have not been characterized, however. We therefore know little about the stability of the complexes as a function of changing solution conditions (e.g. flocculant addition, dewatering) and sorbent identity. Furthermore, without knowledge of the composition and structure of the complexes, we are unable to write reactions that describe complex formation, meaning that no predictive capability has yet resulted from this study.

In the present study we make an exploratory attempt to characterize U sorption complexes on kaolinite as a function of key solution parameters. Uranium has been selected from among U, Pu, and Am because in addition to the need to remove U from the pond waters, U may be expected to serve as an analog for Pu(VI) (Weigel, 1986), and it is the focus of a plethora of other contaminated sites. Because of its relatively high uptake of Pu from solution, kaolinite has been selected as the mineral sorbent for study. A kaolinite reference standard (KGa-2) is used owing to its relative lack of impurities and because it has previously been well characterized (Van Olphen and Fripiat, 1979). Uranium sorption studies reported in the literature suggest that pH and dissolved carbonate concentration are the dominant solution variables in controlling uptake by clay minerals (Muto et al., 1965; Giblin, 1980; Sekine et al., 1991), thus we have varied these parameters in the vicinity of values that maximize U uptake. We have also prepared samples using both Pond C and deionized water to determine whether any of the Pond C water constituents interfere with U uptake or alter the resulting sorption complex. Finally, we use X-ray Absorption Spectroscopy (XAS) as a direct molecular probe to characterize sorbed uranium species, specifically to confirm that uranium is associated with the solid sorbent and to establish the mode of sorption, e.g. inner- vs. outer-sphere, mono- vs. multidentate, mono- vs. polynuclear.

X-ray Absorption Spectroscopy

Technique Capabilities for Sorption Studies[1]

X-ray Absorption Spectroscopy (XAS) has proven to be particularly valuable to the study of sorption at the mineral-water interface for several reasons: (1) its absorber specificity allows study of a selected element in the presence of many elements; (2) backscattering atoms that differ in atomic number (Z) by more than 3 from that of the

[1]Fundamental aspects of the technique were described in Chapter Two.

absorber atom can be distinguished and roughly identified (Brown et al., 1988), and their number can be approximated; (3) interatomic distances can be determined very accurately (±0.02 Å for most backscattering atoms); (4) it is a non-vacuum technique (for absorber Z > 20) usable at ambient temperatures and is therefore applicable to solutions and suspensions as well as solids; and (5) it is sensitive to relatively low concentrations of the absorbing atom (Hayes et al., 1987; Chisholm-Brause et al., 1990a,b; Chisholm-Brause, 1991; Combes et al., 1992; O'Day, 1992).

In the best situations, XAS can verify that sorption has occurred and identify the mode of sorption and structure of the sorption complex (e.g. Combes, 1988; Manceau et al., 1992; O'Day, 1992). To verify sorption, one or more atoms unique to the sorbent must be identified in the coordination environment around the sorbed atom. The number of sorbent atoms should be small enough that absorption or diffusion into the solid can be discounted. Combining interatomic distance information resulting from EXAFS with a knowledge of the structure of the solid sorbent, one can identify the mode of sorption (inner- vs. outer-sphere, mono- vs. multidentate) and in some cases what type of solid site is occupied by the sorbed atom. Number, distance, and identity of neighboring atoms provide information regarding the structure of the sorption complex. Polymerization may be indicated by detection of one or more sorbate ions in the coordination environment of the adion.

Limitations of XAS are not insignificant. Because XAS samples all absorber atoms in the bulk sample, the resulting information represents a sum of all atomic environments in which the absorbing atom is present. Numerical interpretation of EXAFS data relies on theoretical or experimental model compounds, thus the accuracy of resulting numbers is necessarily a function of whether or not a single structure predominates in the sample and how well the model compound represents that unknown structure. Since XAS is insensitive to low Z backscattering atoms under ambient conditions, one cannot use it to discern the arrangement of water molecules at the solid-water interface, except as they can be traced through their oxygen atoms in the near vicinity of an absorber atom. Neither can one use XAS to detect deprotonation or hydrolysis of the sorption site of the adion, inasmuch as the oxygen atoms in water, hydroxide ion or hydroxyl groups, and oxide ions cannot be distinguished because protons scatter extremely weakly.

Particular to the study of uranium sorption at the kaolinite-water interface, pure kaolinite lacks strongly scattering atoms, thus direct verification of sorption may not be possible. In Chapter Two we saw that it is not always possible to identify Si in the coordination environment of U ($R_{U\text{-}Si}$ = 3.1 to 3.8 Å). If we succeed in detecting them at

all, one cannot directly distinguish between Al and Si backscatterers in kaolinite[2], thus potentially precluding determination of the type of solid site occupied by the sorbed U atom. Moreover, because U atoms are such strong scatterers, if more than one U atom is present in the sorption complex, the additional U atoms might contribute to the EXAFS spectrum with such amplitude that they overwhelm the contributions from significantly lighter atoms, including O, Si, and Al. In the absence of evidence for the presence of sorbent atoms among the neighbors of the adion, comparison of XAS data for the solution (i.e. without sorbent) and the solid after equilibration with the solution can reveal differences in atomic environment around U that are consistent with, but not uniquely indicative of, sorption. Despite these limitations, careful sample preparation can result in samples optimized to provide information regarding sorption mode and complex structure.

Sample Preparation Strategy

Although XAS is not inherently surface-sensitive, it can be optimized for surface sensitivity by tailoring sample preparation, as has been done in this and earlier studies by this group (Brown and Parks, 1989). Successful application of XAS to the study of species adsorbed from aqueous solution onto a solid surface requires the following: (1) More than 80% of the mass of the absorber element in the XAS sample must be in the adsorbed phase. Because a small quantity of supernatant is required in the sample to prevent drying, this implies that uptake of the absorber element from solution must be nearly complete, that most of the supernatant must be removed from the sample, and that the concentration of absorber element present in the solid phase bulk structure should be negligible. (2) The concentration of the sorbed element in the XAS sample must be sufficient to produce measurable x-ray fluorescence. For dilute species, this may be achieved by the use of high surface area solids, e.g. clay minerals. (3) To minimize noise produced by matrix (solid and solution) fluorescence, one should select a relatively high Z sorbate and a significantly lower Z sorbent, which makes XAS particularly well-suited to the study of transition metal and higher Z cations on aluminosilicates and other geologically significant oxides. (4) To distinguish between sorption (backscattering from atoms in the solid) and polymer formation (backscattering from other sorbate ions present in the sorption complex), the atomic numbers of the sorbate (x-ray absorber) and sorbent atoms should differ by at least three.

---

[2]Because Al is octahedrally coordinated and Si is tetrahedrally coordinated, one might indirectly distinguish between the two based on bond lengths.

Kaolinite Sorption Sites

Through the arrangement of atoms shared with the adion, knowledge of sorbent crystal structure can help to decipher the structure of an inner-sphere sorption complex and identify the site(s) on the solid where the inner-sphere complex is bound. Because sorbent atoms are not shared with outer-sphere complexes, sorbent structure places fewer constraints on the structures of these complexes.

Kaolinite is a common clay mineral found in a variety of geologic settings, including soil, sedimentary, and hydrothermal environments. In its pure form, kaolinite is composed of a layer of Si atoms tetrahedrally coordinated by O atoms, bonded to a layer of Al atoms octahedrally coordinated by oxygen and hydroxyl groups (Fig. 1) (Grim, 1968). These 1:1 layer packets repeat in the direction perpendicular to the layer planes. Hydroxyl groups line the outside of the Al side (aluminol surface) of each packet, whereas the outside of the Si layer (siloxane surface) is composed of a network of ditrigonal cavities, each of which consists of six corner-shared Si tetrahedra. One Al-bound hydroxyl group is located between the two layers at the center of each ditrigonal cavity. Hydroxyl groups bound to Al atoms, some of which bridge between two Al atoms and some of which are only bound to one, protrude into the interlayer region. The layer packets are held together by weak hydrogen bonds between these interlayer hydroxyl groups and siloxane O atoms.

Cation sorption has been proposed to occur at several sites on the ideal crystal structure of kaolinite (Sposito, 1984; O'Day, 1992). Structural O and OH are expected to participate in sorption of cations, and can be classified in the following manner: (1) surface OH, which bridge between two Al atoms on the aluminol surface; (2) surface O, which bridge between two Si atoms on the siloxane surface; (3) inner OH, singly bonded to an Al atom and located between aluminol and siloxane surfaces; and (4) inner O, which bridge between an Al and a Si. Inner O and OH are exposed along the edges of kaolinite particles. In the presence of water, proton exchange on exposed edge and (001) surface O and OH give rise to a pH-dependent (amphoteric) surface charge.

Imperfections in the crystal structure and impurities are common in natural kaolinites and can provide additional sorption sites. When permanent structural charge exists due to isomorphic substitution (typically Al^{3+} for Si^{4+}), the ditrigonal cavity on the siloxane surface functions as a soft Lewis base. Contamination of kaolinite by separate phase 2:1 phyllosilicate minerals, for which isomorphic substitution is more common, introduces additional charged sites.

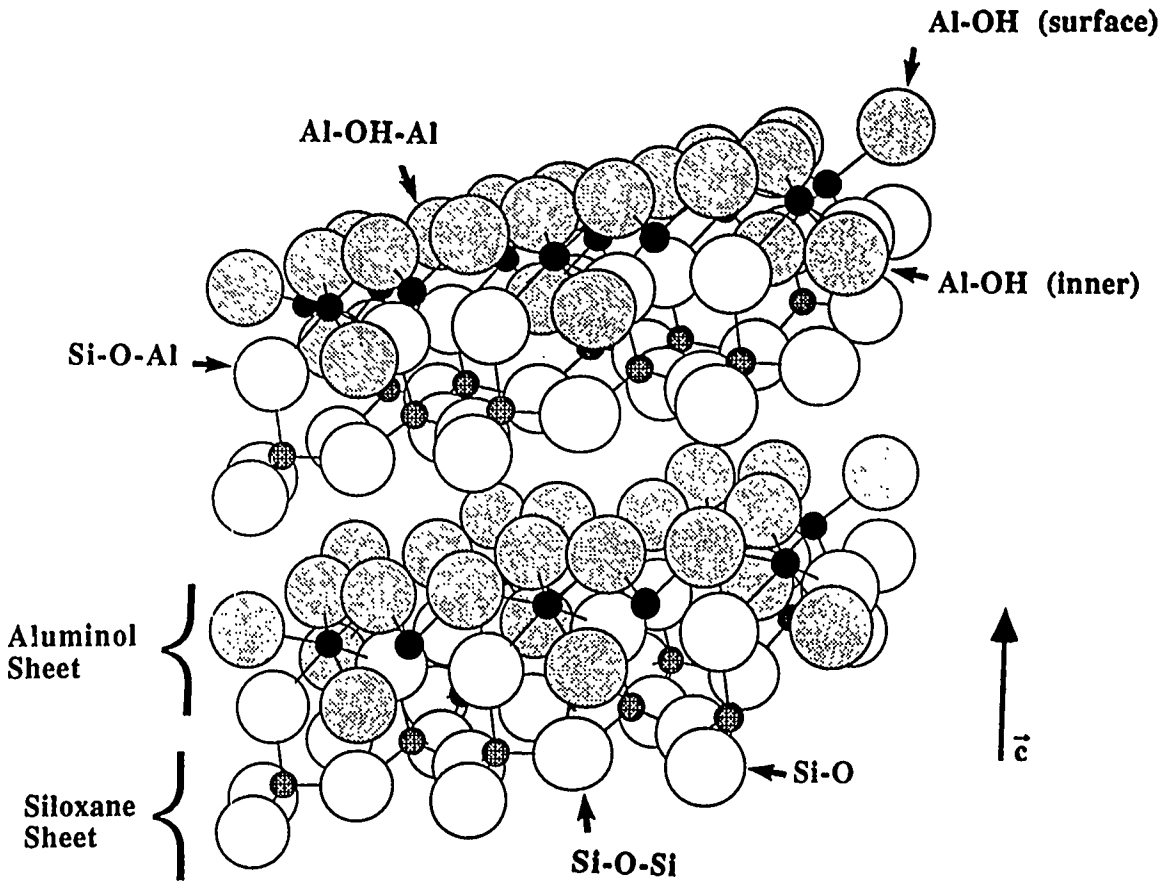

Figure 1. Kaolinite crystal structure showing the aluminol and siloxane 1:1 layers, and surface oxygen atoms exposed on faces that may act as reactive sorption sites. Atoms: Al, solid; Si, hatched; O, open; OH, shaded. (after O'Day, 1992)

Past Sorption Studies

Researchers have consistently assumed (Tripathi, 1984; Hsi and Langmuir, 1985) and demonstrated that the uranyl moiety is preserved upon sorption of U(VI) by a variety of metal oxide solids (Maya, 1982b; Ho and Miller, 1986; Combes, 1988; Chisholm-Brause et al., 1992; Dent et al., 1992; Manceau et al., 1992). The remainder of the structure of U(VI) sorption complexes and the mode of sorption have been subjects of conflicting speculation. In simple systems, aqueous carbonate concentration and solution pH have been shown to affect the extent of U(VI) uptake by solids. It is suspected that these parameters affect uptake by influencing aqueous U(VI) speciation. If this is the case, then aqueous carbonate concentration and pH can reasonably be expected to affect the structures of the resulting sorption complexes and possibly the mode of sorption.

Uranium(VI) uptake by kaolinite, montmorillonite and various amorphous and crystalline iron oxides decreases at solution pH > 6.5 or 7.0 in the presence of air or another gas mixture that has a higher CO_2 content (Muto et al., 1965; Giblin, 1980; Tripathi, 1984; Hsi and Langmuir, 1985; Ho and Miller, 1986; Sekine et al., 1991). This behavior has consistently been attributed to the presence of carbonate in solution because no decrease in uptake is observed in the absence of CO_2 (Tripathi, 1984; Hsi and Langmuir, 1985). The often unstated assumption that accompanies this explanation is that U that desorbs was bound as an inner-sphere sorption complex; carbonate destroys or precludes formation of this inner-sphere complex by strongly complexing U, effectively excluding the solid and other potential ligands from uranium's inner coordination shell. If U were bound as an outer-sphere complex, carbonate ligands could complex U without displacing solid ligands, and therefore would not likely effect its return to the solution phase through carbonate/surface ligand exchange, but it might result in desorption if bonding is largely coulombic. If carbonate is responsible for U desorption by ligand exchange, then one would expect to find U solution species at pH > 6.5 or 7.0 that contain carbonate group(s) in the inner coordination shell. This is consistent with behavior predicted by the Grenthe et al. (1992) thermodynamic database as shown in Figure 3 of Chapter 1, and has been spectroscopically observed (Basile et al., 1978; Madic et al., 1983; Morse et al., 1984). In fact, for a range of ΣU values above pH 8, the tricarbonato uranyl species $[1,0,3]^{4-}$ dominates, in which all equatorial ligand positions are occupied by carbonate O atoms.

The observation that carbonate "removes" U from the solid does not necessarily preclude carbonate from the U sorption complex, however. Uranium(VI) has four to six equatorial ligand positions. In cases in which U(VI) has been shown to be adsorbed to the solid in an inner-sphere fashion, two sorbent O atoms are bonded directly to the U adatom

(Combes, 1988; Manceau et al., 1992). If this is consistent for U on a variety of solids, two to four equatorial positions within the inner-sphere U complex are available for bonding to carbonate (mono- or bidentate) or other ligands.

Considerable disagreement surrounds the possible presence of carbonate in the U(VI) sorption complex. Ho and Miller (1986) observed two carbonate bands in the Fourier Transform infrared (FTIR) spectrum of a dried, U-loaded hematite sample prepared at solution pH values > 6.0. There was a substantial difference between this spectrum and that of hematite after contact with $NaHCO_3$ (no U), indicating that the bands were not attributable to carbonate groups bound directly to hematite. Although they did not demonstrate that the carbonate was bound directly to U, they inferred from their results that uranyl carbonate complexes were present on the hematite.

Using ^{14}C-labeling techniques, Jaffrezic-Renault et al. (1980) found carbonate associated with titanium oxide that had been equilibrated with a solution in which the $[1,0,3]^{4-}$ species dominated (pH 8 to 9). They found the ratio of carbonate retained (by the solid) to U retained equal to 2.0 regardless of ΣU, on which basis they concluded that the U(VI) sorption complex contained two carbonate groups, implying partial release of carbonate upon sorption. Their electrophoretic mobility measurements comparing TiO_2 with U-loaded TiO_2 demonstrate that U sorption from $[1,0,3]^{4-}$ solutions makes TiO_2 particles more negative, which is consistent with a dicarbonato sorption complex (due to the negative charge of $[1,0,2]^{2-}$).

Maya (1982b) offers two lines of evidence for release of carbonate upon U(VI) sorption by hydrous titania, zirconia, and silica gel. In his experiments, sorption was effected from solutions dominated by single uranyl species, namely $[1,0,3]^{4-}$, $[3,0,6]^{6-}$, or $[2,3,1]^{-}$. Solution pH increased during solid equilibration in most of the experiments, which is consistent with the release of carbonate. Acid digestion of solids after equilibration released only 0.05 to 0.1 moles CO_2 per mole of U, which Maya offers as evidence for the absence of carbonate from U(VI) sorption complexes. Yamashita et al. (1980) similarly measured the CO_2:U mole ratio sorbed by hydrous titanium (IV) oxide from $[1,0,3]^{4-}$ solutions and found that carbonate uptake remained constant as uranium uptake increased. They interpreted this to suggest that carbonate is not taken up by the sorbent during U sorption, therefore it is not present in the sorption complex. The actual uptake figures suggest that at least one mole of carbonate is sorbed for each mole of U sorbed at low uptake (0.005 mmol U (g solid)$^{-1}$). The ratio decreases to 0.2 at 0.03 mmol U (g solid)$^{-1}$. These two observations are consistent with at least two interpretations: either carbonate sorbs independently of U and U sorbs as carbonate-free complexes or U sorbs in two modes, one of which includes carbonate.

Results of studies discussed in the preceding three paragraphs suggest that carbonate is probably released when U is sorbed by oxide minerals from solutions in which the $[1,0,3]^{4-}$ complex dominates. The importance of this is in the implication that a fully occupied U equatorial shell must be vacated in order for sorption to occur, thus U sorbs as an inner-sphere complex at high pH in carbonate solutions. The issue of carbonate retention upon sorption of U from solutions dominated by complexes in which the equatorial shell is not fully occupied by carbonato ligands remains unresolved, however. None of the studies mentioned here provide direct *in situ* evidence of carbonate's presence or absence in the sorption complex. Apparent differences in results may be due to a combination of differences in solution conditions, including ΣU, aqueous carbonate concentration, pH, and ionic strength, but they are not so simple as carbonate being present on solids equilibrated at higher carbonate concentration and absent from solids equilibrated at lower concentration. Nonetheless, the role of carbonate in the sorption/desorption of U by metal oxide sorbents remains of critical interest because of the potential control over sorption/desorption equilibria that it might offer. Other dissolved anions might be expected to act similarly to carbonate with respect to U sorption by solids.

The mode of U sorption by solids, i.e. inner- vs. outer-sphere, might be expected to depend in part on the composition and structure of the solid. Combes (1988) and Manceau et al. (1992) have used XAS to demonstrate that U(VI) is bound to hydrous iron oxides in a bidentate, inner-sphere fashion at pH 5 to 6. In spectra of the sorption samples, they were able to identify contributions from Fe neighbors located at distances that would only be possible if U were bound as an inner-sphere complex. The U-Fe distances place constraints on the geometry of bonding that allow determination of the U complex location on the iron oxide surface, assuming an ideal structure for the iron oxides. On the other hand, neither Chisholm-Brause et al. (1992) nor Dent et al. (1992) saw spectral contributions from Si or Al using the same technique to study U sorption by montmorillonite (both) and silica (Dent).

Spectral contribution from Si and Al in the examples cited could be lacking for at least two reasons. Uranium may be sorbed by montmorillonite and silica as an outer-sphere complex, and therefore Si and Al would be too distant from U to be "seen" using XAS. Tsunashima et al. (1981) have measured maximum U uptake values for a Ca-montmorillonite at pH 4 that correspond to the cation exchange capacity (CEC) of that montmorillonite. Furthermore, the amount of U sorbed was equal to the amount of Ca^{2+} released. One can infer from these measurements that U is taken up by montmorillonite in an exchange process; ion exchange in clay minerals is typically thought to involve outer-sphere complexes (Sposito, 1984). Studies of U sorption by silica have not apparently

probed the ion exchange behavior of the system (Stanton and Maatman, 1963; Maya, 1982b; Lieser et al., 1992). Another possible explanation for the absence of Si and Al from the spectra is their weak scattering cross sections, as has been discussed, in which case U could be bound as an inner-sphere complex. We therefore cannot overlook the possibility of more than one type of U sorption complex on any mineral. In fact, the findings of Chisholm-Brause et al. (1992) and Morris et al. (1994) are consistent with the presence of more than one sorption site for U on montmorillonite. In separate experiments, Schindler et al. (1987) measured extent of Cu(II), Cd(II), and Pb(II) uptake by kaolinite as a function of pH at three different ionic strength values (10, 10^2, and 10^3 mol·m^{-3} $NaClO_4$). At low pH, they found much lower uptake from high ionic strength solutions, from which they inferred that competition with Na^+ for ion exchange sites (therefore outer-sphere complexation since Na^+ sorption is known to be weak) dominated sorption behavior at low pH. At high pH (near the top of the uptake vs. pH curve), uptake behavior varied much less with ionic strength, on which basis they proposed a second, amphoteric sorption site at which inner-sphere sorption of metal cations dominates high pH sorption behavior. Sekine et al. (1991) observed a similar ionic strength effect for U sorbed by kaolinite.

Solution pH modulates the extent of sorption in a variety of ways. In the absence of carbonate, the extent of protonation of sorption sites, and hence surface charge, and the distribution of U among hydroxo complexes are both pH-sensitive. Through surface charge and U speciation, pH affects the relative activities of the reactants involved in sorption, and thus must affect the composition of the sorption complex and the extent of sorption. Carbonate is a strong U-complexing ligand that may participate in sorption, and is the conjugate of a weak acid. Changes in solution pH will cause changes in the relative activities of carbonate species and in the distribution of U among hydroxo and carbonato complexes, thus again changing the relative activities of reactants in sorption processes and the composition of the sorption complex and the extent of sorption.

In most of the early U sorption research it was assumed that the dominant solution species sorbed to the solid relatively unchanged (Ho and Doern, 1985; Ho and Miller, 1986). This is particularly true of studies that use geochemical models such as that of Davis et al. (1978) to interpret batch sorption results in terms of complexation reactions (Hsi and Langmuir, 1985). It was early suspected that complexes in the vicinity of the solid-water interface might have different thermodynamic formation constants than in bulk solution. Specifically, formation of polynuclear sorption complexes might be expected under circumstances in which they do not form in bulk solution (James and Healy, 1972; Dillard and Koppelman, 1982). This has been observed in a variety of systems, both in solids dried after they have been equilibrated with aqueous solutions of the sorbing cation

(Co(II) on goethite - Schenck et al., 1983; Cu(II) on gibbsite - McBride et al., 1984; Mn(II) on boehmite - Bleam and McBride, 1985; U(VI) on zeolites - Bartlett and Cooney, 1989) and *in situ* (Co(II) on γ-Al_2O_3 - Chisholm-Brause, 1991; Co(II) on kaolinite - O'Day, 1992). Of the studies employing *in situ* methods to U sorption samples, none have yet observed sorbed polymeric species (Combes, 1988; Chisholm-Brause et al., 1992; Dent et al., 1992; Manceau et al., 1992; Morris et al., 1994).

Because the information resulting from studies of U sorption by kaolinite is limited, we have addressed a variety of solid sorbents in this section with the objective of inferring the composition and structure of U sorption complex(es) and their mode of bonding to kaolinite, bearing structural differences in mind. Although it has not been observed for kaolinite, we can reasonably expect the U-kaolinite sorption complex to contain the uranyl moiety, as it has not been absent from any other U(VI) sorption complex. If this is bonded in an inner-sphere mode by sharing one or two ligands with the surface, then the complex may also contain hydroxo and carbonato groups in equatorial positions. We cannot predict whether carbonate will be present in the sorption complex, but by preparing samples in the presence and absence of CO_2 at pH > 7.0, we hope to detect structural differences in sorption complexes suggestive of carbonate's presence and absence. Based on the ideal structure of kaolinite, the knowledge that U sorbs as an inner-sphere complex to some solids, and analogy with Cu(II), Cd(II), and Pb(II) (Schindler et al., 1987), we might expect U sorption by kaolinite to be dominated by inner-sphere complexes under pH conditions intended for these experiments (6.0 to 8.0). As kaolinite is not a swelling clay and is less prone to isomorphic substitution than smectites, outer-sphere complexation of U by kaolinite is expected to be much less significant than inner-sphere sorption. Finally, we currently have a limited basis for predicting whether sorbed species will be mono- or polynuclear under conditions of our experiments. Rather, we will attempt to determine the extent to which U sorption behavior mimics U solution behavior, in essence, the extent to which the solid plays a role in the structure of the U sorption complex. This could be more thoroughly examined by a comparative study of U sorption by a variety of solids, but our work on kaolinite may provide a starting point for such a study.

Model Compound Selection

To interpret XAS data quantitatively and establish limitations of the technique for the U absorber environment, crystalline and solution model compounds were selected to reflect our expectations regarding the structural environment of uranium at the kaolinite-water interface. Specifically, the complex should contain a uranyl group and be surrounded by 4 to 6 oxygen atoms in the equatorial plane. Reflecting the possibility that

the non-sorbing ligands would be carbonate group(s) or that we might observe a carbonate solution complex, one of the model compounds was a uranyl carbonate. Reflecting the possibility that the sorbed species would be similar to those found in solution, $UO_2^{2+}{\cdot}5H_2O$ (aq) was another model structure. A uranyl silicate mineral and two uranyl phosphate minerals were selected to represent different structural environments that an inner-sphere sorption complex on kaolinite might adopt. Using XAS, Si and P are indistinguishable because their atomic numbers differ by one; because both are typically found in tetrahedral sites surrounded by oxygen, uranyl phosphate structures may be considered as possible analogs for uranyl silicate structures. Finally, uranophane (the silicate) and rutherfordine (the carbonate) could also provide representative environments in which U atoms are in the short- to intermediate-range coordination environment of uranium, i.e., multinuclear complexes.

EXPERIMENTAL

All sorption samples described in this study were prepared by members of the Triay group at Los Alamos National Laboratory (LANL). They were responsible for materials selection and analysis of solutions for U content.

Materials

Kaolinite

The kaolinite used in this study is KGa-2, a poorly crystallized kaolinite standard from the Georgia clay repository. An XRD powder spectrum of KGa-2 was collected to confirm its identity. The KGa-2 XRD spectrum, overlain by the spectrum of another kaolinite, is included in Appendix 2. Agreement of peak location and intensity between the two spectra is good, especially considering that they represent two different kaolinites. In addition, we looked at a sample of KGa-2 using a field emission scanning electron microscope (FE-SEM) to identify particle shape and approximate size. Clay particles range in diameter from 5 to 10 microns and their shapes are irregular. Physical and chemical properties of KGa-2 are reported in Table 1.

Uranium(VI) Stock Solutions

U_3O_8 (NBS 950b) was used in preparation of UK1, UK2, UK3, and UK4. NIST uranium standard solution (10,000 ppm U in 5% HNO_3) was used in preparation of UK5 - UK12. All other reagents, including sodium nitrate, nitric acid, and sodium hydroxide,

Property	KGa-2
Weight % oxides	
SiO_2	43.9
Al_2O_3	38.5
TiO_2	2.08
Fe_2O_3	0.98
FeO	0.15
MnO	n.d.[1]
MgO	0.03
CaO	n.d.
Na_2O	<0.005
K_2O	0.065
P_2O_5	0.045
S	0.02
Cation Exchange Capacity (CEC)	3.3 meq·100g^{-1}
N_2 BET Surface Area	23.50 ± 0.06 m^2·g^{-1}

Table 1. Physical and chemical properties of KGa-2 (after Van Olphen and Fripiat, 1979).

Batch I.D.	U	Al	Ca	Li	Mg	Na	Si	Cl	SO_4	NO_3	pH
#1	1.66e-03	0	49	0	13	130	15	40	50	0	8.1
#2	6.18e-04				*not available*						

Table 2. Chemical constituents of RFP Pond C waters (except pH, in 10^3 mg·m^{-3} (ppm))

were reagent grade. All water used in the preparation of sorption samples, unless otherwise specified, was singly deionized.

All water used in preparation of "Pond C" sorption samples originates from detention pond C-2 on the Rocky Flats Plant (RFP) site. Pond C water used in this study was collected on two different dates from the same location and depth in the pond. Chemical characterization of each collection of RFP Pond C water is presented in Table 2. Pond C water (#1) was used in the preparation of June 1992 sorption samples (UK1-UK4); Pond C water (#2) was used in the preparation of April 1993 sorption samples (UK5-UK12). All Pond C water was stored in a refrigerator; light exposure was not controlled.

Methods

XAS Sorption Sample Preparation

Preparation techniques and starting materials (Pond C water composition) differed significantly and on this basis the samples are divided into two groups: those for which XAS data was collected in June 1992 (UK1 - UK4) and those for which XAS data was collected in April 1993 (UK5 - UK12). For both groups of sorption samples, sorption was effected from solutions made from either Pond C water or deionized (DI) water. Protocols followed for both types of water were very similar. In the protocol description below, the appropriate water type can be substituted for the word water.

Relevant quantities and measurement results are presented in Table 3 for June 1992 and Table 4 for April 1993. With the exception of UK3, which was prepared with Ar-purged water under an inert atmosphere to exclude CO_2, all samples were exposed to laboratory air, hence to CO_2. During the course of their preparation, sorption samples contacted containers made of glass, Nalgene, Teflon, "heavy plastic" (probably HDPE), LDPE, polypropylene, Mylar, and Millipore filters.

<u>June 1992</u>

A stock solution of uranyl nitrate was prepared as follows: The designated quantity of U_3O_8 was dissolved in 5 ml HNO_3 and then heated to dryness. The residue was dissolved in water and brought to total volume to achieve the U concentration ($2 \cdot 10^{-2}$ $mol \cdot m^{-3}$) desired for sorption experiments. To make ionic strength in DI water samples equal to that in Pond C water samples (1.54 $mol \cdot m^{-3}$), the dried uranium residue was dissolved in an appropriate amount of concentrated HNO_3 before addition to the DI water. Prior to kaolinite addition, NaOH was added to the DI water samples to increase the pH to that of the Pond C water samples. Initial pH was measured at this point and aliquots of this

Sample ID	U_3O_8, mg	HNO_3 added, 10^{-6} m^3	Water used	Total Volume, 10^{-3} m^3	Initial pH	UO_2 conc. before KGa-2, $mol \cdot m^{-3}$	pH after filtering	UO_2 conc. after filtering, $mol \cdot m^{-3}$	Percent U uptake
UK1	28.30	0.0	Pond C	5.0	7.93	1.87 E-02	7.95	1.77 E-02	5.35
UK2	28.04	1.31	DI	5.0	7.99	1.90 E-02	6.25	1.30 E-02	31.58
UK3	28.98	1.31	DI/Ar-purged	5.0	8.15	2.08 E-02	7.50	0.147 E-02	92.93
UK4	2.92	0.13	DI	0.5	8.04	1.89 E-02	6.00	0.634 E-02	66.46

Table 3. June 1992 sorption sample preparation data

Sample ID	Water used	Initial pH	Nominal sorption pH	pH before KGa-2 addition	KGa-2 added, g	Adjusted pH after KGa-2 addition	pH after equil.	pH after centrif.
UK5	Pond C	7.37	6.0	6.07	2.522	5.97	6.14	6.77
UK6	DI	4.50	6.0	6.00	2.505	6.12	6.19	6.52
UK7	Pond C	7.48	6.5	6.65	2.515	6.51	6.65	7.29
UK8	DI	4.50	6.5	6.64	2.524	6.60	6.68	7.11
UK9	Pond C	7.36	7.0	7.17	2.505	7.12	7.18	7.8
UK10	DI	4.50	7.0	7.05	2.524	7.16	6.99	7.12
UK11	Pond C	7.50	7.5	7.56	2.526	7.55	7.67	8.15
UK12	DI	4.50	7.5	7.52	2.501	7.92	7.13	7.34

Table 4. April 1993 sorption sample preparation data

solution were taken for total initial uranium content analysis by Neutron Activation Analysis.

Kaolinite was added to each aliquot with mixing. Stirring of the resulting dispersion continued for 24 hours, after which the suspension was allowed to stand. After 2 hours of standing, the supernatant was decanted and centrifuged at 5000 rpm for one hour. Resulting centrifugates were filtered through a 0.45 μm Millipore filter. The pH of the filtered solutions was measured and aliquots of this solution were taken for total uranium content analysis by Neutron Activation Analysis. Uranium content data and calculated percent uptake values are included in Table 3. To make XAS samples, the solid centrifuge residue was loaded without drying into a 3 mm thick polyethylene holder with Mylar windows. Several milliliters of the filtered supernatant solution from preparation of UK2 were loaded into a Teflon holder with Mylar windows for XAS data collection.

April 1993

NIST uranium standard solution was added to 5000 ml of water with stirring to achieve the U concentration ($2 \cdot 10^{-2}$ mol·m^{-3}) desired for sorption experiments. Initial pH was measured at this time. To make ionic strength in DI water samples equal to that in Pond C water samples (4 mol·m^{-3}), the designated amount of sodium nitrate was added to DI water solutions. All solutions were shaken on an orbital shaker for 1 hour at 80 rpm, after which pH was adjusted using $2 \cdot 10^{3}$ mol·m^{-3} NaOH or $2 \cdot 10^{3}$ mol·m^{-3} HNO_3 to the nominal sorption pH value. The solution was shaken for 24 hours, after which pH was measured and adjusted to the designated sorption value if drift had occurred. Aliquots of this solution were taken for total initial uranium content analysis by inductively coupled plasma-mass spectroscopy (ICP-MS).

Kaolinite was added with mixing, and the pH was periodically adjusted over the following 24 hours to maintain the designated sorption value while stirring continued. Twenty-four hours after the kaolinite was added, approximately 2000 ml of the suspension was filtered through a 0.45 μm filter paper. The remaining suspension was centrifuged for 10 minutes at 12,000 rpm. After pouring off the centrifuged supernatant, clay residue was poured onto the filter paper. Samples of the centrifuged supernatant were taken for total U content analysis by ICP-MS. To make XAS samples, clay from the filter paper was loaded into a Teflon holder with Mylar windows. For all but the UK11 sample, a piece was cut from the center of the filter paper and loaded into the Teflon holder on the side to be placed most distant from the incoming x-ray beam for XAS data collection. The filter paper was included in the sample holder because it was suspected that the finest kaolinite grains, on which the highest per mass loadings of U should be found, were trapped on the filter

paper. Several milliliters of the filtered supernatant solutions from preparation of UK10 and UK12 were loaded into a Teflon holder with Mylar windows for XAS data collection.

Uptake results for April 1993 samples were intended to further explore the effect of Pond C water on sorption as well as the role of pH. Problems experienced during the ICP-MS analysis of April 1993 samples at LANL produced false results for all of the samples, the cause of which is unknown. Solution and supernatant samples were not kept to enable repetition of the analysis, nor would the results necessarily be applicable to XAS sample data given potential changes in solution composition with time. For this reason, no uptake data are available for the April run. Samples were used for XAS data collection, however, because the presence of uranium was verified by observation of x-ray absorption.

XAS Data Collection

Uranium L_{III}-edge XAS spectra were collected over the energy range ~17 - 18 keV at the Stanford Synchrotron Radiation Laboratory (SSRL) during dedicated beam conditions (~3 GeV and 40-90 mA), using high flux wiggler beam line IV-2 (18 kG wiggler field). The x-ray beam was unfocused on a Si(220) monochromator crystal, cut #2 (ϕ=90°). Sorption sample and supernatant solution spectra were collected in fluorescence mode with the sample oriented 45° to the incident beam. Fluorescence detection was accomplished with a 13-element Ge-array detector. Harmonic rejection was effected by 40-80% detuning of the incident beam. Three to sixteen scans were collected for each sample.

XAS Data Analysis

Data analysis up to but not including the least-squares fit was conducted as for the model compounds in Chapter Two, with the following differences. In PROCESS, polynomials of order +1 were fit to pre-edge spectra and subtracted. Reference phase shift and effective scattering amplitude parameters calculated in Chapter Two were used to fit sorption sample EXAFS data. For shells of backscattering atoms (axial O and U) that could be isolated in model compound experimental EXAFS data, empirical phase shift and amplitude parameters were extracted using a Gaussian window. These were alternately substituted for theoretical parameters to fit similar shells in sorption sample EXAFS data, in order to corroborate the N, R, and σ^2 values resulting from use of the FEFF parameters.

Unfiltered sorption data were fit without further refinement (e.g., deglitching)[3] using a multi-shell approach. In accordance with the findings of Chapter Two, the value of S_0^2 was fixed to 1.0 in all fits. The same value of ΔE_0 was assigned to each coordination shell. This value was allowed to adjust while remaining equal for all shells. The axial shell was fit by fixing N=2 and floating R and σ^2. Because the first neighbor equatorial shell in our sorption samples appears to split into two subshells (as in uranophane), several strategies were employed to keep the number of variables in the least-squares fit small enough to prevent the system from being indeterminate. Spectra for each sample were alternately fit assuming one and two equatorial oxygen shells. When assuming a single shell, N was fixed at 5, and R and σ^2 were allowed to vary from initial values of 2.4 Å and 0.01, respectively. When assuming 2 equatorial subshells, N and σ^2 values could not be varied simultaneously without underdefining the system, thus two fitting strategies were employed. In the first, both σ^2 values were fixed to 0.002 (borrowed from the uranophane fit), and both N and R values were varied. Using the second strategy, the sum of the two N values was fixed at 5 (average of expected values) and both R and σ^2 values were allowed to vary.

Fourier transform features ultimately attributed to Si/Al neighbors were isolated using a Gaussian window and fit in the absence of other spectral components. The amplitude envelope of the windowed EXAFS function was examined for the characteristic shape of Si and Al, which peaks around k = 8 $Å^{-1}$ when multiplied by k^3. The resulting N and σ^2 values for Si/Al were allowed to adjust in a multi-shell fit of the unfiltered spectra; R remained fixed at the value determined during the fit of filtered data. Unlike Si, U contributions could be fit without isolation because of their significant amplitude. For each U shell, N, R, and σ^2 were allowed to adjust in a multi-shell fit while other shell parameters were held fixed.

XANES features positions were measured and labeled as for model compounds in Chapter Two.

---

[3]Single-point deglitching of UK2, 5, 6, and 12 resulted in significant differences only for UK2. The poor quality of UK2 data are believed to be the source of the differences resulting from deglitching of UK2 data. The lack of change observed for UK5, 6, and 12 would suggest that deglitching beyond that which results from ratioing the data to I_0 is not necessary.

RESULTS

X-ray Absorption Spectroscopy - Qualitative Analysis

As was demonstrated in Chapter Two for model compounds, qualitative analysis of EXAFS spectra and their FTs provides the basis for selecting atom pair parameters to use in fitting the data. This is particularly true for samples of unknown structure, as is the case for our sorption samples.

Within the signal-to-noise limitations of the data, EXAFS spectra for sorption samples UK3, 5, 6, 7, 8, 10, and 12 are qualitatively similar to each other (Fig. 2 and Fig. 3). A single frequency dominates the EXAFS spectra, although there is more than one feature in each FT, suggesting that at least two frequencies contribute to each EXAFS spectrum. Visual comparison of these FTs with those of the model compounds suggests that the sorption sample FT peaks at 1.3 and 1.9 Å[4] are attributable to axial and first equatorial shell ligands, respectively. Further inspection of sorption FTs reveals that the equatorial contribution appears to break into two distinct shells (1.9 and 2.2 Å), as was found to occur for uranophane.

Features indicative of more distant backscatterers are present in FTs of UK3, 5, 6, 8, 10, and 12 spectra. A peak that is clearly significant above background is present at 3.0 Å in all of these spectra. Based on distance and known sample constituents, the most likely candidates for backscattering atoms that produce the 3.0 Å peak are Si or Al in the kaolinite structure, as Si is located 3.1 to 3.8 Å from U in uranyl silicate minerals, and it (or Al) might be expected to be found at a similar distance if U is sorbed as an inner-sphere complex by kaolinite. The peak is too distant for O_{eq}, nitrate-N, or carbonate-C, and too close for a nearest neighbor U atom.

A more distant FT peak is discernible above background at 3.8 Å in UK3, 10 and 12 spectra. This distance is typical of U neighbors. Furthermore, the prominence of this peak at relatively large distance suggests that the backscattering atom(s) must have a significant backscattering cross section. Of the atoms present in significant concentrations in these samples, this is uniquely true for U.

Spectra for UK2 and UK9 stand out as being qualitatively different from spectra for all other sorption samples, with the exception of the O_{ax} shell. To the extent that noise can be ignored, they are similar to each other. Noise is a significant factor in both spectra, however. Both show evidence in the low k region of their EXAFS spectra of the frequency that produces the 1.3 Å FT peak, attributable to axial oxygens. The second peak in both FTs (1.9 Å) is significantly larger than the dominant equatorial feature (1.9 Å) in

[4]In this and the following sections, FT peak positions are reported uncorrected for phase shift, which typically moves the peak to higher R than observed by 0.2 to 0.4 Å.

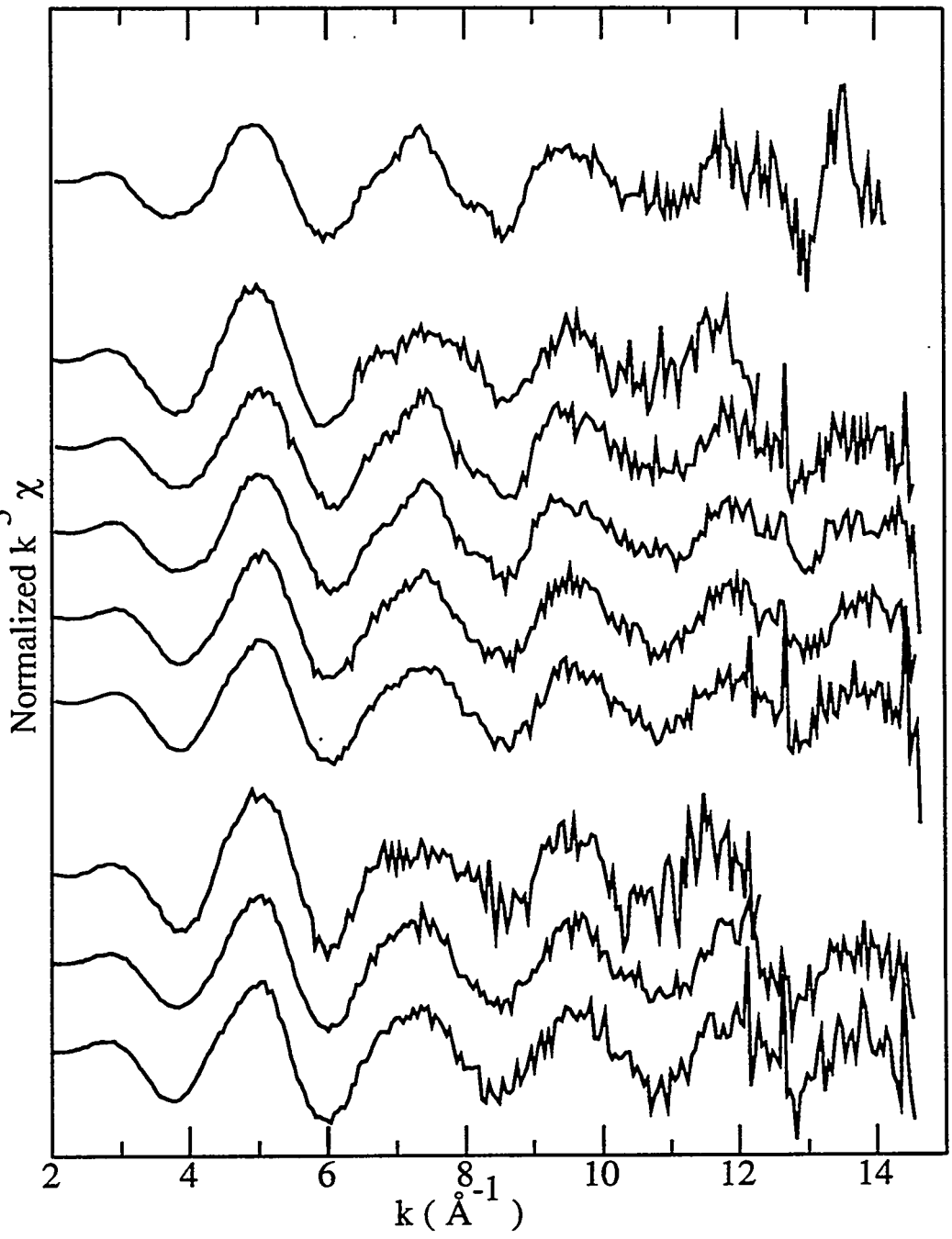

Figure 2. EXAFS spectra for sorption samples. From bottom to top, spectra are grouped as Pond C water/CO_2 present, deionized water/CO_2 present, and deionized water/CO_2 absent. Within each group, pH increases moving upward. Sample numbers from bottom to top are UK5, UK7, UK9; UK6, UK8, UK10, UK12, UK2; and UK3.

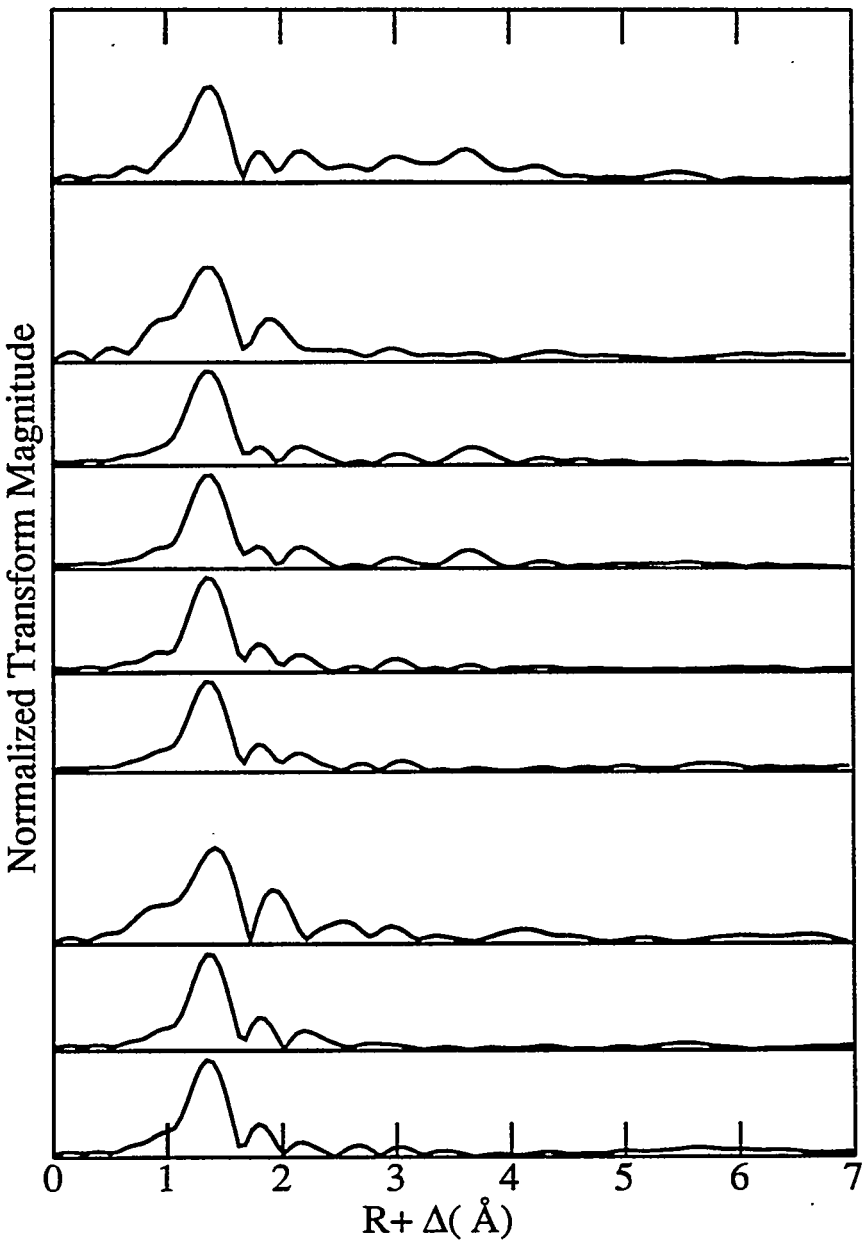

Figure 3. Fourier transforms of EXAFS spectra for sorption samples. From bottom to top, spectra are grouped as Pond C water/CO_2 present, deionized water/CO_2 present, and deionized water/CO_2 absent. Within each group, pH increases moving upward. Sample numbers from bottom to top are UK5, UK7, UK9; UK6, UK8, UK10, UK12, UK2; and UK3.

other sorption sample FTs. Although there appear to be features at higher R in the UK9 FT, the amount of noise in the data makes assessment of the quality of fit using additional shells of backscattering atoms equivocal, at best. In addition to the noise level, the shortened usable data range in UK2 and UK9 spectra make the observed differences from other sorption samples in the equatorial shell questionable, because resolution between two equatorial subshells would be lost as the difference between $R_{U\text{-}Oeq(1)}$ and $R_{U\text{-}Oeq(2)}$ (ΔR) approaches or falls below $\pi/2\Delta k$ (see Chapter Two). For the other sorption samples, ΔR averages 0.20 Å. The required minimum data range (Δk) for resolving a ΔR of 0.20 Å is 7.85 $Å^{-1}$. As all of the transforms in this study begin at or slightly above k=3 $Å^{-1}$, this would require usable data through k=11 $Å^{-1}$. By k=11 $Å^{-1}$, the UK9 and to a lesser extent, UK2 spectra are already noisy, which may account for the lack of resolution of the equatorial shell into two subshells.

Data are not presented for UK1, UK4, or UK11 because the data quality is too poor for analysis. Poor data quality is most likely due to the low U uptake in all three samples, as well as the absence of the solution filtration filter from the UK11 sample, resulting in a lack of contribution from U sorbed to small kaolinite particles trapped on the filter. Data quality in the XANES region of UK4 and UK11 was good enough to suggest the presence of the uranyl moiety; only a very weak feature not clearly identifiable as an edge was present in the UK1 spectrum.

Spectra of supernatant solutions expected to contain the highest concentrations of U for each group of samples (UK2, UK11, UK12) failed to reveal a U x-ray absorption edge, indicating U concentrations too low to contribute to EXAFS spectra. This confirms that sorption sample spectra do not reflect species in the solution phase contained in the samples.

X-ray Absorption Spectroscopy - Quantitative Analysis

UK3, 5, 6, 7, 8, 10, and 12

Based on qualitative similarities between the uranophane spectrum and the sorption spectra, phase shift and amplitude parameters from FEFF calculations employing the uranophane structure were used to fit the sorption data (Appendix 5). The uranyl $U\text{-}O_{ax}$ distance was found to be within 0.01 Å of 1.80 Å for all of the sorption samples (Table 5). Equatorial oxygens in all sorption samples except UK2 and UK9 were best fit using two subshells. The significant improvement over fitting with one equatorial shell is most apparent in the FT fits (App. 5).

The two O_{eq} shell fitting strategies, i.e. fixing both O_{eq} σ^2 values to 0.002 and fixing the sum of O_{eq} N values to 5, resulted in fits of equal quality. The balance between

SAMPLE	LIGAND	*Fixed O_{eq} σ^2 values* N	R (Å)	σ^2 (Å^2)	*Fixed O_{eq} N values* N	R (Å)	σ^2 (Å^2)
Deionized Water							
UK6	O_{ax}	2	1.79	0.0032	2	1.79	0.0032
	$O_{eq(1)}$	1.1	2.30	0.002	2.0	2.28	0.0068
	$O_{eq(2)}$	1.5	2.47	0.002	3.0	2.47	0.0076
UK8	O_{ax}	2	1.80	0.0029	2	1.80	0.0029
	$O_{eq(1)}$	1.1	2.30	0.002	2.1	2.29	0.0068
	$O_{eq(2)}$	1.3	2.47	0.002	2.9	2.48	0.0077
UK10	O_{ax}	2	1.80	0.0034	2	1.80	0.0034
	$O_{eq(1)}$	1.0	2.29	0.002	2.1	2.27	0.0059
	$O_{eq(2)}$	1.2	2.48	0.002	2.9	2.49	0.0077
	U	1	3.88	0.0051	1	3.88	0.0043
UK12	O_{ax}	2	1.80	0.0032	2	1.80	0.0032
	$O_{eq(1)}$	0.9	2.28	0.002	2.0	2.26	0.0066
	$O_{eq(2)}$	1.0	2.48	0.002	3.0	2.48	0.0092
	U	1	3.87	0.0043	1	3.87	0.0041
UK2	O_{ax}	2	1.81	0.0040			
	O_{eq}	3.5	2.44	0.0113			
UK3	O_{ax}	2	1.80	0.0029	2	1.80	0.0027
	$O_{eq(1)}$	1.3	2.29	0.002	2.1	2.28	0.0039
	$O_{eq(2)}$	1.4	2.48	0.002	2.9	2.49	0.0048
	U	2	3.87	0.0045	2	3.87	0.0045
Pond C Water							
UK5	O_{ax}	2	1.79	0.0024	2	1.79	0.0024
	$O_{eq(1)}$	1.4	2.30	0.002	2.2	2.28	0.0059
	$O_{eq(2)}$	1.5	2.46	0.002	2.8	2.46	0.0072
UK7	O_{ax}	2	1.80	0.0028	2	1.80	0.0028
	$O_{eq(1)}$	1.4	2.32	0.002	2.2	2.31	0.0047
	$O_{eq(2)}$	1.5	2.49	0.002	2.8	2.50	0.0057
UK9	O_{ax}				2	1.81	0.0036
	O_{eq}				5	2.40	0.0140

Table 5. Results of sorption sample EXAFS analysis. Samples are divided into two groups: those prepared with deionized water and those prepared with Pond C water. Within each group, the sorption pH increases as one descends in the column. Data quality was poor and data range was short in UK2 and UK9, which may account for the lack of equatorial oxygen shell splitting.

N and σ^2 for each shell necessarily varied depending on the fitting strategy employed, however R values did not vary beyond the error limits of the method (± 0.02 Å) with fit strategy. Because the R values did not vary significantly, we conclude that both resulting sets of N, R, and σ^2 parameters are equally valid. Among samples, parameters can only be compared within a single strategy. Because our knowledge basis for fixing N values (all uranyl compounds) is significantly greater than that for σ^2 (one model compound - uranophane), and the first fitting strategy consistently underestimates by two to three the expected average O_{eq} coordination number of five, we focus on the parameters resulting from the second strategy (last three columns in Table 5).

Fixing the sum of equatorial oxygens to 5, the distance from U to the closer equatorial subshell ($R_{U\text{-}Oeq(1)}$) lies between 2.26 and 2.31 Å and the longer distance ($R_{U\text{-}Oeq(2)}$) lies between 2.46 and 2.50 Å. Rounding to whole numbers of atoms, equatorial oxygens consistently divide into two at the shorter distance and three at the longer distance.

Unfortunately, the 3.0 Å peak observed in most FT spectra does not produce significant features in the corresponding EXAFS spectra. Thus, the source of this peak must be determined and evaluated from filtered spectra and on the basis of its improved modeling of the unfiltered FT features (Fig. 4). As expected, the amplitude function of the filtered spectrum (for the 3.0 Å peak) is characteristic of atoms with atomic numbers near Si (Teo and Lee, 1979). The filtered spectra are well fit by 0.3 to 1.0 Si atoms located approximately 3.3 Å from U (σ^2 = 0.001 to 0.005 Å^2) in UK3, 5, 6, 8, 10, and 12.[5] These same N, R, and σ^2 values can be used to fit the 3.0 Å peak in the unfiltered spectra, but it is desirable to allow N and σ^2 to adjust because they can be under- or overestimated when filtering is done in a region that is not isolated from other backscattering atoms, as is the case for the region under discussion. Unfortunately, allowing these values to vary simultaneously tends to result in values that are clearly outside of reasonable ranges. This is not surprising given that the Si contribution to the spectra at this distance is relatively small, and it therefore a minor factor in directing a least-squares fit. For these reasons we consider the N and σ^2 values associated with these Si shells to be very approximate and they have therefore not been reported in Table 5. Distance values should not be significantly affected by the filtering process, unless more than one Si atom contributes to the spectrum from slightly different distances from U or large termination ripples from O_{eq} or U overlap with the Si feature. Both of these possibilities are quite realistic, therefore we have not reported R for Si neighbors in Table 5 because we think it might be misleading. We are nonetheless confident that the FT features discussed correspond to Si/Al neighbors.

[5]Although we cannot distinguish between Si and Al, as discussed, we will refer to this shell as the Si shell for simplicity in the remainder of this chapter.

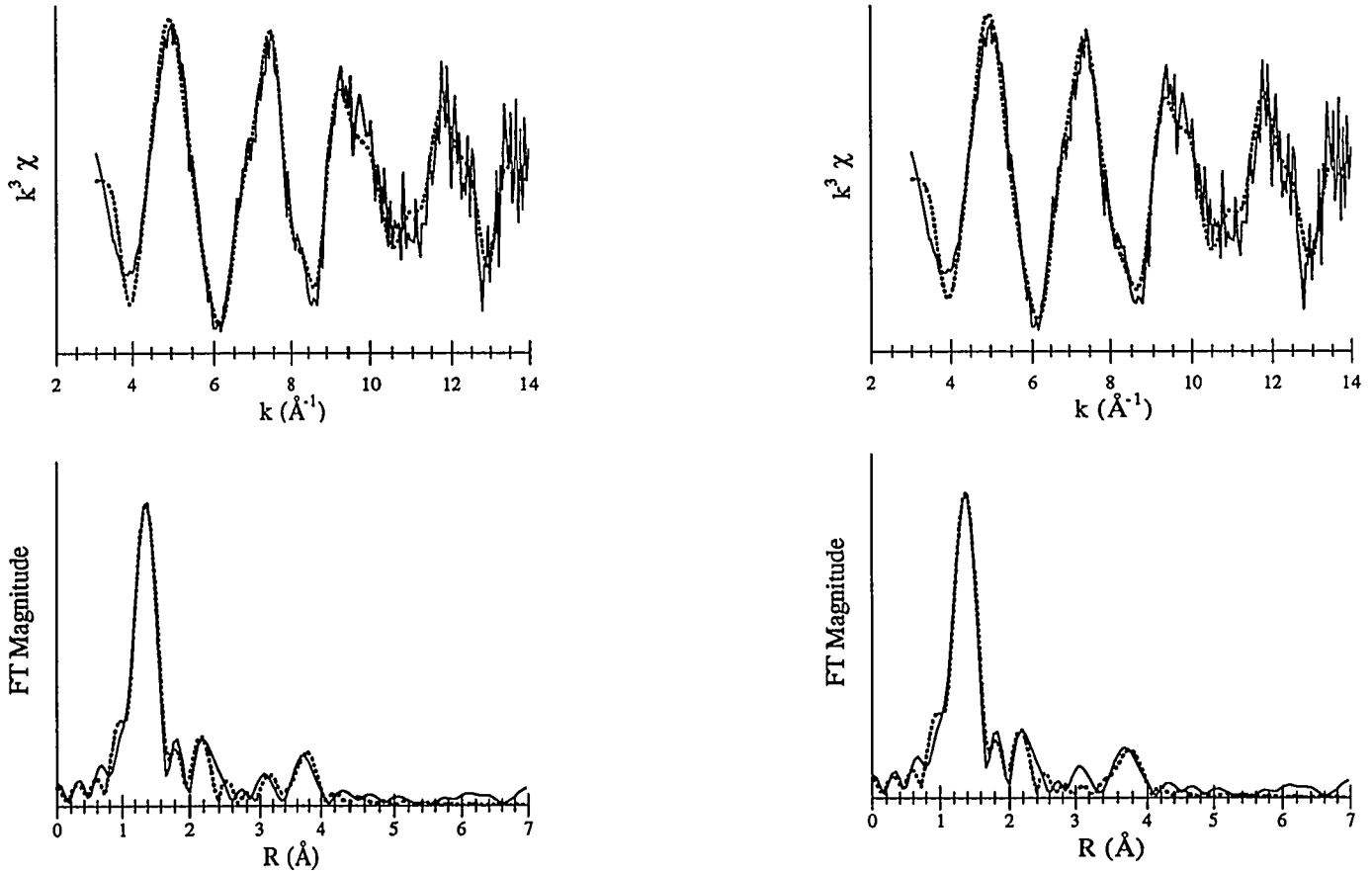

Figure 4. Fits of UK12 spectra with and without a shell of Si neighbors at 3.3 Å. Fourier transform spectra are uncorrected for phase shift. Solid lines are experimental spectra; dotted lines are fits. In all fits, two equatorial oxygen subshells were included. Fit in left pair of spectra contains a Si shell; fit in right pair of spectra does not. Note the improved fit of the 3.1 Å FT peak in the fit that includes the Si neighbor.

The only alternative explanation, given constraints on the structure place by U structural chemistry, is that these are multiple-scattering features. This is highly unlikely given the asymmetric nature of the solid-water interface.

The 3.8 Å peak in transforms of UK3, 10, and 12 spectra is well fit using phase shift and amplitude parameters for U, resulting in one U atom (fixed N) at 3.87 to 3.89 Å in UK10 and 12 and 2 U atoms at the same distance in UK3. Deconvolution of the resulting fits suggests that the U backscatterers are responsible for subtle features in the corresponding EXAFS spectra, including peak shoulders at k=6.5, 8, 11, and 12.5 $Å^{-1}$. Debye-Waller terms for the U shells are similar for all three fits (0.0043 to 0.0053) and very close to those found for two U neighbors at 4.3 and 3.9 Å in rutherfordine and uranophane, respectively. In fact, the number of U atoms was set to 2 in UK3 because its Debye-Waller term was unusually small (0.0013) for such a distant neighbor when N was set equal to 1.0. The very high correlation between N and σ^2 is reflected here. The agreement for both values between uranophane and UK3 suggests that the values obtained for UK3 are realistic because we established in Chapter Two that 0.005 $Å^2$ is a reasonable σ^2 value for 2 U atoms at this distance. For the same reason, the discrepancy between N values (but not σ^2 values) for uranophane and UK10 and 12 suggests that both N and σ^2 values for UK10 and 12 should be larger or both should be smaller than the values in Table 5. Without additional information, it is difficult to ascertain correct values of either.

Sorption sample UK3 has additional structure on the high R side of the 3.8 Å peak and around 5.5 Å in its FT which is most likely attributable to additional U neighbors because of the elements present in the sample, only U is expected to scatter strongly enough to be seen at these distances. Due to significant overlap in the 3.8 Å region and the relatively small size of the 5.5 Å feature, this structure would be difficult to fit confidently.

Disorder parameter (σ^2) values are generally consistent with those found for similar backscattering shells in the model compounds. Sorption sample O_{ax} σ^2 values are at the high end of the range found for model compounds, suggesting slightly weaker U-O_{ax} bonds (higher vibrational disorder) and/or a greater difference between the two U-O_{ax} bond lengths (higher static disorder) for the uranyl moiety at the solid-water interface. Among other explanations, the former could be caused by stronger equatorial bonds or participation of the axial oxygens in a second bond, the latter by unequal environments for the two O_{ax} atoms. Either way, the difference is quite small and possibly insignificant.

Sorption sample O_{eq} subshell σ^2 values are similar to each other within a reasonably narrow range. Compared to uranophane, sorption sample σ^2 values are larger, but within the same order of magnitude. Consistently larger σ^2 values in the sorption samples are indicative of more O_{eq} shell disorder (static and/or vibrational) than in uranophane.

COMPOUND	White Line (eV)	A (eV)	Δ_1[1] (eV)	$R_{U\text{-}Oax}$ (Å)	B (eV)	Δ_2[2] (eV)	$R_{U\text{-}Oeq}$ (Å)
UK2	17172	17182	10	1.81	17208	36	2.44
UK3	17171	17181	10	1.80	17209	38	2.28, 2.49
UK5	17169	17181	12	1.79	17207	38	2.28, 2.46
UK6	17172	17182	10	1.79	17210	38	2.28. 2.47
UK7	17170	17180	10	1.80	17208	38	2.31, 2.50
UK8	17172	17184	12	1.80	17210	38	2.29, 2.48
UK9	17172	17182	10	1.81	17210	38	2.40
UK10	17171	17181	10	1.80	17210	39	2.27, 2.49
UK12	17171	17182	11	1.80	17210	39	2.26, 2.48

[1]Energy difference between peak of white line (first derivative = 0) and maximum slope of A feature (first derivative = local maximum)
[2]Energy difference between peak of white line (first derivative = 0) and peak of B feature (first derivative = 0)
[3]Equatorial oxygens are best fit in most of the sorption samples using two separate shells.

Table 6. Comparison of relative energy positions of sorption sample XANES features with interatomic distances. Feature designations correspond to Figure 2 of Chapter Two.

Thus the immediate atomic environment (O_{ax} and O_{eq} shells) of U in UK3, 5, 6, 7, 8, 10, and 12 is quite uniform, despite the varied conditions under which the samples were prepared. There appears to be a minor, possibly insignificant trend toward decreasing $R_{U\text{-}Oeq(1)}$ (from 2.30 to 2.26 Å) with increasing pH (from 6.0 to 7.1) in DI water exposed to air. No such trend is apparent in Pond C water samples, but we are limited to data from two samples. Uranium neighbors are detectable in the higher pH DI water samples prepared in the presence (UK10-pH 7.0; UK12-pH 7.1) and absence (UK3-pH 8) of CO_2. Uranium neighbors are not detectable in any of the Pond C water samples. This may be attributable to the poor data for high pH samples (UK9-pH 7.0; UK11-pH 7.5; UK1-pH 8.0), or otherwise to Pond C water constituents that inhibit polynuclear species formation.

XANES

The presence of features A and B in the XANES region of all sorption sample spectra confirms the presence of the uranyl moiety in the samples. As for the model compounds in Chapter Two, peak positions relative to the x-ray absorption edge ("white line") correspond to $R_{U\text{-}Oax}$ and $R_{U\text{-}Oeq}$ (Table 6). Because the local U environment varies little among the sorption samples, so do the relative positions of XANES features.

DISCUSSION

In this study we have utilized XAS to establish the structure of U sorption complexes at the kaolinite-water interface in response to changes in aqueous carbonate presence, RFP Pond C water constituents, and solution pH. To a lesser extent, we have observed the effects of the same three parameters on the uptake of U by kaolinite through the quality (i.e. signal-to-noise ratio) of the resulting XAS data. We use the resulting structural information to attempt to identify the mode of sorption.

Over the range of solution conditions explored in this study, the U sorption complex is characterized by a uranyl moiety ($R_{U\text{-}Oax} \approx 1.80$ Å) surrounded by 5 equatorial O atoms for which the U-O bond lengths separate into two groups of three long (≈ 2.48 Å) and two short (≈ 2.28 Å). Silicon (and/or aluminum) is present in the coordination environment under most of the conditions studied, although the number and location of Si neighbors are not well known. For samples prepared in DI water in contact with air at solution pH values $8.0 > pH \geq 7.0$ (UK10 and UK12), an uncertain number of U neighbors are located approximately 3.9 Å from the central U. Uranium neighbors approximately 3.9 Å from the central U are also present in the sample from which CO_2 was excluded, prepared at pH 8.0 (UK3).

Carbonate presence must explain the apparent absence of U neighbors from UK2 (carbonate present, pH 8.0) spectra compared with their definite presence in UK3 (CO_2 excluded, pH 8.0) spectra, as it is the only condition the two samples do not share. Despite the shortened data range in UK2 spectra, we would expect to see evidence for U neighbors if they were present, because U visibly contributes to the EXAFS spectrum as early as $k = 7.5$ Å^{-1}. The lack of U neighbors in our UK2 data suggests that carbonate inhibits U polynuclear formation at pH 8.0 in the presence of a solid. Although we do not observe a contribution for C neighbor(s) in the UK2 spectra (we would not expect to see such a weak scatterer in such a noisy spectrum), carbonate must be bound directly to U in the sorption complex to inhibit polynuclear formation. Thus under conditions of UK2 preparation, carbonate is assumed to be present in the sorption complex. Although our result does not suggest that carbonate is present in all U sorption complexes that have been exposed to air, it certainly suggests that there is no need for complete loss of carbonate from the U equatorial shell in order for sorption to occur.

Furthermore, we know from our own and others' U uptake measurements that carbonate presence reduces uptake by kaolinite at pH 8 (from 92% in UK3 to 31% in UK2 in our studies), presumably due to uneven competition between carbonate and the solid surface for U. This is reflected in the reduction in the UK2 signal-to-noise ratio relative to UK3.

Although we might have predicted differences in sorption complex structures resulting from waters of different composition, sorption from pH 6.0 to 6.5 Pond C water produces a U sorption complex that is virtually indistinguishable from that sorbed from DI water in the same pH range.[6] Data quality for the three higher pH Pond C water sorption samples (UK9, UK11, and UK1) is too poor for quantitative analysis whereas the higher pH DI water sorption spectra (UK10, 12, and 2) are of good to reasonable quality. Reduced uptake from Pond C water relative to that from DI water likely accounts for the poorer data quality in UK9, UK11, and UK1 spectra. In fact, the increasing effect of Pond C water constituents on U uptake at higher pH is similar to the trend observed for carbonate effect on U uptake. Furthermore, EXAFS spectra from our pH 7.0 Pond C water sample (UK9) and our pH 8.0, CO_2-exposed DI water sample (UK2) are qualitatively similar. Without further structural analysis of these samples or comprehensive chemical analysis of Pond C water, we might conclude that a high carbonate content of Pond C water relative to DI water accounts for the observed CO_2-like effect of Pond C water on U uptake.

[6]The only notable difference can be found in the pH 6.5 Pond C water sample (UK7) spectra, in which there is no evidence for Si neighbors.

The effect of pH on U sorption complex structure is consistent with that observed for U solution complexes. The formation of polynuclear species increases with pH (over the range 6.0 to 7.1) for the DI water/atmospheric carbonate series of samples (UK6, UK8, UK10, UK12). The structures of these four sorption complexes are almost identical with the exception of the U shell, which is nonexistent at pH 6.0 and 6.5 and definitely present at pH 7.0 and 7.1. At pH 8.0 in the DI water series (UK2), polynuclear species are not present, most likely due to competition with carbonate ligands, as discussed above. In fact, comparison of the stoichiometries of these sorption complexes (except UK2[7]) with those of dominant solution species expected at each pH reveals a remarkable similarity, assuming that precipitation of the hydrous uranyl oxide has not occurred in our samples for kinetic reasons (Fig. 5). We can infer that U sorption behavior in pH 6.0 to 8.0, low ionic strength, DI water solutions containing kaolinite parallels its solution behavior under similar conditions. This is similar to inferences (James and Healy, 1972) and observations (Dillard and Koppelman, 1982; Chisholm-Brause, 1991; O'Day, 1992) that Co(II) sorption behavior parallels its solution behavior, although for Co(II) the surface appears to enhance polymer formation, which is not apparent from our study of U(VI). The more significant role played by the solid in the Co(II) system compared with U(VI) may result from the more stringent geometric constraints placed on bonding by the regular CoO_6 octahedron as compared with the uranyl pentagonal or hexagonal bipyramid, in which the U-O_{eq} bond lengths and angles vary considerably, resulting in a more "adaptable" sorbate.

The same trend cannot be established for the Pond C water samples as the data quality at pH 7.0 and above is too poor to discern a U contribution, but we would expect polynuclear species to be absent from Pond C water samples above pH 7.0 due to the increased carbonate-like effect already observed in these samples.

Sorption Mode

Although we have addressed the short-range environment of U in our sorption samples, we have yet to discuss how U is associated with kaolinite. Given the composition of the XAS samples (primarily solid with a small amount of supernatant), U could be found in one or more of three different phases: dissolved in aqueous solution, precipitated from solution, and sorbed by kaolinite. We have ruled out the first possibility by finding no x-ray absorption edge in XAS spectra of the supernatants, suggesting that they could not be responsible for sorption sample spectra.

[7]Solution pH dropped as low as 6.25 after filtration of UK2, thus although sorption was initiated at pH 8.0, the extent of sorption and composition of the sorption complex may have been altered as pH dropped.

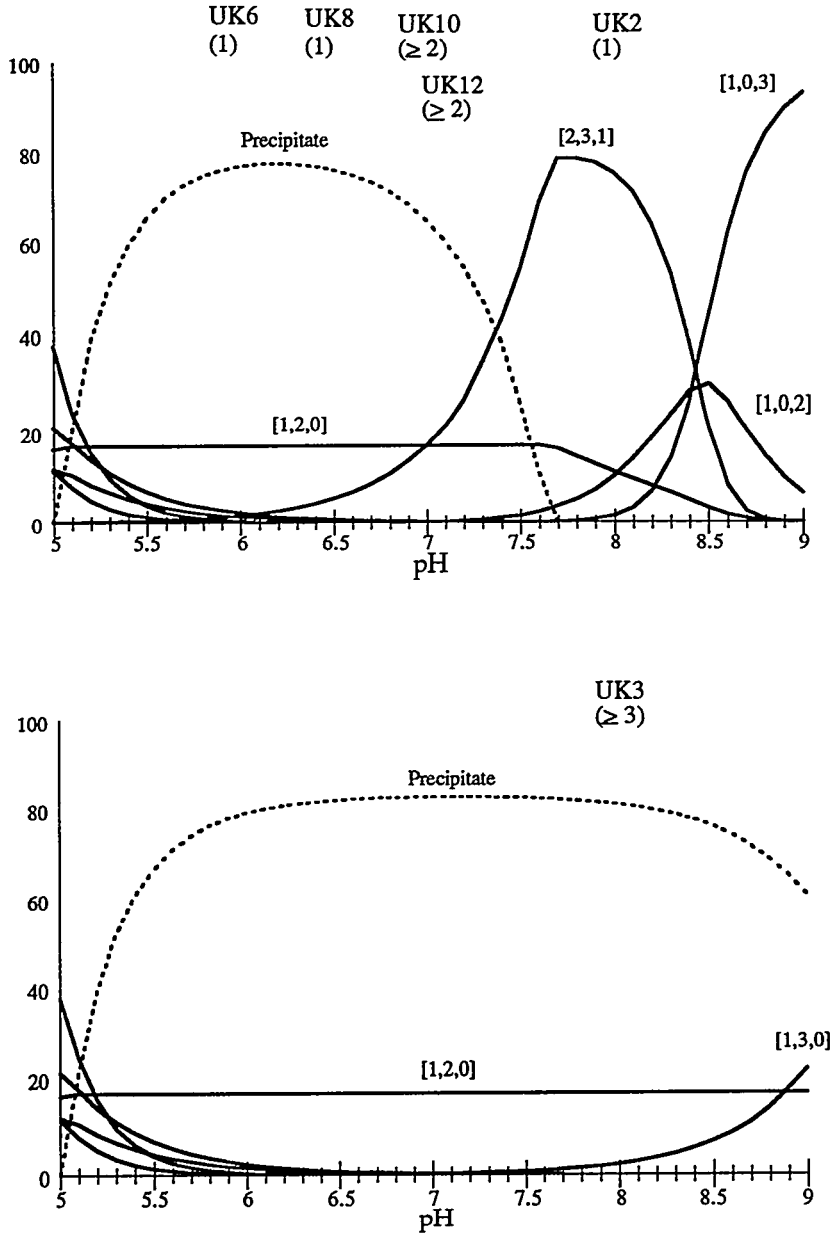

Figure 5. Equilibrium U(VI) distribution as a function of pH for $\Sigma U = 10^{-1.7}$ mol·m^{-3}, ionic strength = 1 mol·m^{-3} $NaNO_3$ (i.e., initial conditions in the sorption experiments) in the presence (top) and absence (bottom) of atmospheric CO_2. Kaolinite is included in the calculation and is allowed to come to equilibrium with the solution, but sorption is not explicitly accounted for. Both solutions are supersaturated with respect to $UO_3 \cdot 2H_2O$ and β-$UO_2(OH)_2$ in the mid-pH range, shown with dashed lines. The CO_2-free solution is additionally supersaturated with respect to soddyite between pH 7.5 and 9.0. Sorption sample designations, along with the number of U atoms in the corresponding sorption complex derived from EXAFS spectra (in parentheses), are located in the horizontal vicinity of their nominal pH of preparation; vertical location is not intended to imply anything. See Appendix One for details of calculation.

Precipitation of a U solid phase must be seriously considered, because initial solutions from which U was sorbed to prepare UK3, 6, 8, 10, and 12 were supersaturated with respect to uranyl trioxide dihydrate ($UO_3 \cdot 2H_2O$) and a uranyl hydroxide phase (β-$UO_2(OH)_2$) (Grenthe et al., 1992) and UK3 was additionally supersaturated with respect to soddyite, a uranyl silicate, assuming that an equilibrium amount of kaolinite dissolved (Nguyen et al., 1992). (Because the composition of the Pond C water is not completely known, the same determination cannot be made for the Pond C water samples.) Furthermore, we have observed polynuclear complex formation in some of our samples, which could be indicative of precipitation. The structure of the dihydrate has not been determined, but it is believed to consist of pseudo-hexagonal layers of $[UO_2(OH)_2]_n$ in which each U has six O_{eq} neighbors, each of which joins three U atoms (Christ and Clark, 1960). The uranyl hydroxide phase similarly consists of sheets, but each U has four O_{eq} neighbors, each of which joins two U atoms (Roof et al., 1964). Relying on known distances in similar structures, both of these precipitates would be expected to have U-U distances on the order of 3.9 Å, similar to those found for our sorption samples. To our knowledge, the structure of soddyite has not been refined.

With the exception of UK3, precipitation of a U phase probably did not occur in our samples for several reasons. No precipitation was observed during sample preparation. Perhaps more convincing, there are no U neighbors in the EXAFS spectra for several of the sorption samples that were prepared under conditions of supersaturation (UK6 and UK8). Of the samples for which U neighbors were observed in the coordination environment of U (UK10 and UK12), Si is present in the spectra in the vicinity of 3.3 Å, which is inconsistent with the structures of the dihydrate and the hydroxide phases. This raises the question of a mixed U and Si solid phase, but of those that have been reported and for which heats of dissolution have been determined (soddyite, sodium boltwoodite, and sodium weeksite), none are predicted to form under these conditions (Nguyen et al., 1992). We can furthermore preclude the possible formation in UK10 and UK12 of an amorphous solid phase, which would be more likely to form than a crystalline phase during the relatively short duration of the sorption experiments, because its formation would require greater over saturation than crystalline phases of similar composition (Stumm and Morgan, 1981; Morse and Casey, 1988).

If we accept our inference that U sorption behavior roughly parallels its solution behavior, then it appears quite likely that we may be sampling a precipitate, or its precursor, in UK3. Spectra for UK3 definitely indicate the presence of U neighbors, whereas no polynuclear solution species are predicted under conditions of UK3 preparation. Without good structural refinements for the solids with respect to which the

UK3 solution is supersaturated, we cannot establish whether similarities exist between the UK3 sorption complex and these solids.

Sorption by kaolinite is therefore the most likely fate of U in all of our sorption samples for which the spectra are of good quality (UK2, 3, 5, 6, 7, 8, 10, and 12). Silicon has been fit as a backscatterer in the coordination environment of U for all of these but UK2 and UK7, thus (with some uncertainty) confirming inner-sphere complexation of U. Sorption of U on low Z (< 26) oxides has previously been studied using EXAFS (Chisholm-Brause et al., 1992; Dent et al., 1992), but sorbent metal atoms have never been seen in the U coordination environment. Although we are unable to constrain the number of Si neighbors in the U coordination environment, the relatively small size of the Si contribution to the spectra as well as the presence of U neighbors in many of the samples' spectra precludes the possibility that U is absorbed into the kaolinite structure.

We observe a small peak at 3.0 Å that stands above background in the UK2 FT, but because of the higher level of noise in UK2 spectra compared with those in which this feature was fit, UK2 fitting results for this peak would be equivocal. We suspect that the small 3.0 Å peak is attributable to Si, on which basis we infer that U in UK2 is bound in an inner-sphere fashion to kaolinite. There is no evidence of Si in the coordination environment of U in UK7. This does not preclude inner-sphere sorption, as we observed in uranophane, meta-autunite, and meta-ankoleite in Chapter Two that Si and P backscatterers are not always seen in this distance range from U. Furthermore, we have not seen any evidence in this study that the structural environment of U in UK7 should be dramatically different from that in UK5. Nonetheless, we have no direct evidence for inner-sphere sorption of U by kaolinite in UK7 and must simply conclude that U is sorbed by kaolinite in UK7 in an unknown manner.

We cannot establish the exact bonding geometry between U and kaolinite for several reasons. First of all, we cannot distinguish between Al and Si backscatterers, and therefore do not know to which sites on kaolinite sorption is limited. We assume that bonding to Si/Al occurs through O_{eq} atoms, because O_{ax} atoms seldom participate in bonds other than the one with U, and when they do, the U-O_{ax} bond length has been predicted to lengthen on the order of 0.1 Å (Hoekstra and Siegel, 1973), which is not observed here. Whereas U-Oeq bond lengths and angles might be used to determine binding sites on kaolinite based on common interatomic distances (e.g. O-O as was done by O'Day (1992)), the equatorial O shell in all of our sorption samples is too statically disordered to determine O-U-O angles. In the uranophane structure, short U-O_{eq} bond lengths (2.3 Å) are characteristic of monodentate silicate ligands, in which the O_{eq} that bridges between Si and U does not also bridge to neighboring U atoms; long U-O_{eq} bond lengths (2.5 Å) in the

same structure are characteristic of bidentate silicate ligands in which both O_{eq} atoms that bridge between Si and U also bridge to neighboring U atoms. The corresponding U-Si distances in uranophane are 3.7 and 3.1 Å, respectively. Using uranophane as a potentially analogous structure, the presence of both long and short U-O_{eq} bond lengths in the sorption complexes could mean both monodentate and bidentate linkage of U to Si, for which a U-Si distance of 3.3 Å provides no obvious limitations.

Polynuclear sorption complexes are present in UK10 and UK12; UK3 contains either polynuclear sorption complexes or a precipitate. Drawing from the structures of a large number of uranyl solids and solution complexes, the U-U distance of approximately 3.9 Å constrains each pair of U neighbors to be bound by two bridging O (or OH) groups. In the case of UK3, for which an average of 2 U neighbors has been estimated for each U atom, an equilateral triangular arrangement of three U atoms as proposed by Åberg (1970) for a triuranyl solution species is consistent with our data. We do not have enough information to uniquely determine the structure of the UK3 sorption complex, however.

Chisholm-Brause et al. (1992) found Debye-Waller factors for the O_{eq} shell of U sorbed by montmorillonite similar to values we obtain when fitting O_{eq} atoms as a single shell, which they interpreted as evidence for multiple sites or sorption complexes. This interpretation is not inconsistent with our data, however we observed in our model compound study that σ^2 values in the vicinity of 0.01 Å^2 are not unusually high for a single U coordination environment. In fact, a σ^2 value in this range for the O_{eq} shell of a sorption complex should not seem high given the asymmetric U coordination environment (solid on one side, water on the other).

RFP Pond Water Remediation

As regards the removal of U from RFP pond water, our uptake results reaffirm the observations of others, namely that high pH enhances U uptake, hence removal, unless carbonate is present. When carbonate is present, high pH inhibits uptake. Our XAS results suggest that carbonate limits uptake by inhibiting polymerization to form multinuclear surface complexes. Thus carbonate concentration should be limited in the process designed for removal of U from RFP pond water in order to achieve maximum uptake. Conversely, the carbonate effect might be exploited to effect the removal of U from kaolinite or any other solid sorbent after the U-loaded solid has been removed from the pond water. Furthermore we have observed strong parallels in the pH dependence of U solution and sorption behavior, thus the extensive body of knowledge regarding U(VI) solution behavior can be expected to provide reasonable guidelines for optimizing U uptake. Finally, Pond C water constituents that were not present in the deionized water

sorption samples did not cause any observable differences in the structure and composition of U sorption complexes resulting from Pond C water solutions. This result suggests that the use of laboratory samples made from deionized, rather than Pond C water may be a reasonable approach to optimizing the conditions under which sorption is effected.

APPENDIX ONE
Thermodynamic Calculations

We have used thermodynamic calculations in this work to predict solution speciation and solid dissolution/precipitation as a function of pH. Calculations were made using the computer program HYDRAQL (Papelis et al., 1988) and the U thermodynamic database of Grenthe et al. (1992). This database was selected from those available for three reasons: it has taken advantage of more recent literature than most, it has been carefully reviewed for internal consistency, and it is being used by a number of researchers who study U and therefore is under stringent scrutiny.

The logarithms of the formation constants for all of the solids and solution complexes considered in the calculations are contained in the table in this appendix. These equilibrium constants are based on formation of the solid or complex from "components" as defined for HYDRAQL. Thus, for the $[2,3,1]^-$ complex,

$$2UO_2^{2+} + 3H_2O + CO_3^{2-} \leftrightarrow (UO_2)_2(OH)_3CO_3^- + 3H^+$$

$$K = ((UO_2)_2(OH)_3CO_3^-)(H^+)^3 / (UO_2^{2+})^2(CO_3^{2-}) = 10^{-0.77}$$

where () represents the activity of each component. The Davies' equation is used to calculate activity coefficients (Stumm and Morgan, 1981). Similarly for a solid, β-$UO_2(OH)_2$,

$$UO_2^{2+} + 2H_2O \leftrightarrow \beta\text{-}UO_2(OH)_2 + 2H^+$$

$$K = (H^+)^2 / (UO_2^{2+}) = 10^{-4.95}$$

Formation constants for kaolinite (May et al., 1986) and soddyite, sodium boltwoodite, and sodium weeksite (Nguyen et al., 1992) were taken from other sources, as they were not included in the Grenthe et al. (1992) database. The U minerals have been adjusted for internal consistency with the Grenthe et al. (1992) database.

In calculations that resulted in the speciation diagram (Chapter One, Fig. 3), ΣU, ionic strength, and carbonate concentration were selected to duplicate conditions under which sorption samples were prepared. All solids listed in the table for which all components were present in solution were allowed to reach equilibrium with respect to precipitation.

In Chapter Two our objective was to determine a set of ΣU, pH, and ionic strength conditions under which a single solution complex dominates. We were further restricted to working at a U concentration that would produce a strong x-ray absorption signal (for U transmission XAS, ≥ 5 mol·m^{-3}). The low pH (< 3.0) end of the speciation diagram tends to be the least cluttered, from which we selected the fully hydrated UO_2^{2+} ion.

In Chapter Three we made calculations to verify that kaolinite was not dissolving in our sorption experiments nor was any other phase precipitating. We therefore included kaolinite in the calculation as a Type IV, or "precipitated but allowed to dissolve" solid. All of the remaining solids from the table were included in the calculation as Type V, or "allowed to precipitate" solids. Because HYDRAQL only allows one Type V solid to precipitate at a time, solids that were found to precipitate ($UO_3 \cdot 2H_2O$ and β-$UO_2(OH)_2$) were moved to the Type VI category, meaning they were not taken into account in the mass balance. This allowed us to repeat the calculation to determine whether the solution was supersaturated with respect to any other solids.

log K	Solution Complex	log K	Solid
-5.20	$[1,1,0]^+$	-9.20	α-$UO_3 \cdot 0.9\ H_2O$
-10.30	$[1,2,0]^0$	-4.95	β-$UO_2(OH)_2$
-19.20	$[1,3,0]^-$	-4.83	$UO_3 \cdot 2H_2O$
-33.00	$[1,4,0]^{2-}$	-11.98	$UO_2(NO_3)_2$
-2.70	$[2,1,0]^{3+}$	-8.51	$UO_2(NO_3)_2 \cdot H_2O$
-5.62	$[2,2,0]^{2+}$	-4.92	$UO_2(NO_3)_2 \cdot 2H_2O$
-11.90	$[3,4,0]^{2+}$	-3.67	$UO_2(NO_3)_2 \cdot 3H_2O$
-15.55	$[3,5,0]^+$	-2.25	$UO_2(NO_3)_2 \cdot 6H_2O$
-31.00	$[3,7,0]^-$	-30.18	α-Na_2UO_4
-21.90	$[4,7,0]^+$	-22.70	$Na_2U_2O_7$
9.68	$[1,0,1]^0$	14.47	UO_2CO_3
16.94	$[1,0,2]^{2-}$	26.94	$Na_4UO_2(CO_3)_3$
21.60	$[1,0,3]^{4-}$	17.57	Soddyite
-0.77	$[2,3,1]^-$	17.24	Sodium boltwoodite
0.74	$(UO_2)_3O(OH)_2(HCO_3)^+$	136.35	Sodium weeksite
36.96	$[11,12,6]^{2-}$	38.41	Kaolinite
54.00	$[3,0,6]^{6-}$		
0.30	$UO_2NO_3^+$		

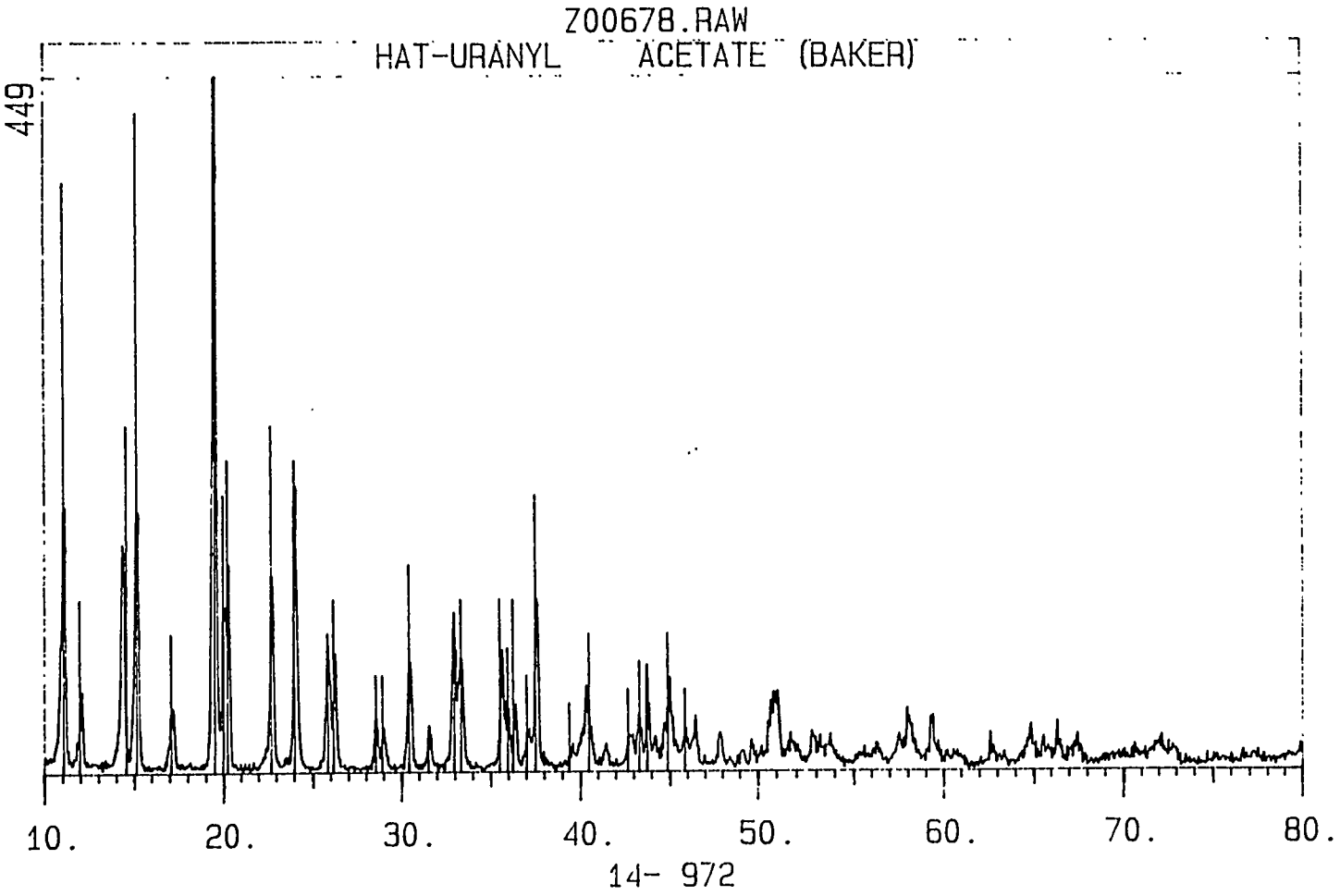
Z00678.RAW
HAT-URANYL ACETATE (BAKER)
449
10.
20.
30.
40.
50.
60.
70.
80.
14- 972

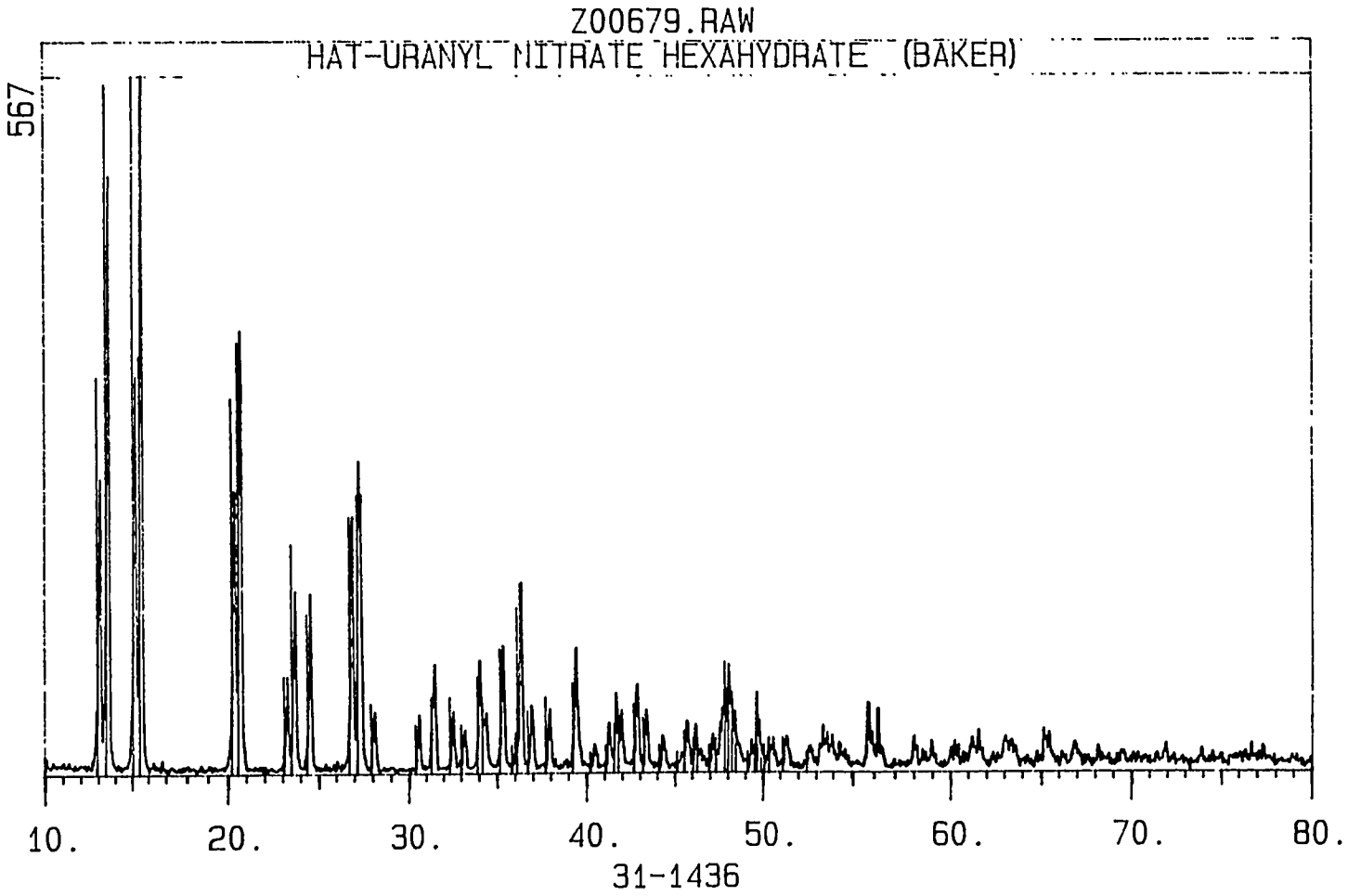
Z00679.RAW
HAT-URANYL NITRATE HEXAHYDRATE (BAKER)
567
10.
20.
30.
40.
50.
60.
70.
80.
31-1436

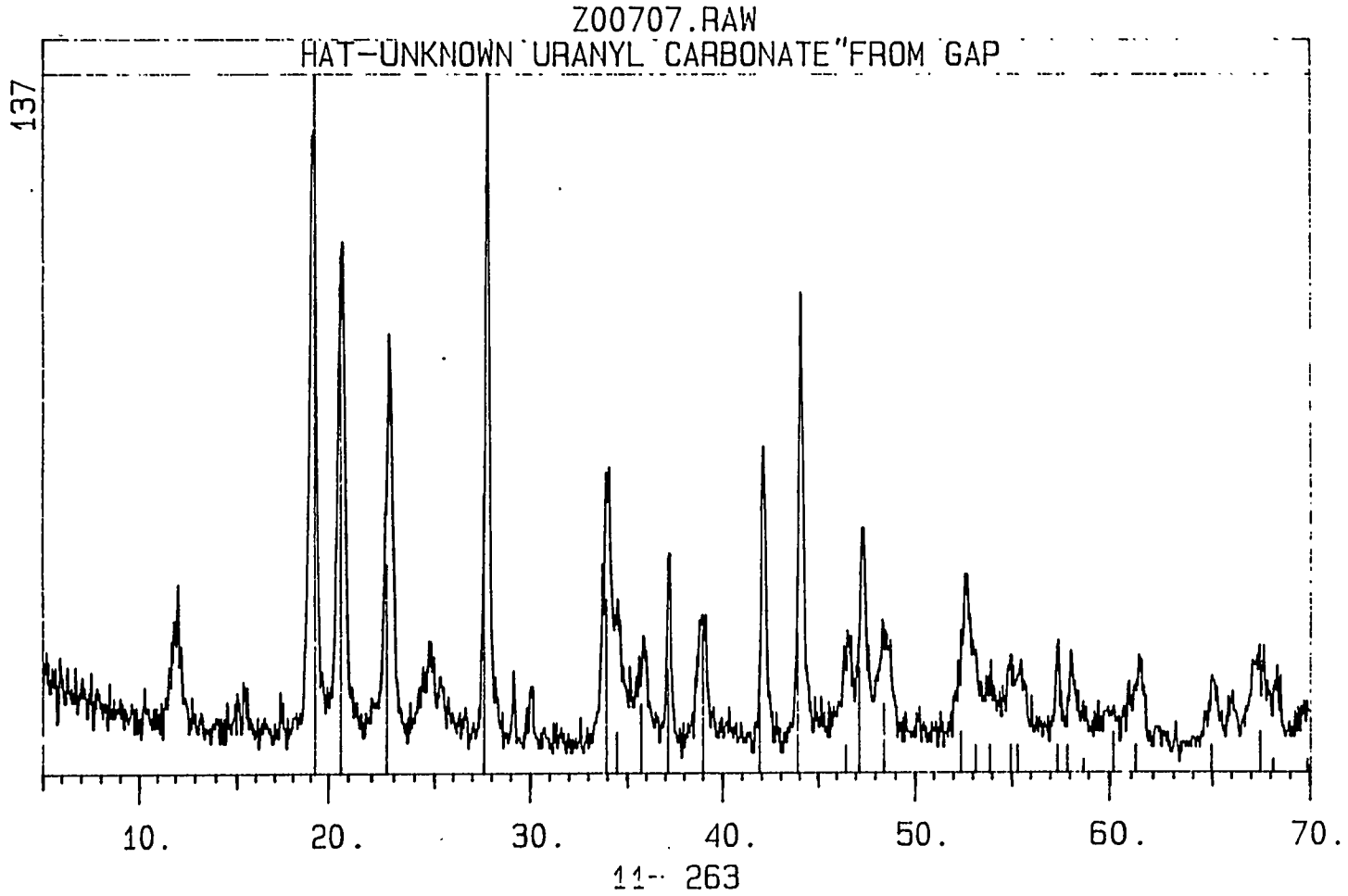
Z00707.RAW
HAT-UNKNOWN URANYL CARBONATE"FROM GAP
137
10.
20.
30.
40.
50.
60.
70.
11-· 263

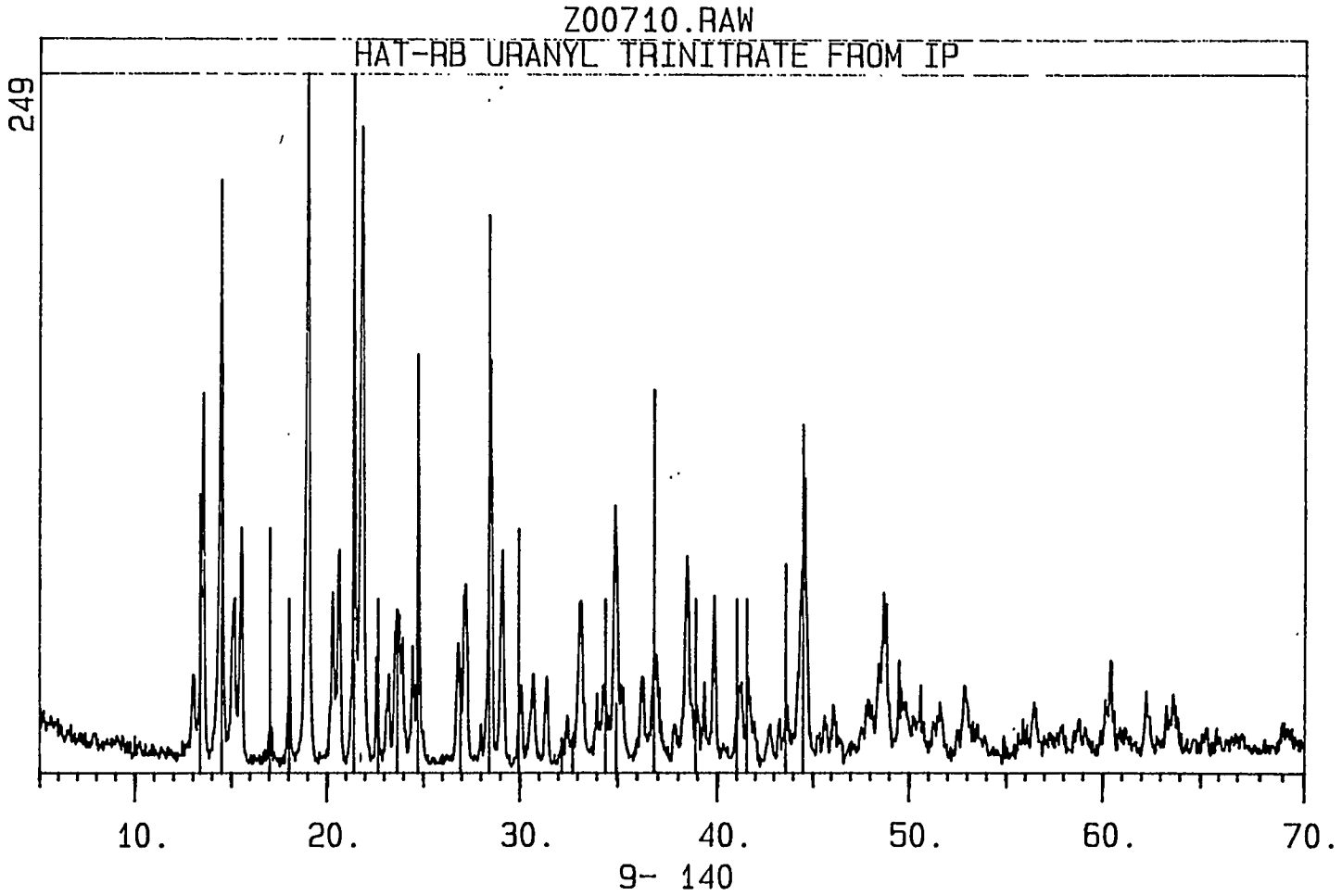
Z00710.RAW
HAT-RB URANYL TRINITRATE FROM IP
249
10.
20.
30.
40.
50.
60.
70.
9- 140

Uranophane, 39-1360

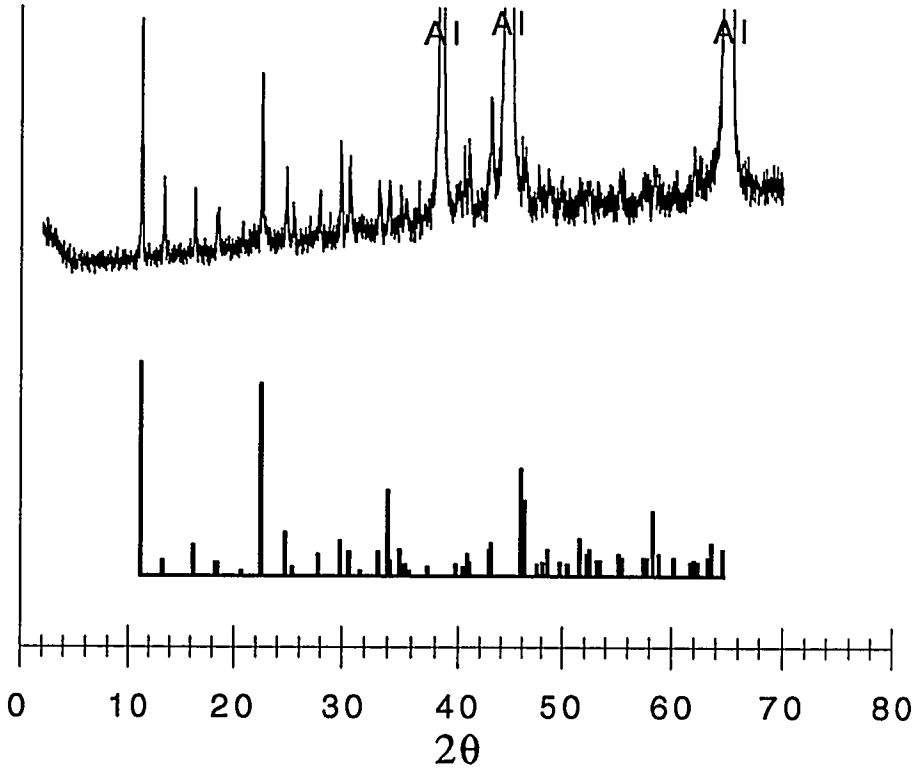

Meta-Autunite, 39-1351

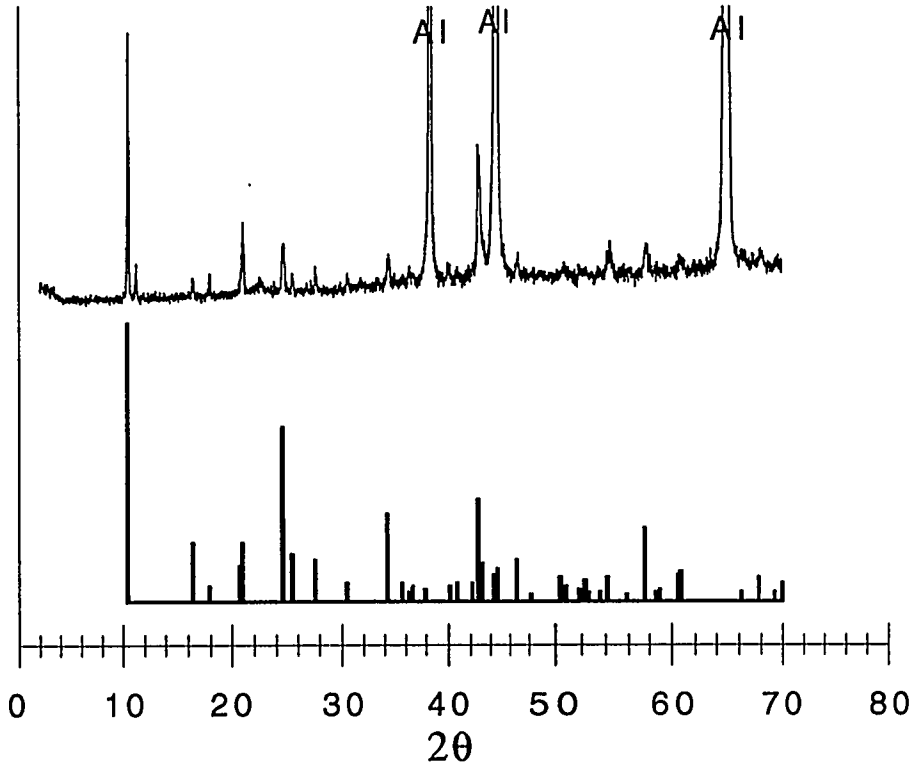

Meta-ankoleite, 29-1061

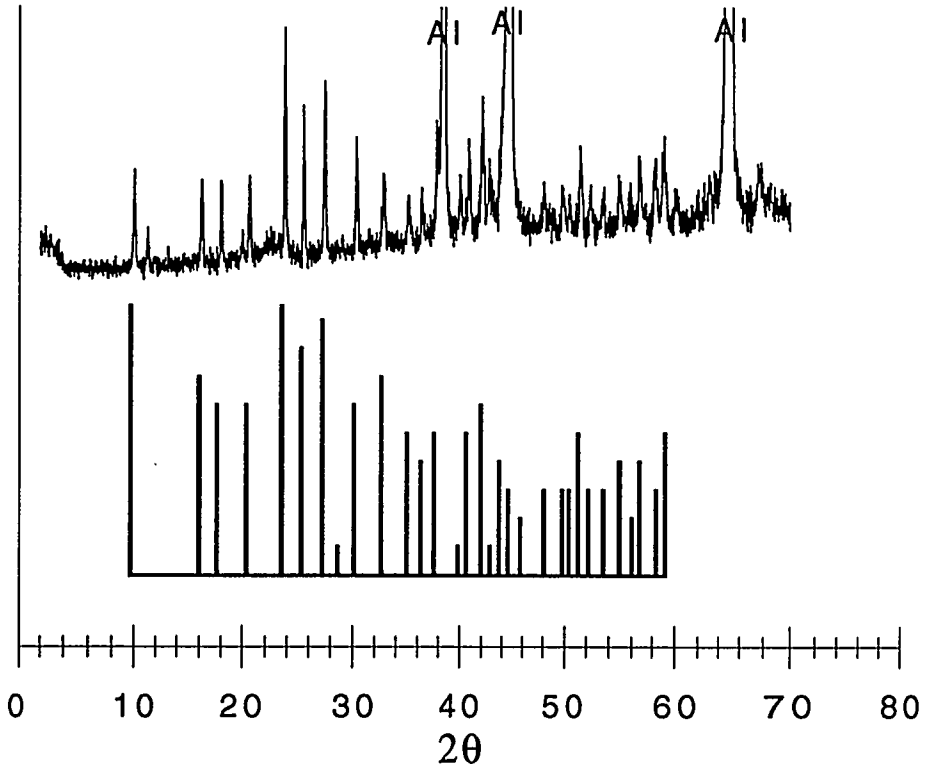

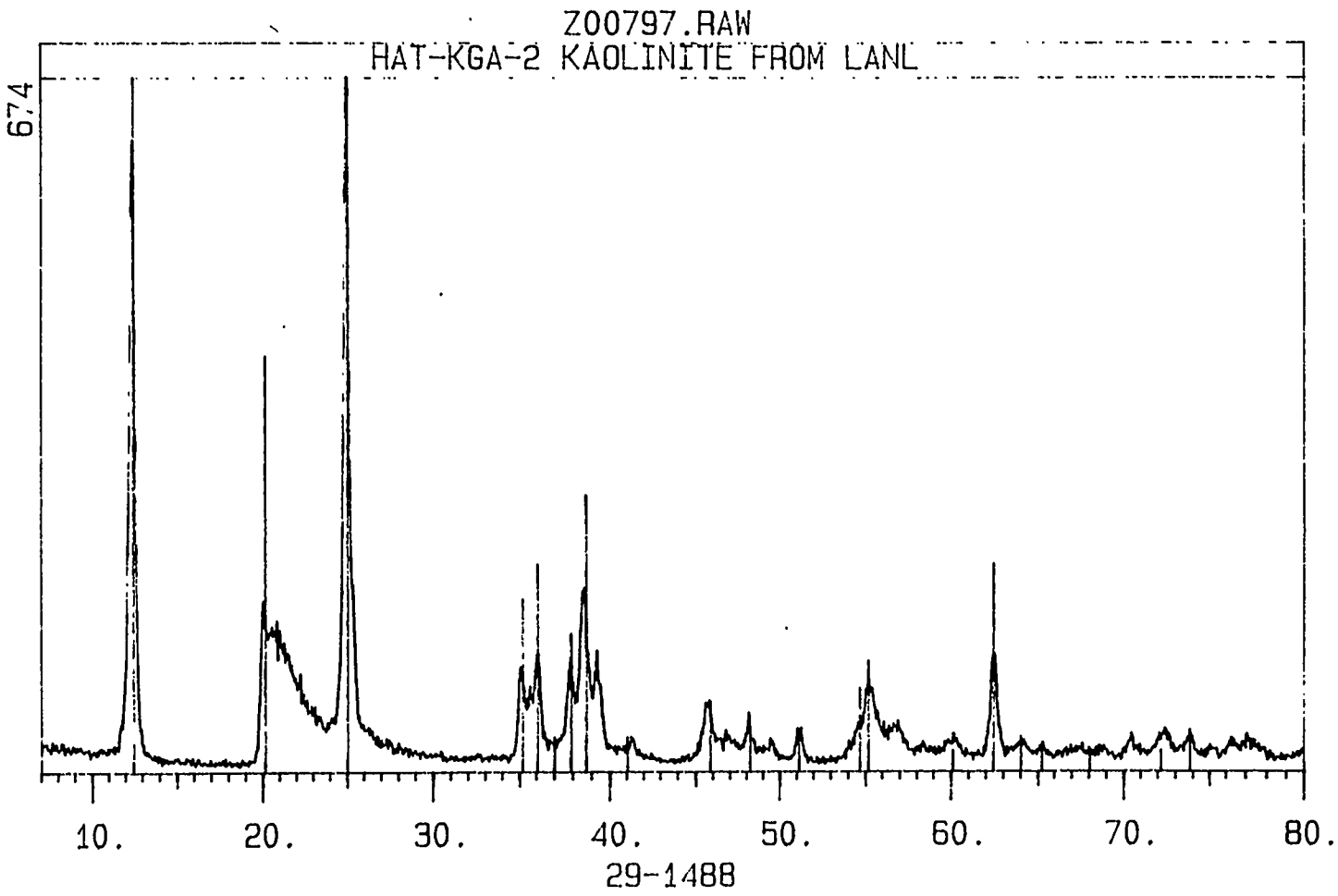
Z00797.RAW
RAT-KGA-2 KAOLINITE FROM LANL
67.4
10.
20.
30.
40.
50.
60.
70.
80.
29-1488

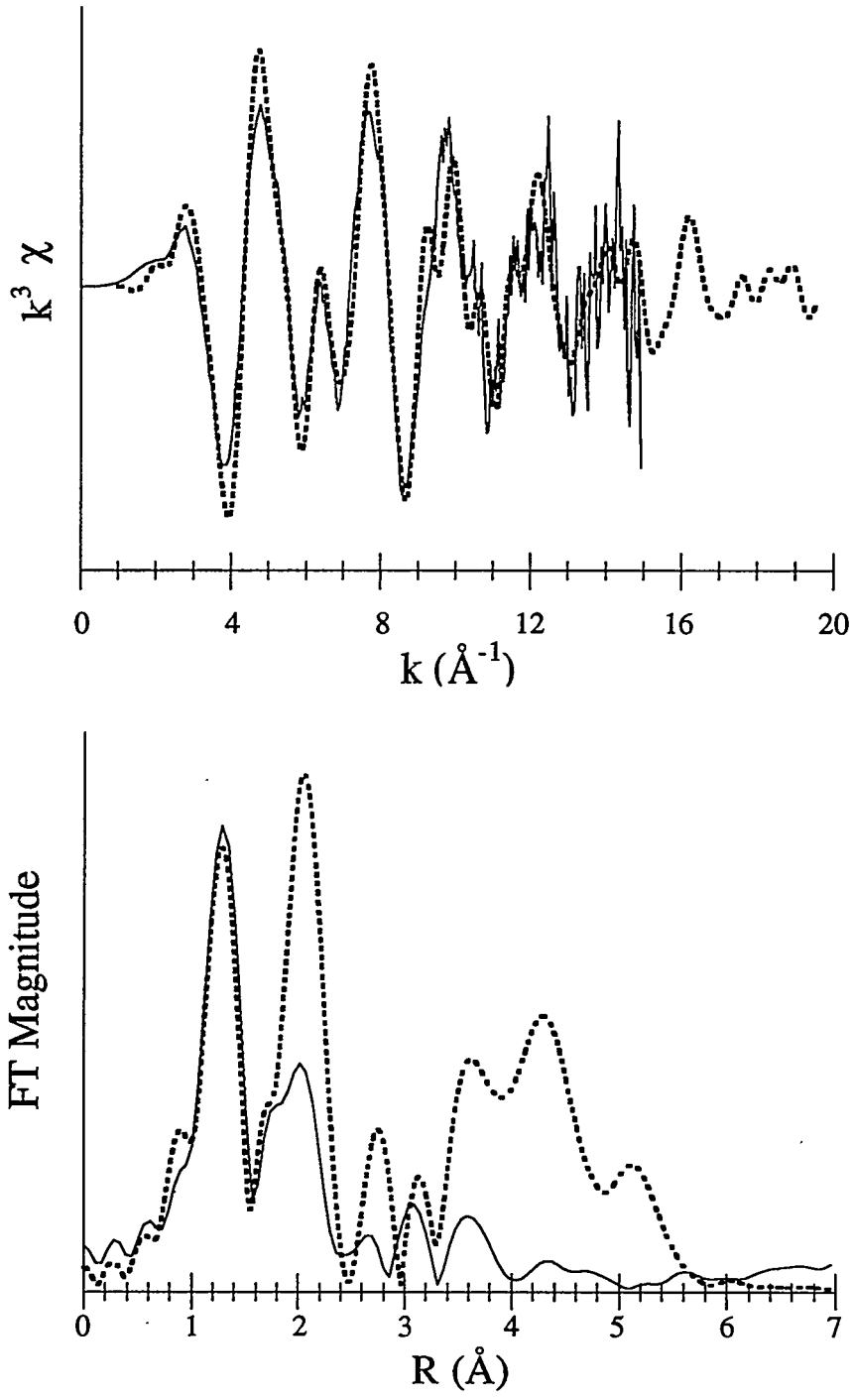

3-1. Uranyl nitrate hexahydrate. Dotted line is FEFF-calculated spectrum; solid line is experimental spectrum.

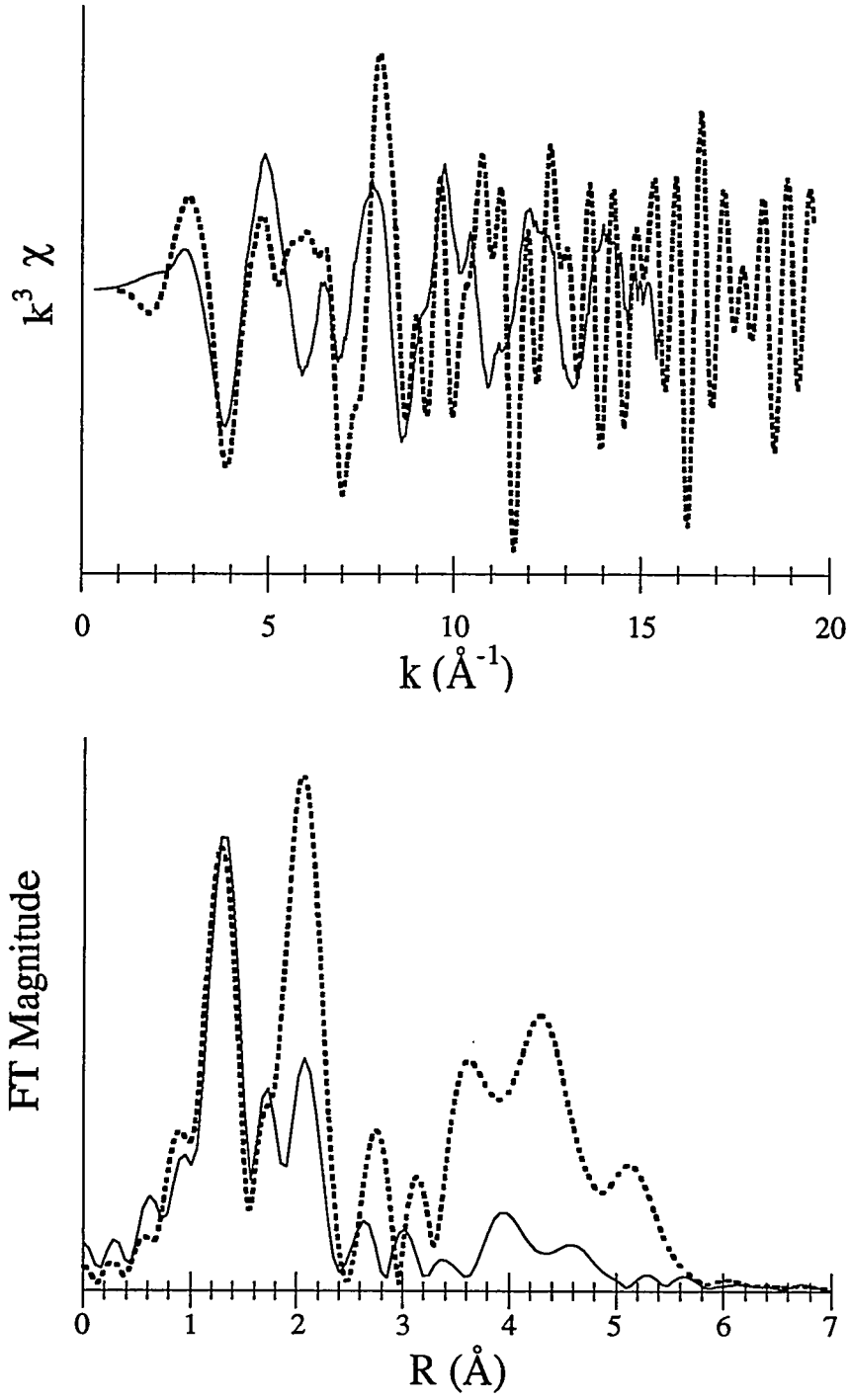

3-2. Rutherfordine. Dotted line is FEFF-calculated spectrum; solid line is experimental spectrum.

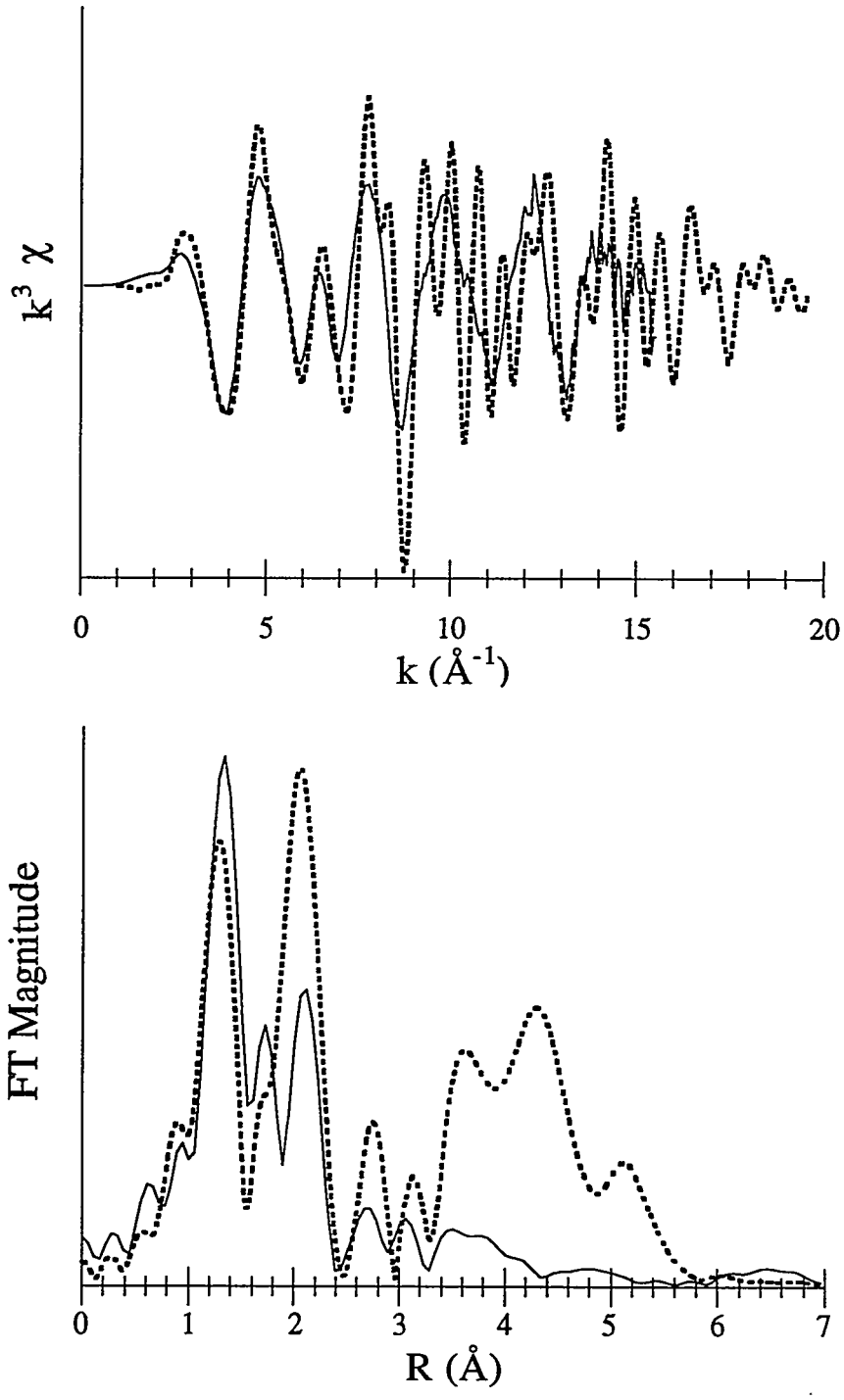

3-3. Rubidium uranyl nitrate. Dotted line is FEFF-calculated spectrum; solid line is experimental spectrum.

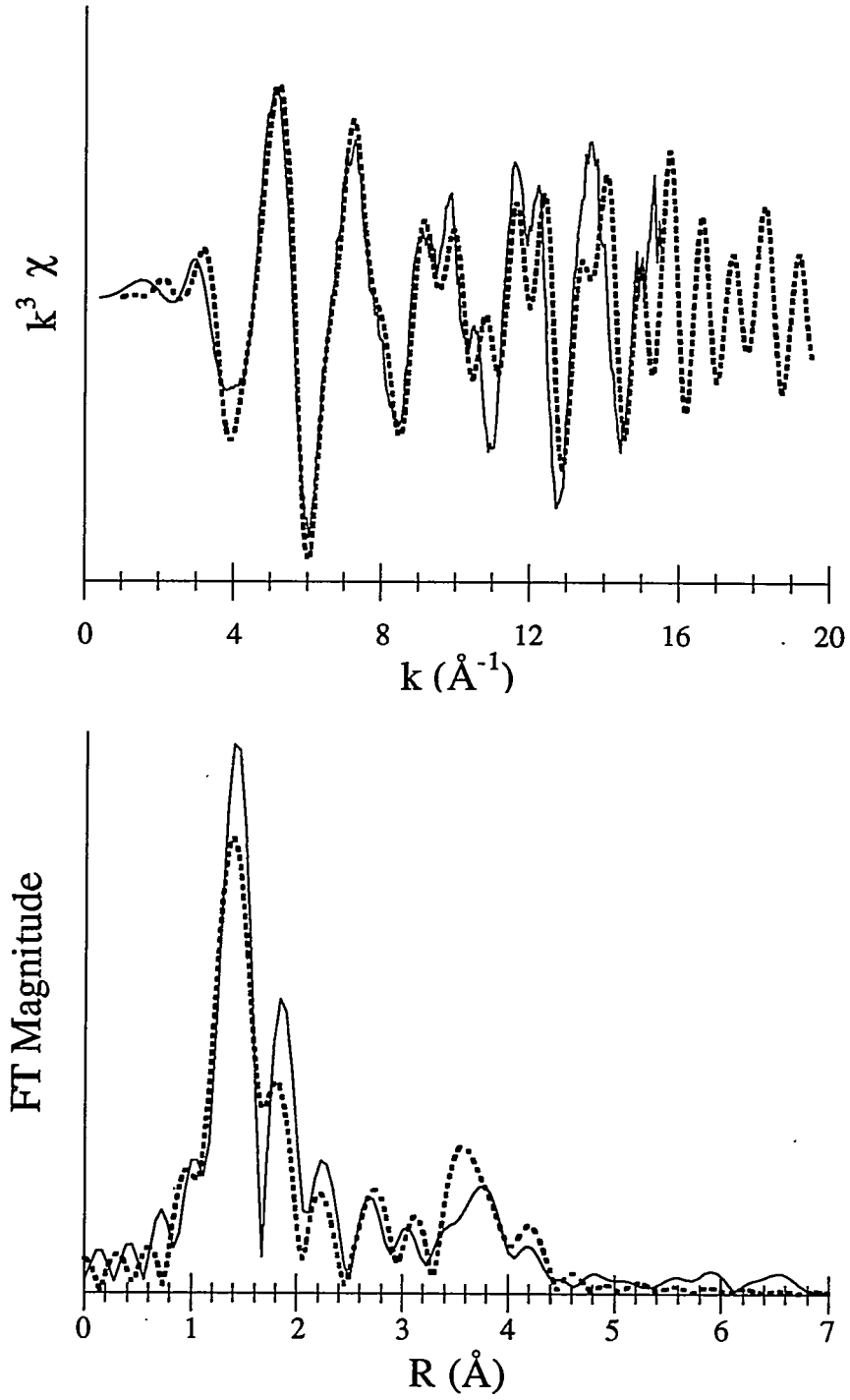

3-4. Uranophane. Dotted line is FEFF-calculated spectrum; solid line is experimental spectrum.

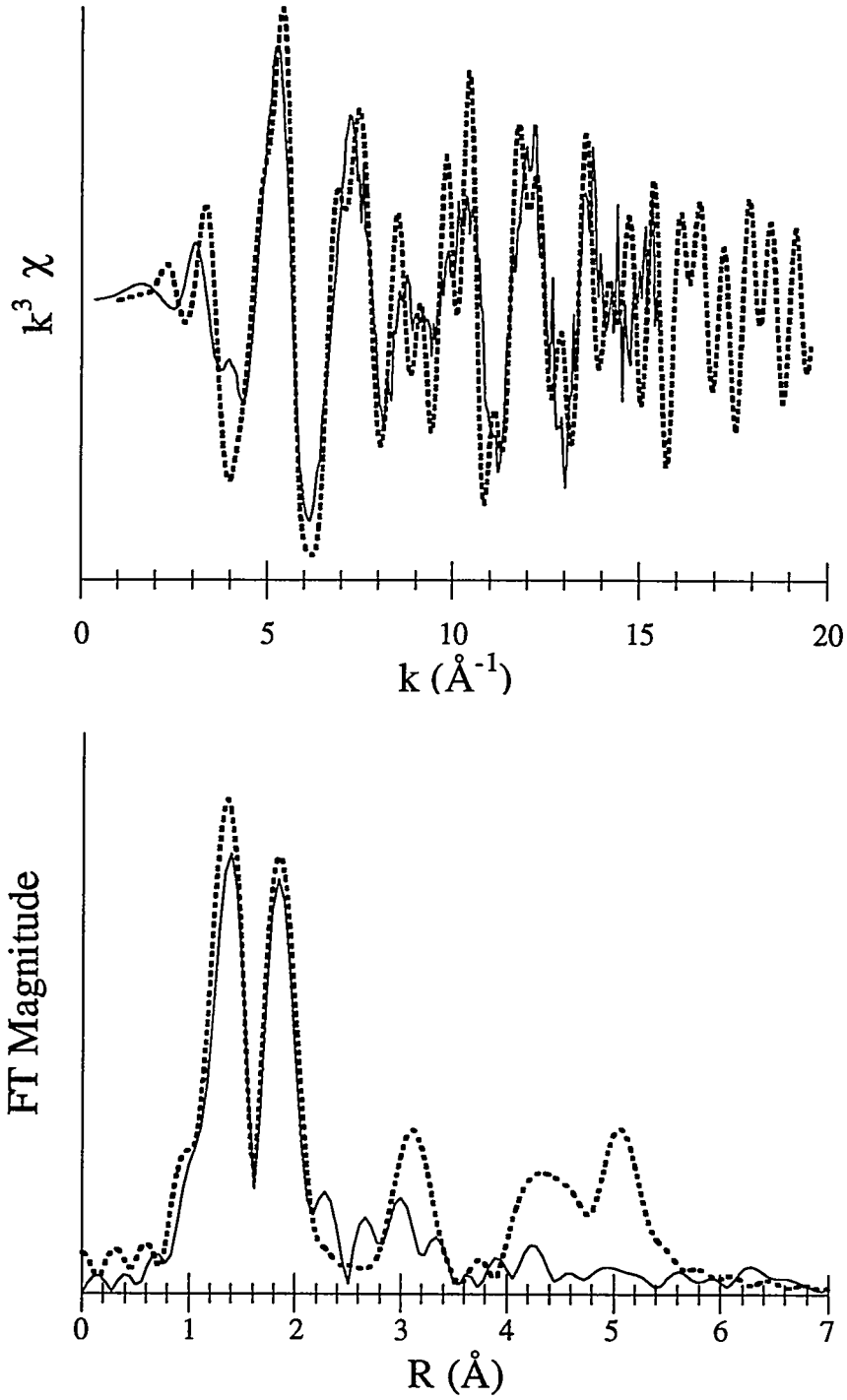

3-5. Meta-autunite. Dotted line is FEFF-calculated spectrum; solid line is experimental spectrum.

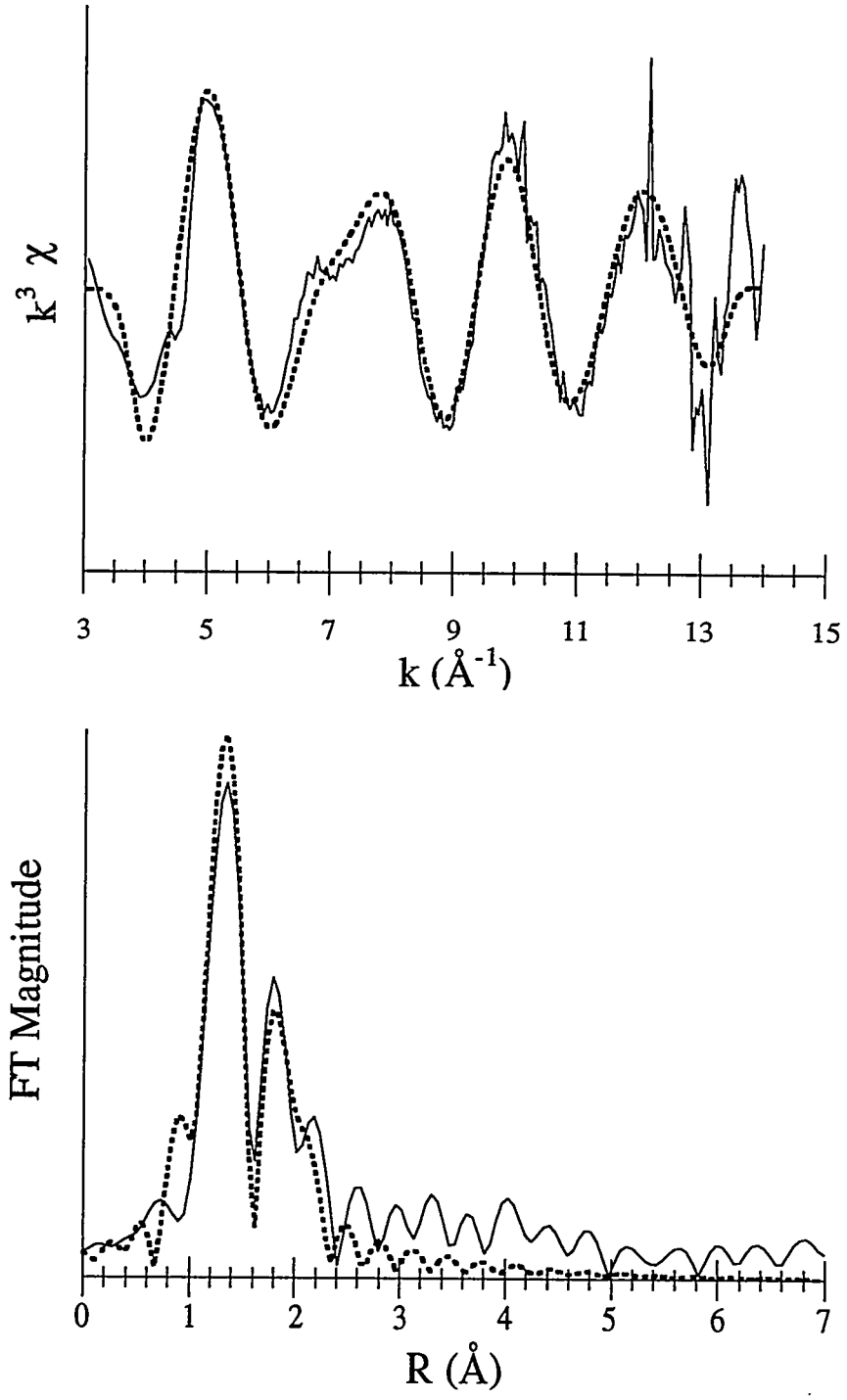

4-1. Unhydrolyzed monomeric aqueous uranyl ion. Dotted line is fit; solid line is experimental spectrum.

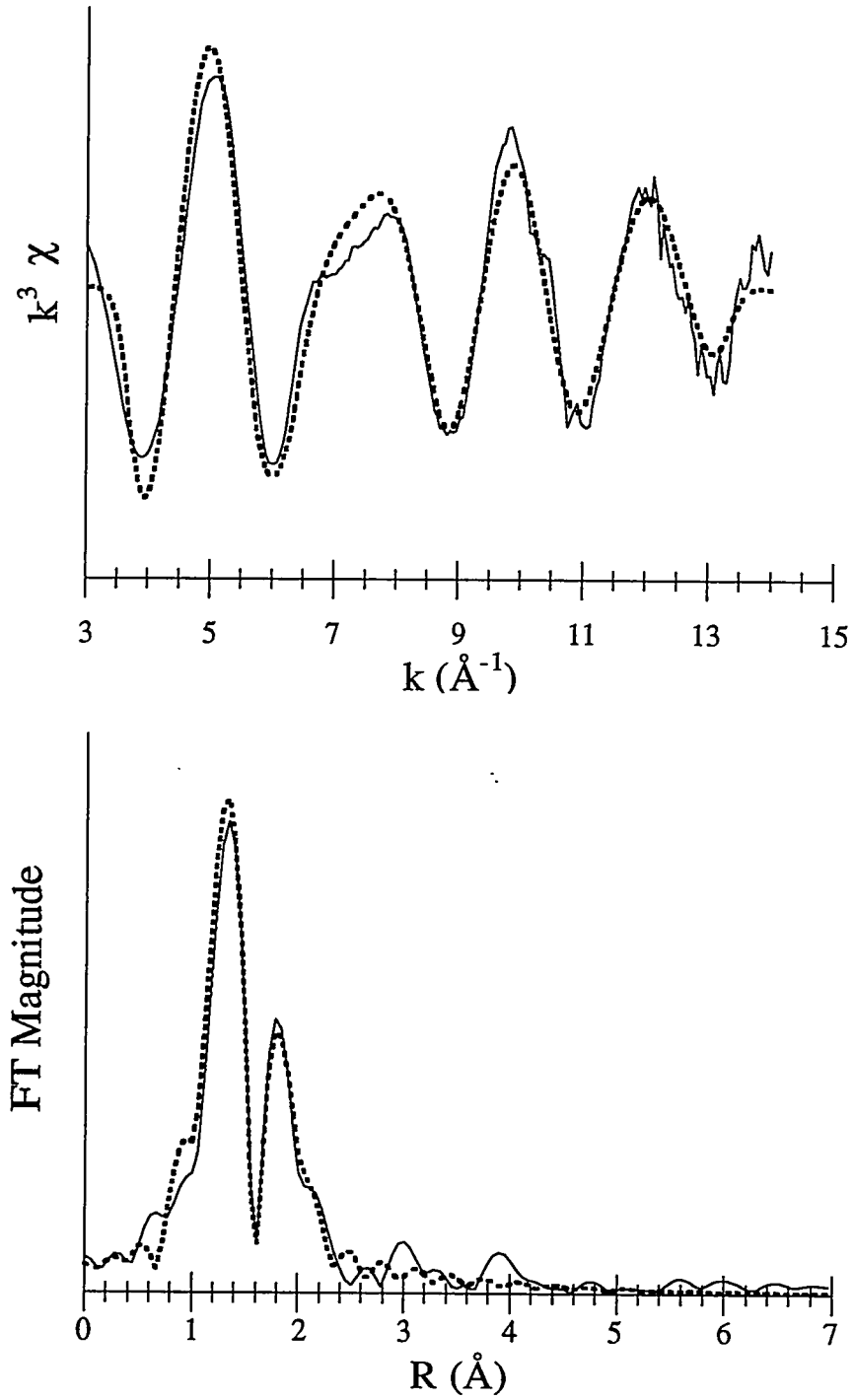

4-2. Uranyl (di)acetate. Dotted line is fit; solid line is experimental spectrum.

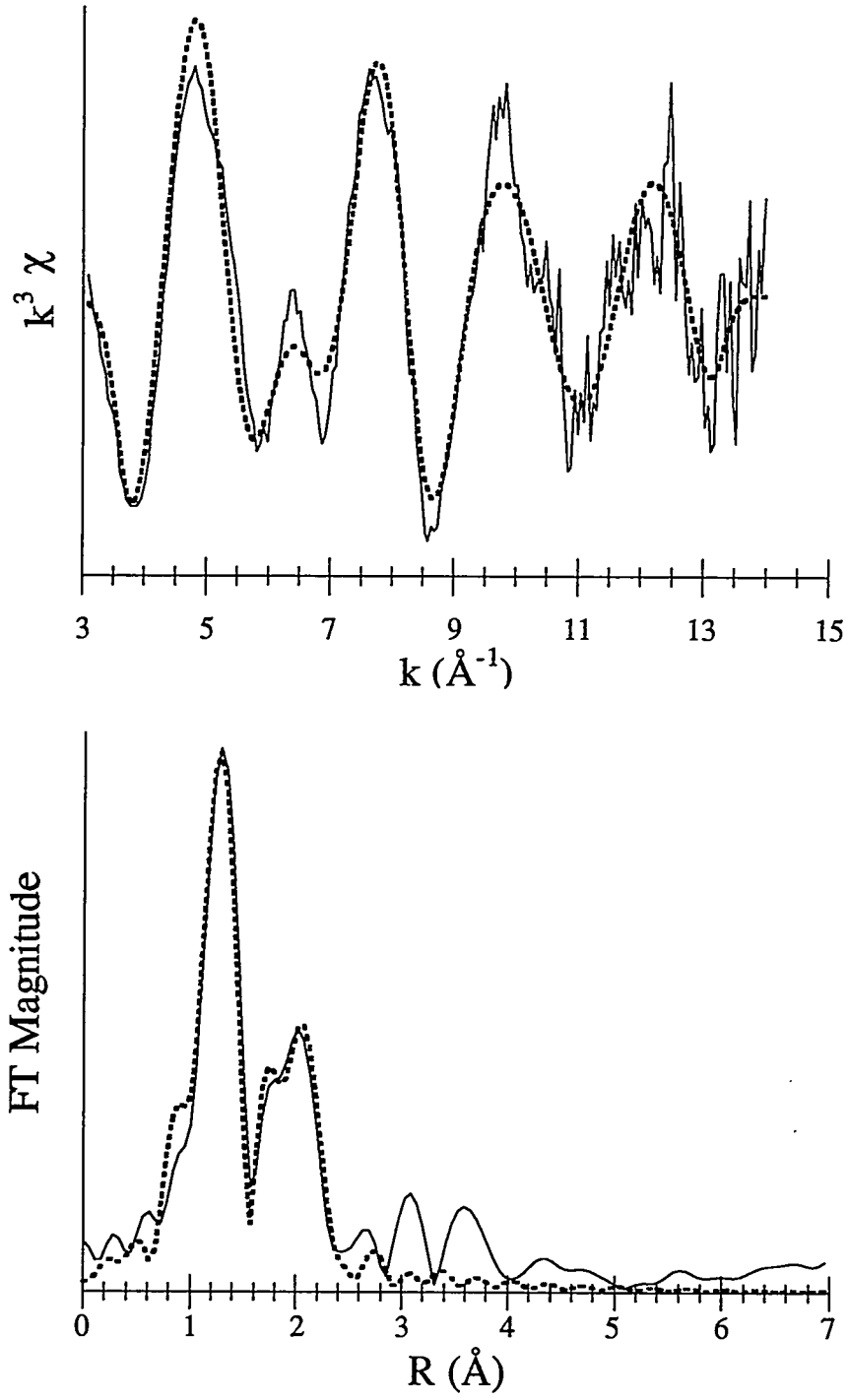

4-3. Uranyl nitrate hexahydrate. Dotted line is fit; solid line is experimental spectrum.

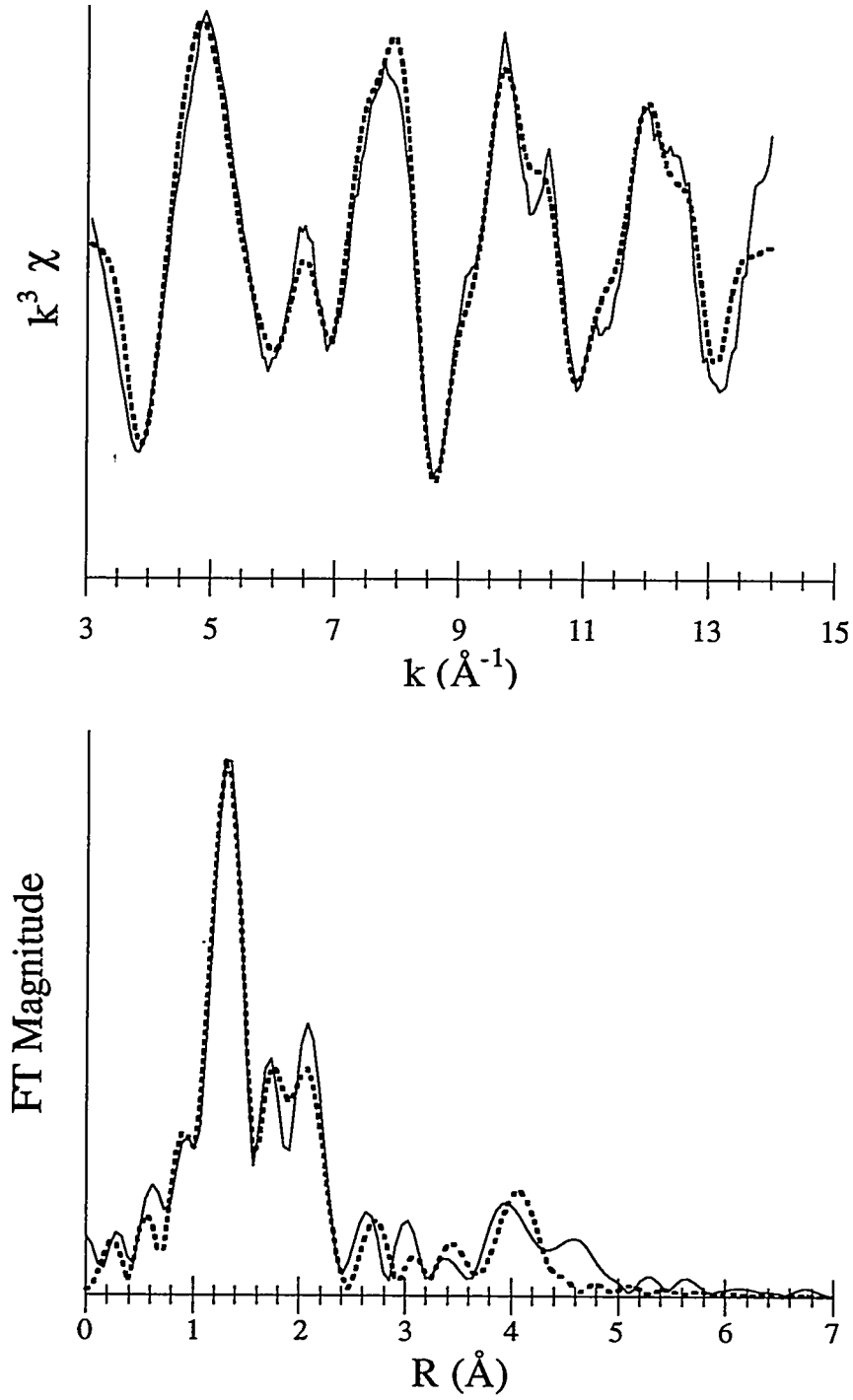

4-4. Rutherfordine. Dotted line is fit; solid line is experimental spectrum.

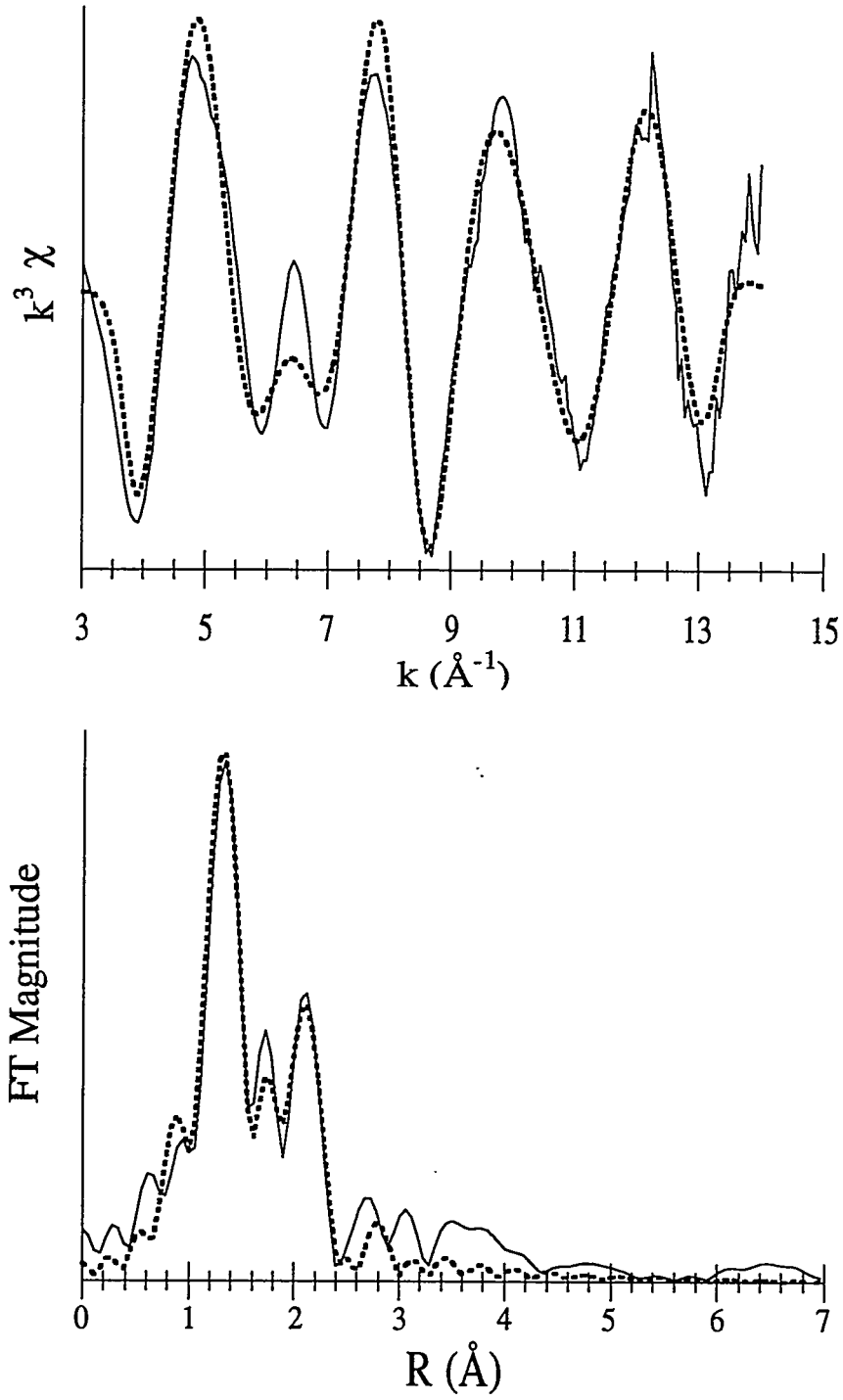

4-5. Rubidium uranyl nitrate. Dotted line is fit; solid line is experimental spectrum.

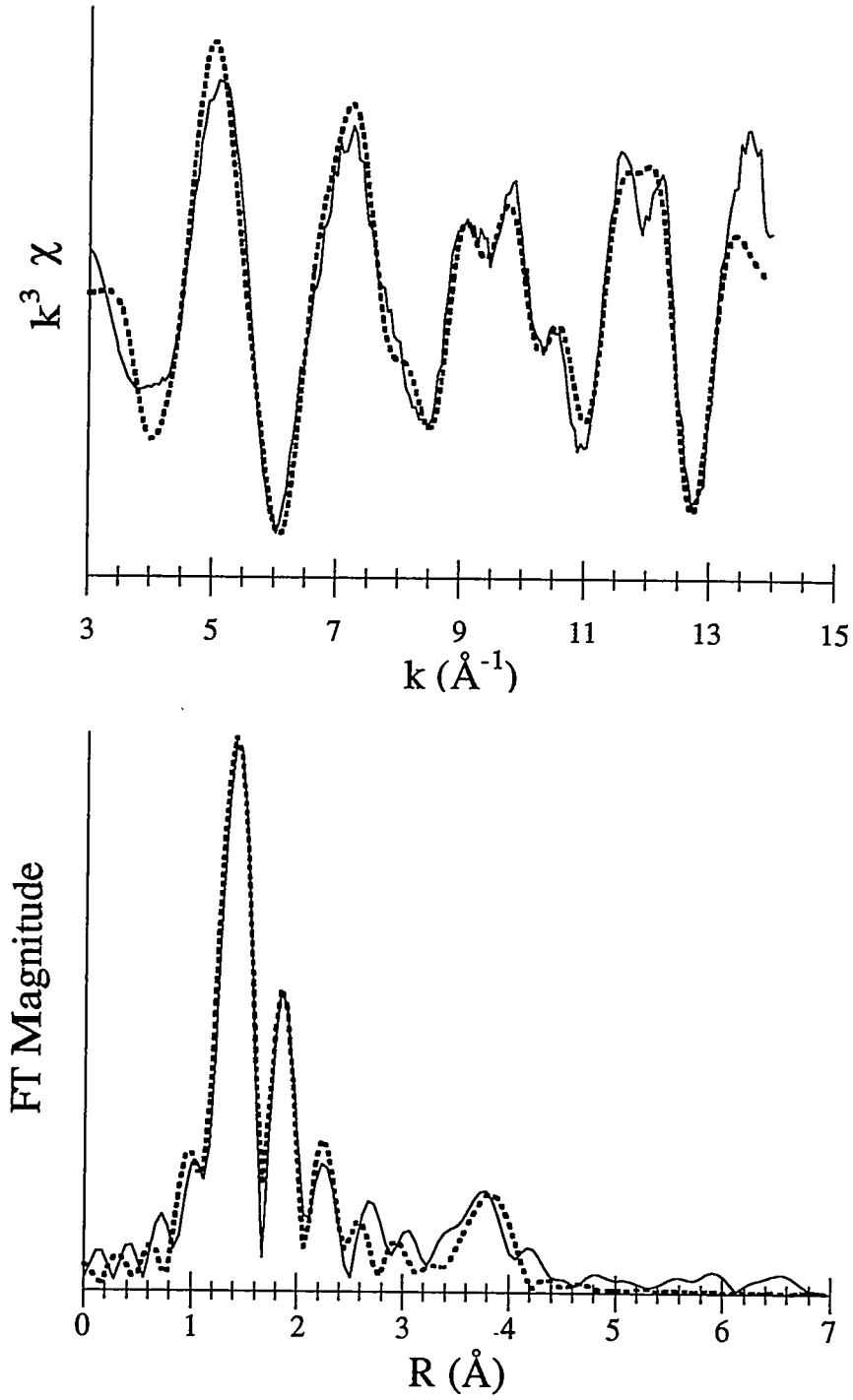

4-6. Uranophane. Dotted line is fit; solid line is experimental spectrum.

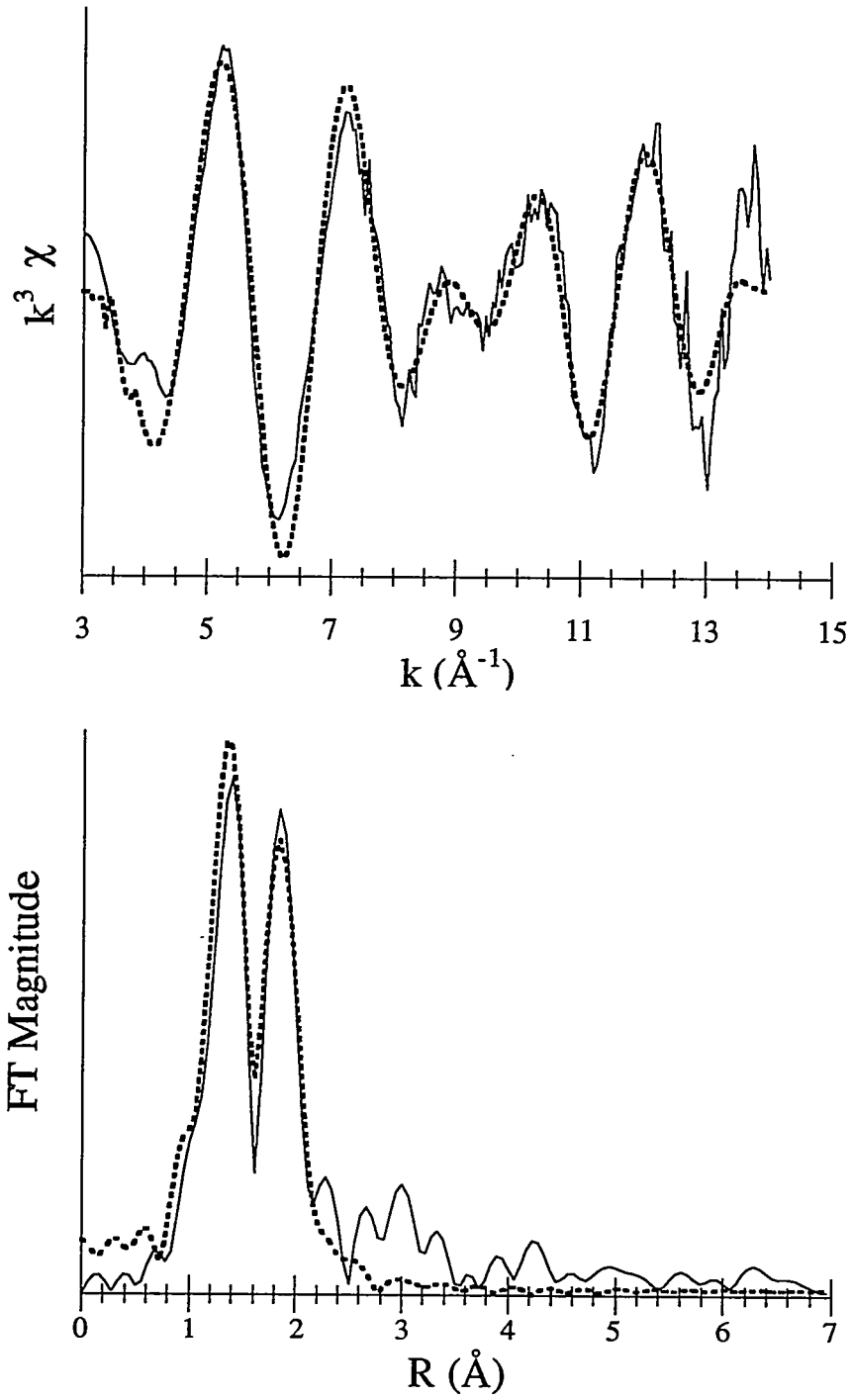

4-7. Meta-autunite. Dotted line is fit; solid line is experimental spectrum.

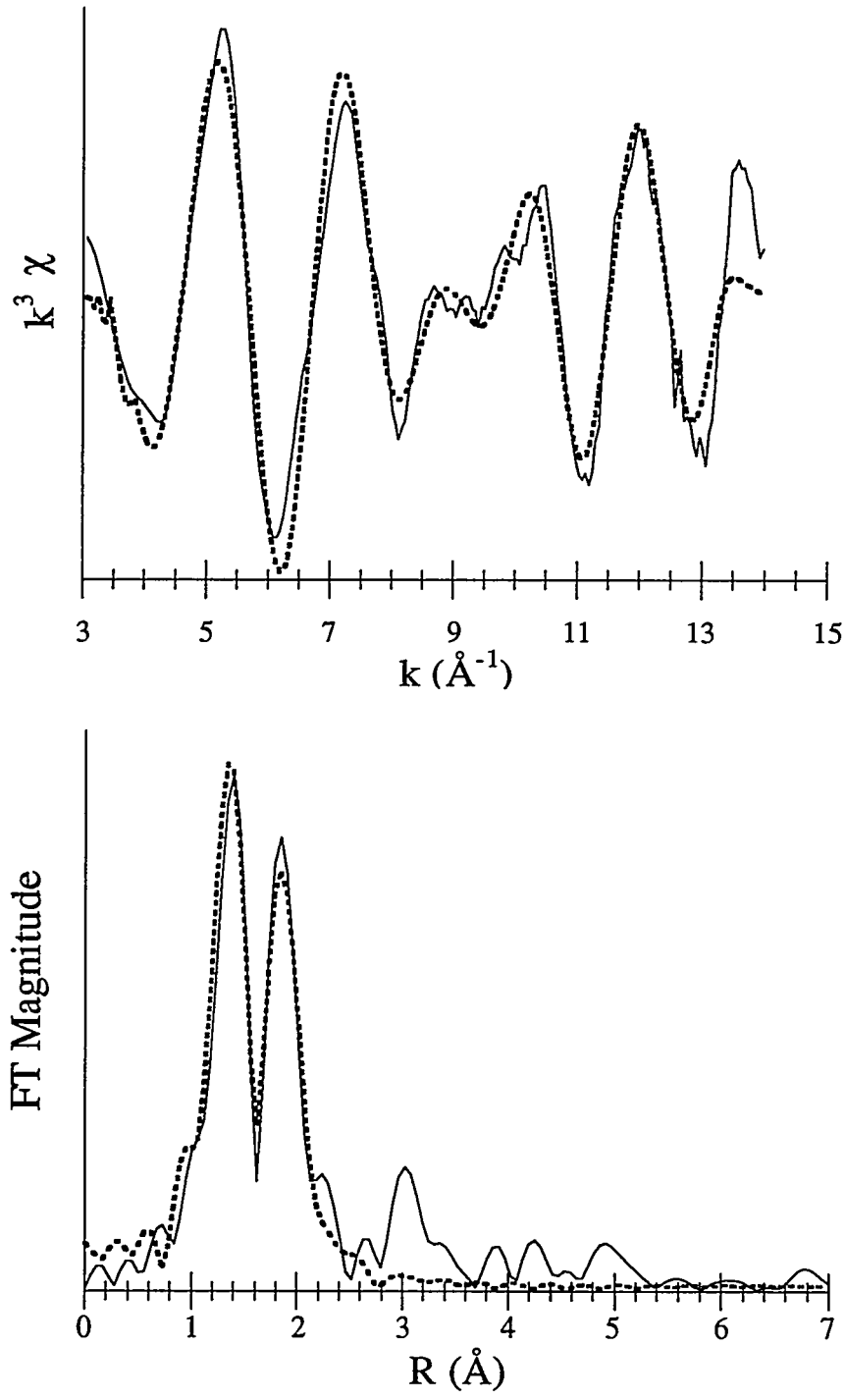

4-8. Meta-ankoleite. Dotted line is fit; solid line is experimental spectrum.

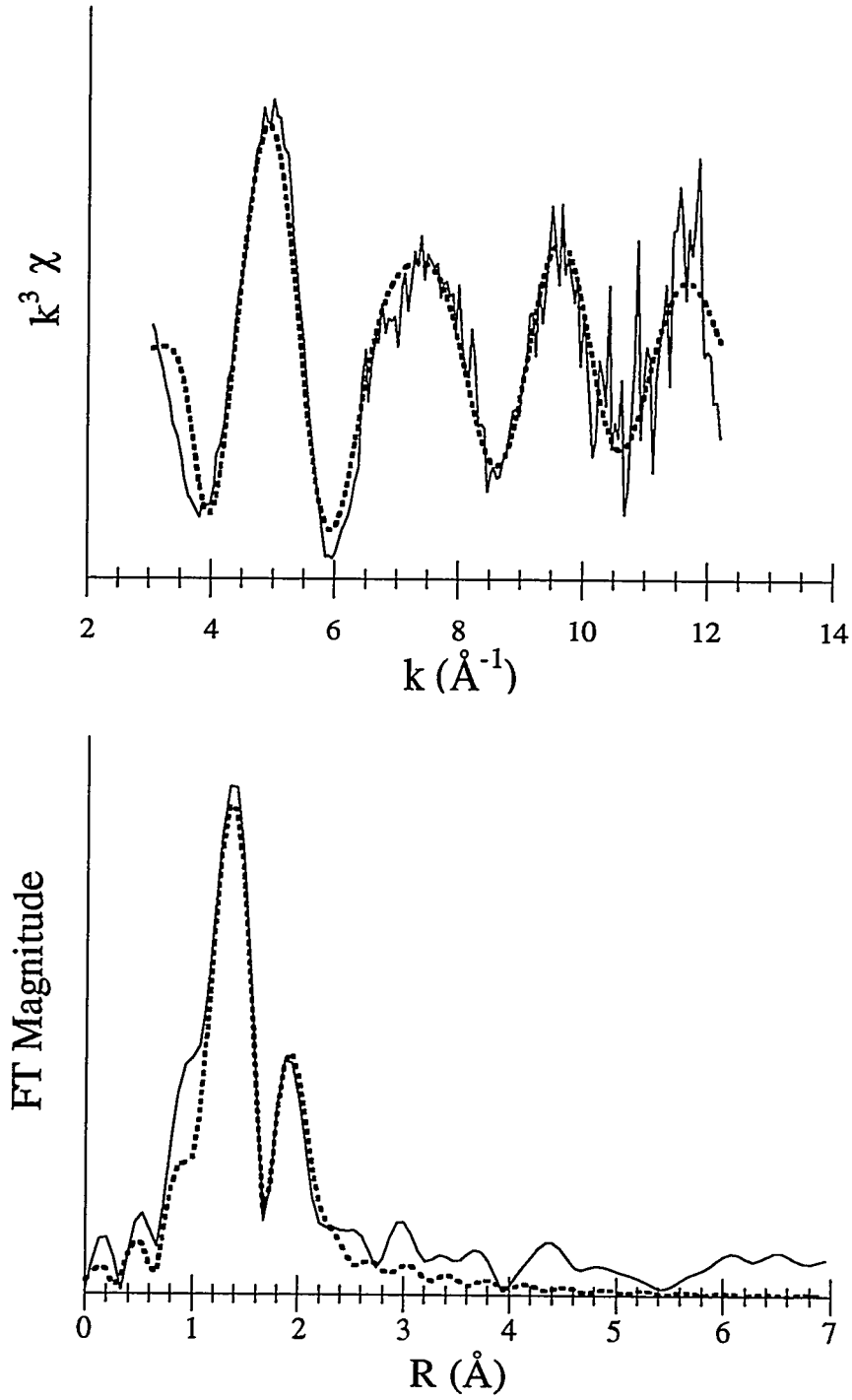

5-1. UK2. Dotted line is fit; solid line is experimental spectrum.

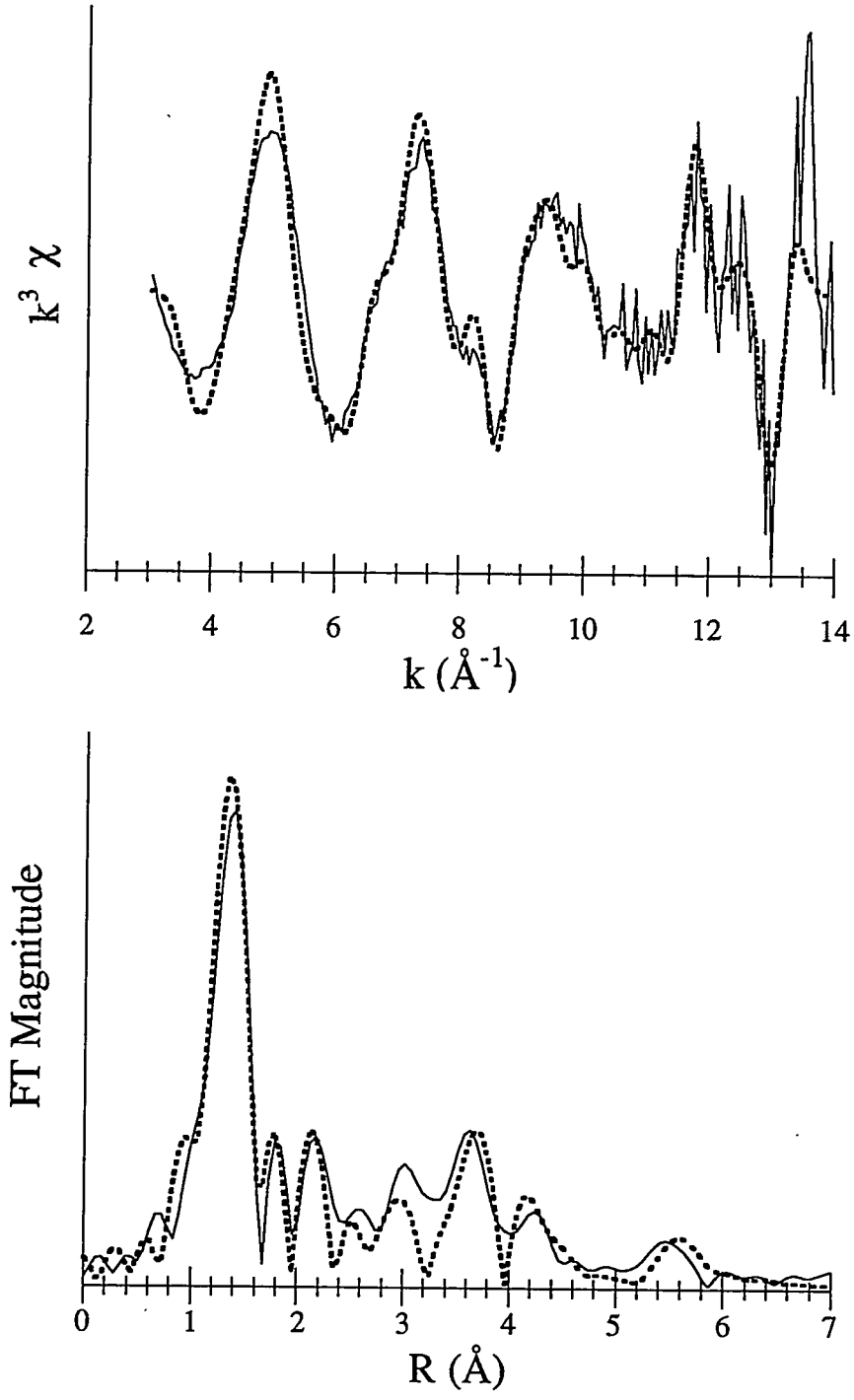

5-2. UK3. Dotted line is fit; solid line is experimental spectrum.

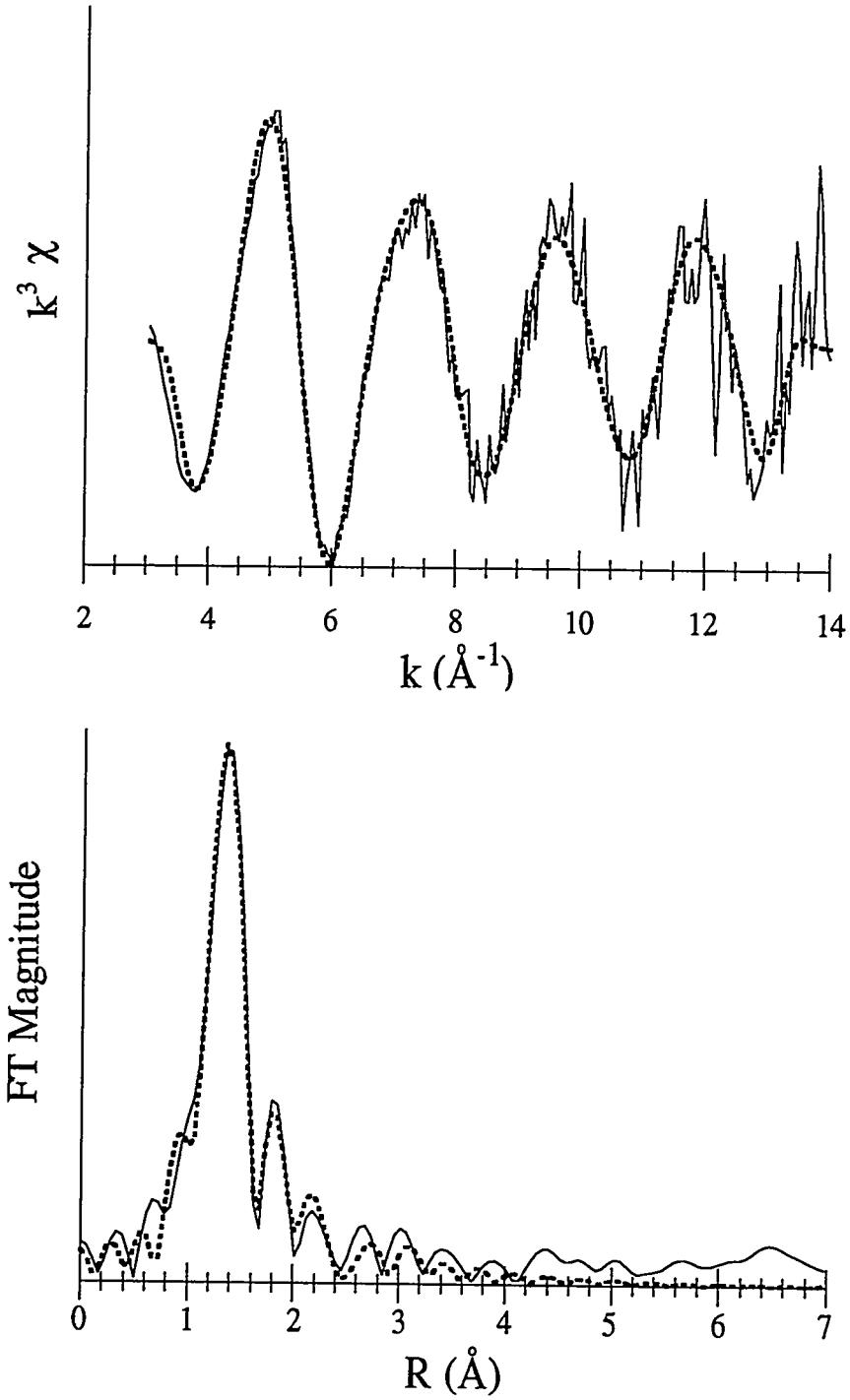

5-3. UK5. Dotted line is fit; solid line is experimental spectrum.

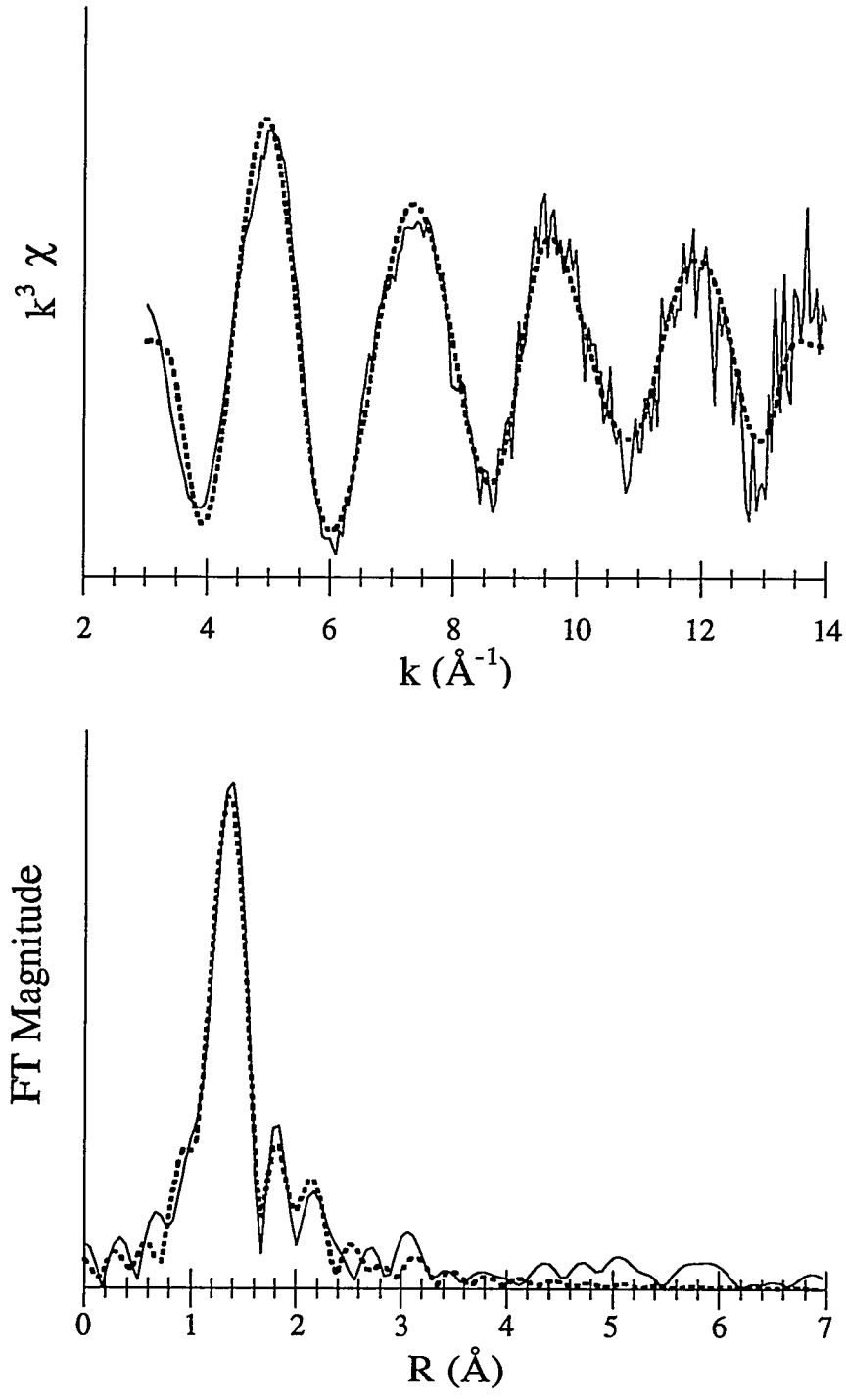

5-4. UK6. Dotted line is fit; solid line is experimental spectrum.

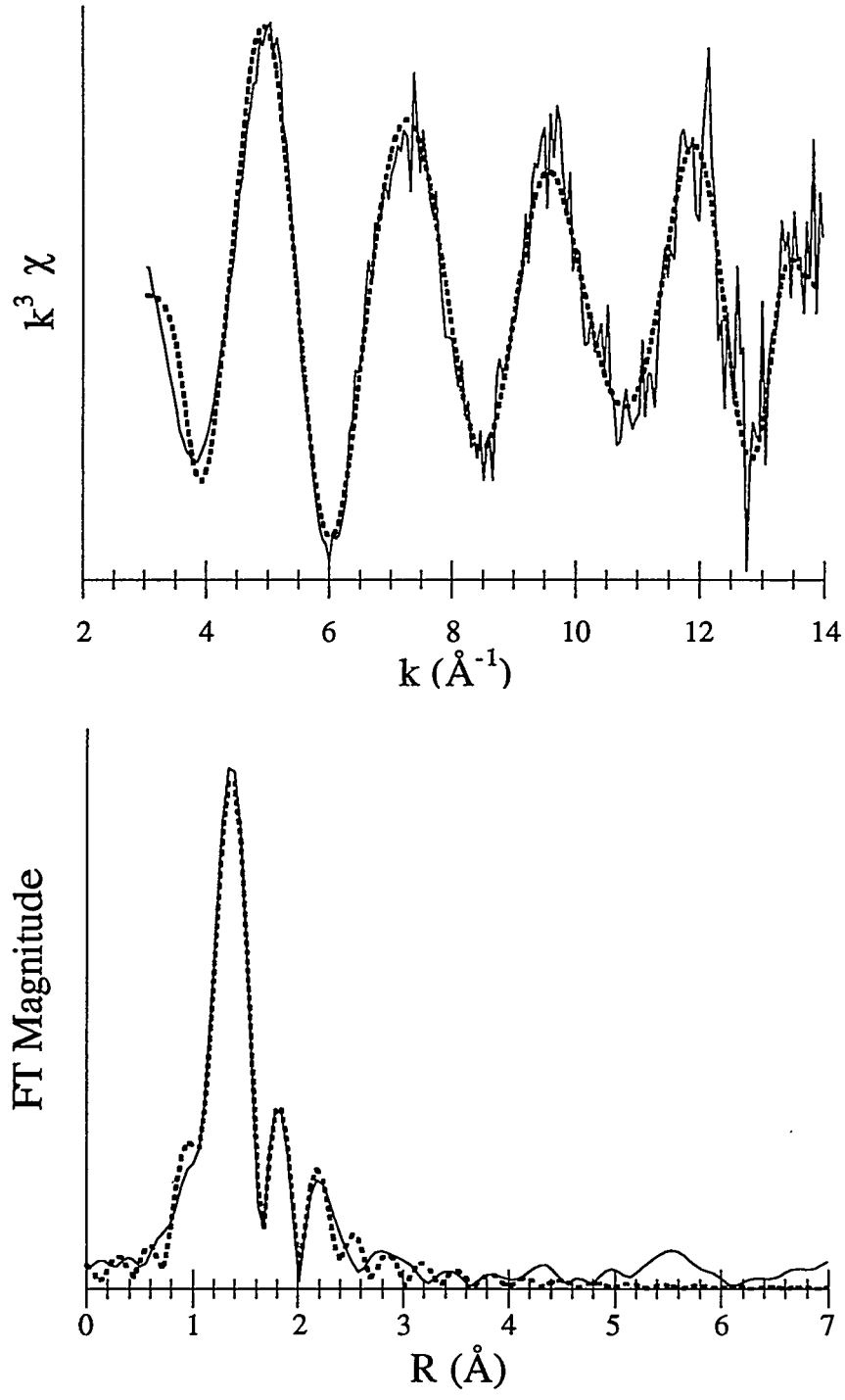

5-5. UK7. Dotted line is fit; solid line is experimental spectrum.

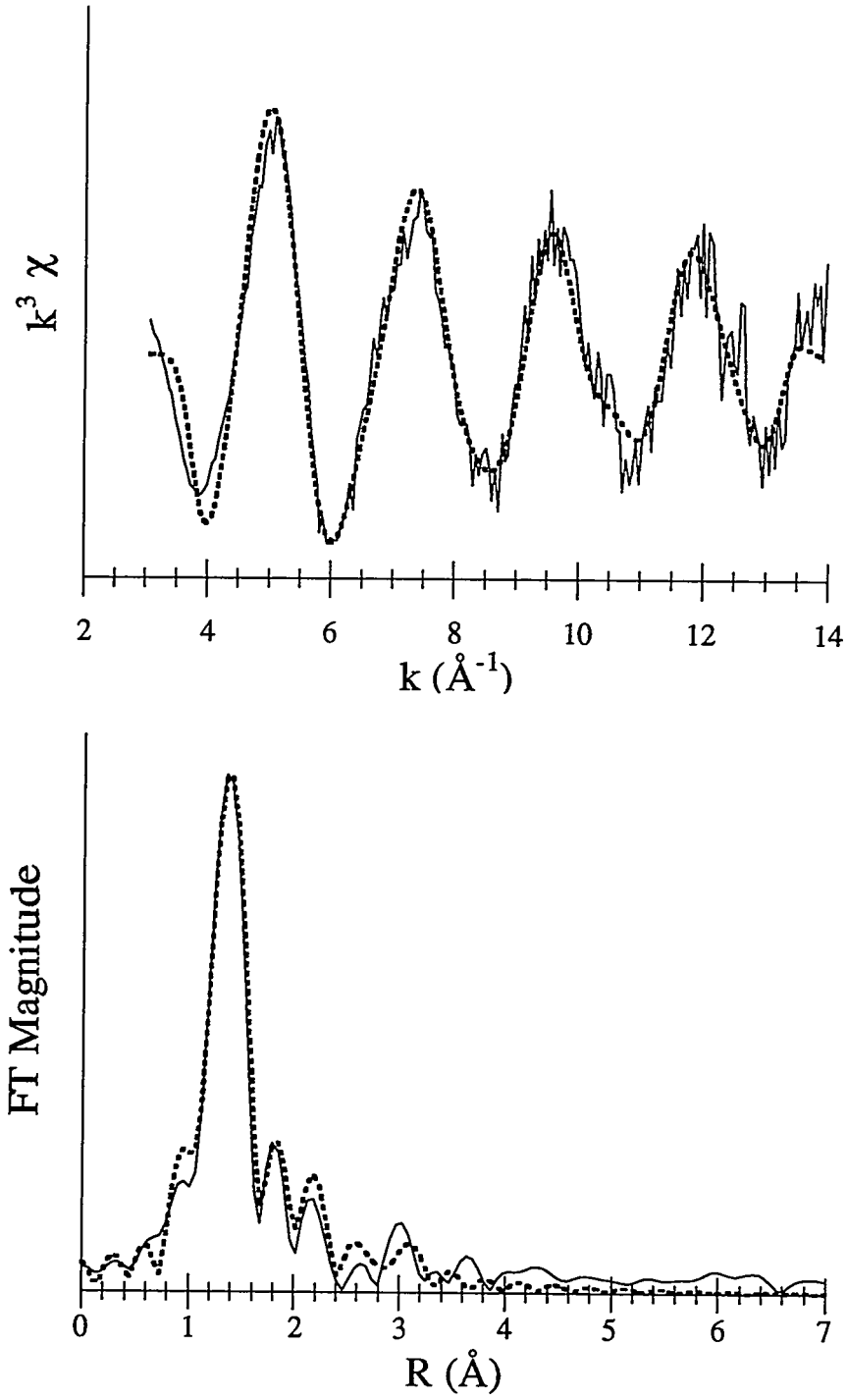

5-6. UK8. Dotted line is fit; solid line is experimental spectrum.

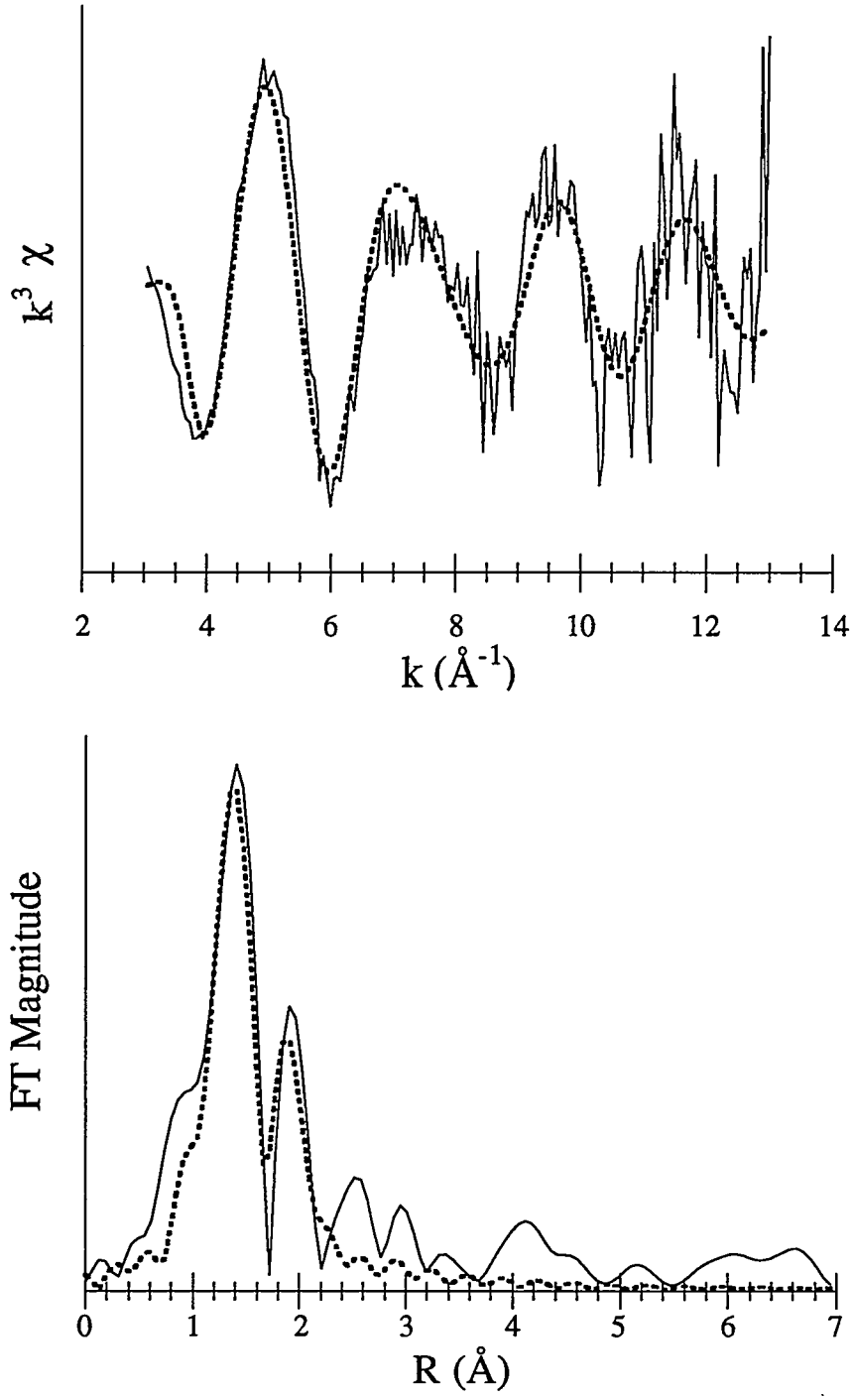

5-7. UK9. Dotted line is fit; solid line is experimental spectrum.

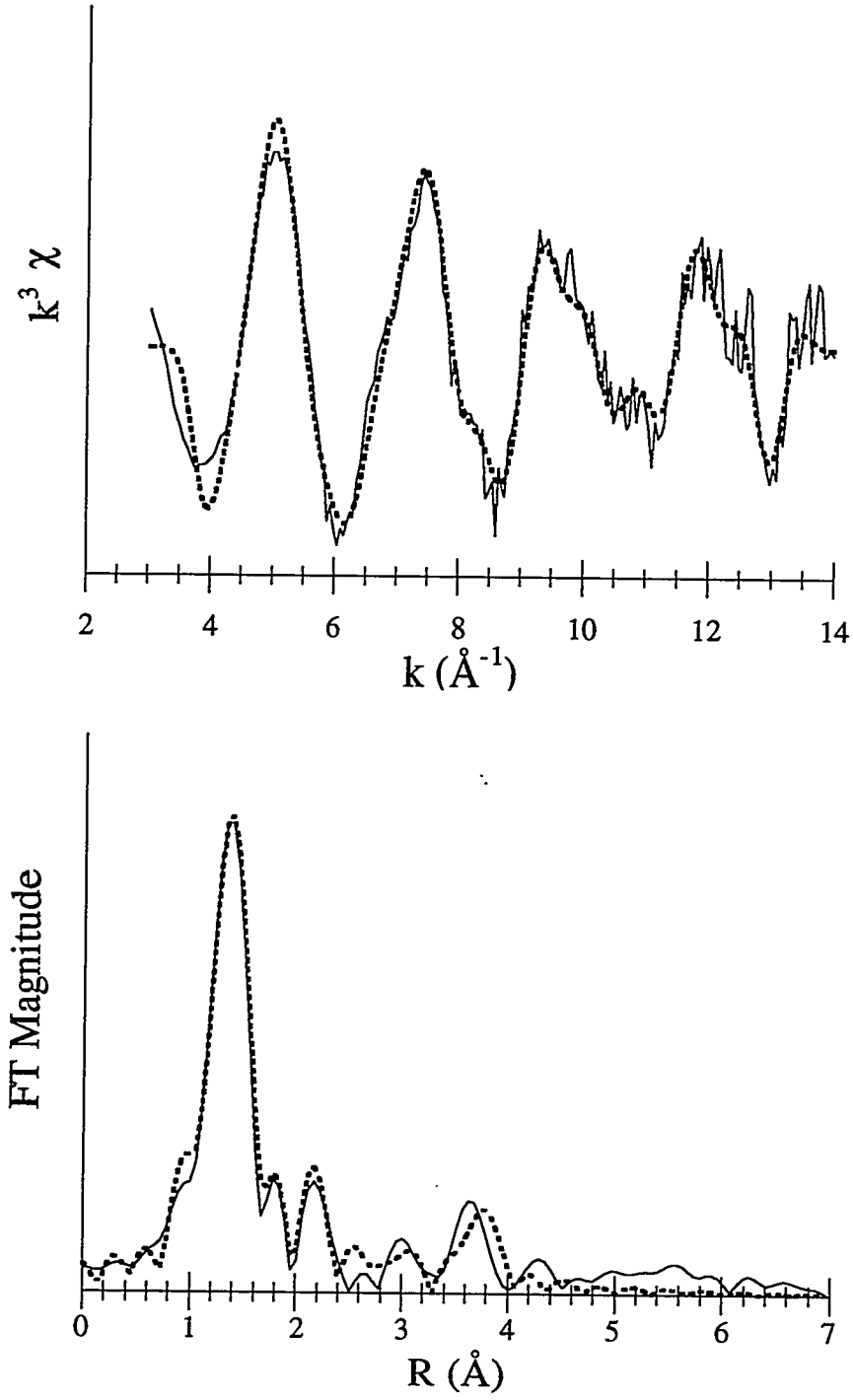

5-8. UK10. Dotted line is fit; solid line is experimental spectrum.

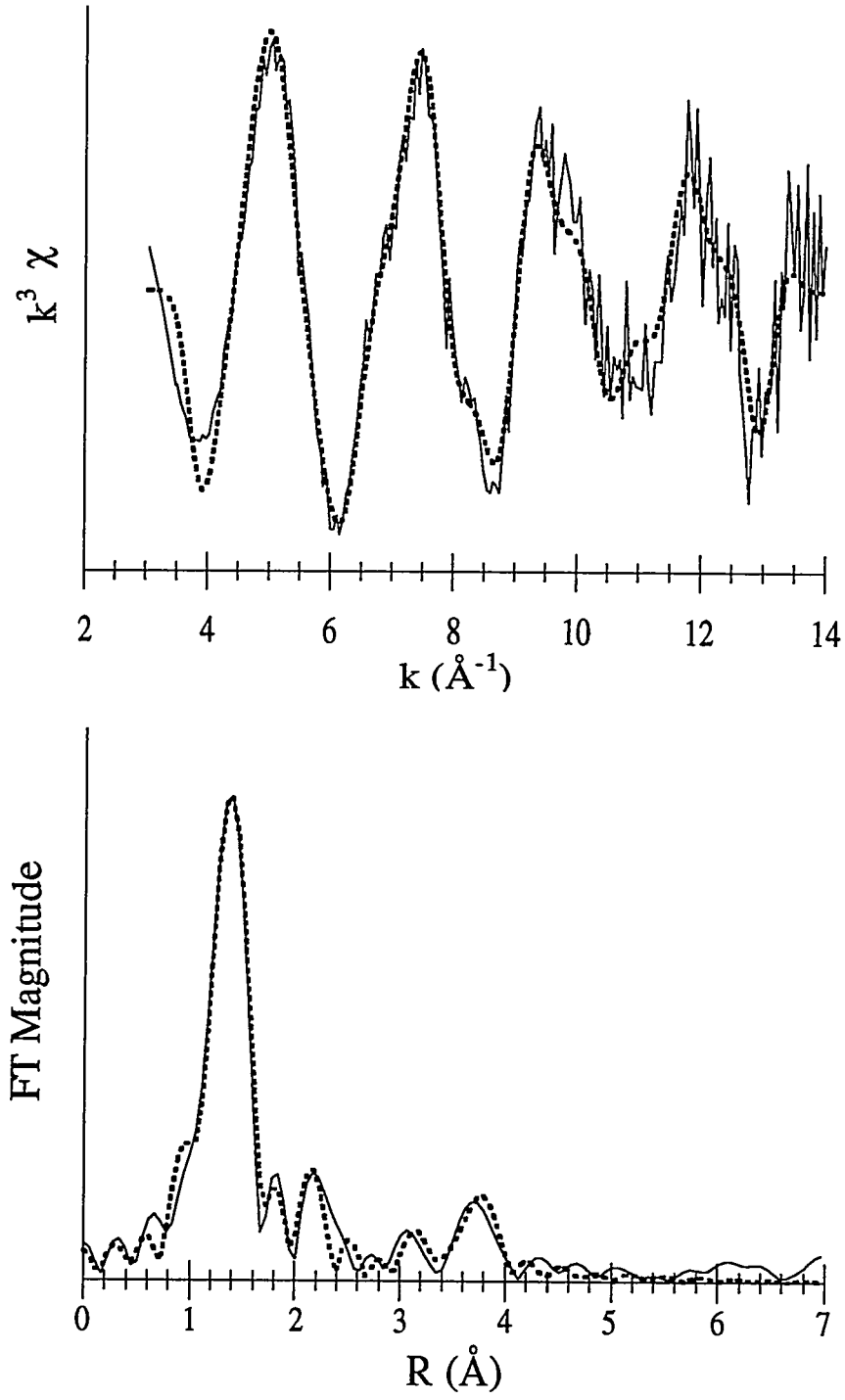

5-9. UK12. Dotted line is fit; solid line is experimental spectrum.

REFERENCES

Åberg, M. (1969) The crystal structure of $[(UO_2)_2(OH)_2Cl_2(H_2O)_4]$. *Acta Chem. Scand.* **23,** 791-810.

Åberg, M. (1970) On the structures of the predominant hydrolysis products of uranyl (VI) in solution. *Acta Chem. Scand.* **24,** 2901-2915.

Åberg, M. (1971) On the crystal structure of a tetranuclear hydroxo complex of uranyl (VI). *Acta Chem. Scand.* **25,** 368-369.

Åberg, M., Ferri, D., Glaser, J., and Grenthe, I. (1983) Studies of metal carbonate equilibria. 8. Structure of the hexakis(carbonato)tris[dioxouranate(VI)] ion in aqueous solution. An x-ray diffraction and ^{13}C NMR study. *Inorg. Chem.* **22,** 3981-3985.

Anderson, A., Chieh, C., Irish, D. E., and Tong, J. P. K. (1980) An x-ray crystallographic, raman, and infrared spectral study of crystalline potassium uranyl carbonate, $K_4UO_2(CO_3)_3$. *Can. J. Chem.* **58,** 1651-1658.

Andreyev, P. F., and Chumachenko, A. P. (1964) Reduction of uranium by natural organic substances. *Geokhimiya* **1,** 12-22.

Baes, C. F. J., and Mesmer, R. E. (1976) *The Hydrolysis of Cations*. John Wiley & Sons, 489 p.

Barrett, N. T., Greaves, G. N., Willis, B. T. M., Antonini, G. M., and Thornley, F. R. (1988) Anharmonic vibrations in UO_2 as determined by EXAFS. *J. Phys. C: Solid State Phys.* **21,** L791-L796.

Bartlett, J. R., and Cooney, R. P. (1989) Raman spectra of zeolites exchanged with uranyl (VI) cations - I. Zeolite Y. *Spectrochim. Acta* **45A,** 541-547.

Basile, L. J., Ferraro, J. R., Mitchell, M. L., and Sullivan, J. C. (1978) The raman scattering of actinide (VI) ions in carbonate media. *Appl. Spectrosc.* **32,** 535-537.

Bianconi, A., Fritsch, E., Calas, G., and Petiau, J. (1985) X-ray-absorption near-edge structure of 3d transition elements in tetrahedral coordination: the effect of bond-length variation. *Phys. Rev. B* **32,** 4292-4295.

Bleam, W. F., and McBride, M. B. (1985) Cluster formation versus isolated-site adsorption. A study of Mn(II) and Mg(II) adsorption on boehmite and goethite. *J. Colloid Interface Sci.* **103,** 124-132.

Borovec, Z. (1981) The adsorption of uranyl species by fine clay. *Chem. Geol.* **32,** 45-58.

Brown, G. E., Jr., Calas, G., Waychunas, G. A., and Petiau, J. (1988) X-ray absorption spectroscopy and its applications in mineralogy and geochemistry. In *Spectroscopic Methods in Mineralogy and Geology* (ed. F. C. Hawthorne); *Reviews in Mineralogy* (ed. P. H. Ribbe), **18;** Mineralogical Society of America, Washington, D.C., 431-512 pp.

Brown, G. E., Jr., and Parks, G. A. (1989) Synchrotron-based x-ray absorption studies of cation environments in earth materials. *Reviews of Geophysics* **27,** 519-533.

Charpin, P., Dejean, A., Folcher, G., Rigny, P., and Navaza, P. (1985) EXAFS sur des composes de coordination de l'uranium en phase solide et en solution. *J. Chim. Phys. Phys. Chim. Biol.* **82,** 925-932.

Chisholm-Brause, C., Conradson, S. D., Eller, P. G., and Morris, D. E. (1992) Changes in U(VI) speciation upon sorption onto montmorillonite from aqueous and organic solutions. In *Proc. Scientific Basis for Nuclear Waste Management XV* (ed. C. G. Sombret) **257,** 315-322. Materials Research Society.

Chisholm-Brause, C. J. (1991) *Spectroscopic and equilibrium study of cobalt(II) sorption complexes at oxide/water interfaces.* Ph.D., Stanford University.

Chisholm-Brause, C. J., Hayes, K. F., Roe, A. L., Brown, G. E., Jr., Parks, G. A., and Leckie, J. O. (1990a) Spectroscopic investigation of Pb(II) complexes at the gamma-Al2O3/water interface. *Geochim. Cosmochim. Acta* **54, 7,** 1897-1909.

Chisholm-Brause, C. J., O'Day, P. A., Brown, G. E., Jr., and Parks, G. A. (1990b) Evidence for multinuclear metal-ion complexes at solid/water interfaces from x-ray absorption spectroscopy. *Nature* **348,** 528-530.

Christ, C. L., and Clark, J. R. (1960) Crystal chemical studies of some uranyl oxide hydrates. *Am. Mineral.* **45,** 1026-1061.

Christ, C. L., Clark, J. R., and Evans, H. T. J. (1955) Crystal structure of rutherfordine, UO2CO3. *Science* **121,** 472-473.

Clark, J. R., and Christ, C. L. (1957) Some observations on rutherfordine. *Am. Mineral.* **41,** 844-850.

Combes, J.-M. (1988) *Evolution de la structure locale des polymeres et gels ferriques lors de la cristallisation des oxydes de fer. Application au piegeage de l'uranium.* Docteur, l'Universite Pierre et Marie Curie.

Combes, J.-M., Chisholm-Brause, C. J., Brown, G. E., Jr., Parks, G. A., Conradson, S. D., Eller, P. G., Triay, I. R., Hobart, D. E., and Meijer, A. (1992) EXAFS spectroscopic study of neptunium(V) sorption at the alpha-FeOOH/water interface. *Environ. Sci. Technol.* **26,** 376-382.

Cramer, S. P., and Hodgson, K. O. (1979) X-ray absorption spectroscopy: a new structural method and its applications to bioinorganic chemistry. *Prog. Inorg. Chem.* **25,** 1-39.

Cromer, D. T., and Harper, P. E. (1955) The length of the uranyl ion in uranyl carbonate. *Acta Crystallogr.* **8,** 847-848.

Davis, J. A., James, R. O., and Leckie, J. O. (1978) Surface ionization and complexation at the oxide/water interface, I. Computation of electrical double layer properties in simple electrolytes. *J. Colloid Interface Sci.* **63,** 480-499.

Dent, A. J., Ramsay, J. D. F., and Swanton, S. W. (1992) An EXAFS study of uranyl ion in solution and sorbed onto silica and montmorillonite clay colloids. *J. Colloid Interface Sci.* **150,** 45-60.

Dik, T. A., Nikanovich, M. V., and Umreiko, D. S. (1988) Spectral-structural analysis of the state of nitrate groups in $UO_2(NO_3)_2$. *J. Appl. Spectrosc.* **48,** 503-507.

Dillard, J. G., and Koppelman, M. H. (1982) X-ray photoelectron spectroscopic (XPS) surface characterization of cobalt on the surface of kaolinite. *J. Colloid Interface Sci.* **87,** 46-55.

Evans, H. T., Jr. (1963) Uranyl ion coordination. *Science* **141,** 154-158.

Farges, F., Ponader, C. W., Calas, G., and Brown, G. E., Jr. (1992) Structural environments of incompatible elements in silicate glass/melt systems: II. U(IV), U(V), and U(VI). *Geochim. Cosmochim. Acta* **56,** 4205-4220.

Frondel, C., Riska, D. D., and Frondel, J. W. (1956) X-ray powder data for uranium and thorium minerals. *U.S. Geol. Surv. Bull.* **B 1036-G,** 91-153.

George, G. N., and Pickering, I. J. (1993) Manual for EXAFSPAK: A suite of computer programs for analysis of x-ray absorption spectra. 63 pp.

Giblin, A. M. (1980) The role of clay adsorption in genesis of uranium ores. In *Proc. International uranium symposium on the Pine Creek Geosyncline* (ed. J. Ferguson and A. B. Goleby) 521-529.

Ginderow, P. D. (1988) Structure de l'uranophane alpha, Ca(UO2)2(SiO3OH)2.5H2O. *Acta Crystallogr.* **C44,** 421-424.

Görller-Walrand, C., and Colen, W. (1982) On the coordination symmetry of the hydrated uranyl ion. *Chem. Phys. Lett.* **93,** 82-85.

Grenthe, I., Fuger, J., Konings, R. J. M., Lemire, R. J., Muller, A. B., Nguyen-Trung, C., and Wanner, H. (1992) *Chemical Thermodynamics of Uranium*. North-Holland, 715 p.

Grim, R. E. (1968) *Clay mineralogy*. McGraw-Hill, 596 p.

Hayes, K. F., Roe, A. L., Brown, G. E., Jr., Hodgson, K. O., Leckie, J. O., and Parks, G. A. (1987) In situ x-ray absorption study of surface complexes: selenium oxyanions on α-FeOOH. *Science* **238,** 783-786.

Healy, T. W., James, R. O., and Cooper, R. (1968) The adsorption of aqueous Co(II) at the silica/water interface. In *Adsorption from Aqueous Solution* (ed. W. J. Weber Jr. and E. Matijevic); *Advances in Chemistry Series* **79;** American Chemical Society, Washington, D.C., 62-73 pp.

Ho, C. H., and Doern, D. C. (1985) The sorption of uranyl species on a hematite sol. *Can. J. Chem.* **63,** 1100-1104.

Ho, C. H., and Miller, N. H. (1986) Adsorption of uranyl species from bicarbonate solution onto hematite particles. *J. Colloid Interface Sci.* **110,** 165-71.

Hoekstra, H. R. (1963) Uranium-oxygen bond lengths in uranyl salts: uranyl fluoride and uranyl carbonate. *Inorg. Chem.* **2,** 492-495.

Hoekstra, H. R., and Siegel, S. (1973) The uranium trioxide-water system. *J. Inorg. Nucl. Chem.* **35,** 761-779.

Hsi, C. D., and Langmuir, D. (1985) Adsorption of uranyl onto ferric oxyhydroxides: application of the surface complexation site-binding model. *Geochim. Cosmochim. Acta* **49,** 1931-1941.

Jaffrezic-Renault, N., Poirier-Andrade, H., and Trang, D. H. (1980) Models for the adsorption of uranium on titanium dioxide. *J. Chromatog.* **201,** 187-192.

James, R. O., and Healy, T. W. (1972) Adsorption of hydrolyzable metal ions at the oxide-water interface II. Charge reversal of SiO_2 and TiO_2 colloids by adsorbed Co(II), La(III), and Th(IV) as model systems. *J. Colloid Interface Sci.* **40,** 53-64.

Karim, D. P., Georgopoulos, P., and Knapp, G. S. (1980) Extended X-ray absorption fine structure studies of actinide ions in aqueous solution. *Nucl. Technol.* **51,** 162-168.

Krauskopf, K. B. (1992) Environmental Geochemistry. In *Encyclopedia of Physical Science and Technology* (ed. R. A. Meyers); **6;** Academic Press, Inc., San Diego, 185-214 pp.

Langmuir, D. (1978) Uranium solution-mineral equilibria at low temperatures with applications to sedimentary ore deposits. *Geochim. Cosmochim. Acta* **42,** 547-569.

Lieser, K. H., Quandt-Klenk, S., and Thybusch, B. (1992) Sorption of uranyl ions on hydrous silicon dioxide. *Radiochim. Acta* **57,** 45-50.

Madic, C., Hobart, D. E., and Begun, G. M. (1983) Raman spectrometric studies of actinide (V) and -(VI) complexes in aqueous sodium carbonate solution and of solid sodium actinide(V) carbonate compounds. *Inorg. Chem.* **22,** 1494-1503.

Manceau, A., Charlet, L., Boisset, M. C., Didier, B., and Spadini, L. (1992) Sorption and speciation of heavy metals on hydrous Fe and Mn oxides. From microscopic to macroscopic. *Appl. Clay Sci.* **7,** 201-223.

May, H. M., Kinniburgh, D. G., Helmke, P. A., and Jackson, M. L. (1986) Aqueous dissolution, solubilities and thermodynamic stabilities of common aluminosilicate clay minerals: kaolinite and smectites. *Geochim. Cosmochim. Acta* **50,** 1667-1677.

Maya, L. (1982a) Hydrolysis and carbonate complexation of dioxouranium (VI) in the neutral-pH range at 25 C. *Inorg. Chem.* **21,** 2895-2898.

Maya, L. (1982b) Sorbed uranium (VI) species on hydrous titania, zirconia, and silica gel. *Radiochim. acta* **31,** 147-151.

McBride, M. B., Fraser, A. R., and McHardy, W. J. (1984) Cu2+ interaction with microcrystalline gibbsite. Evidence for oriented chemisorbed copper ions. *Clays Clay Miner.* **32,** 12-18.

McGlynn, S. P., Smith, J. K., and Neely, W. C. (1961) Electronic structure, spectra, and magnetic properties of oxycations. III. Ligation effects on the infrared spectrum of the uranyl ion. *J. Chem. Phys.* **35,** 105-116.

McMaster, W. H., Kerr del Grande, N., Mallet, J. H., and Hubbell, J. H. (1969) *Compilation of x-ray cross sections.* Rpt. UCRL-50174, Section II, Revision 1, Lawrence Radiation Lab, Univ. Calif.

Mentzen, B., and Giorgio, G. (1970) Caracterisation a l'etat solide de l'acetate d'uranyle dihydrate. *J. Inorg. Nucl. Chem.* **32,** 1509-1516.

Morosin, B. (1978) Hydrogen uranyl phosphate tetrahydrate, a hydrogen ion solid electrolyte. *Acta Crystallogr.* **B34,** 3732-3734.

Morris, D. E., Chisholm-Brause, C. J., Barr, M. E., Conradson, S. D., and Eller, P. G. (1994) Spectroscopic evidence for discrete multiple sorption sites for UO_2^{2+} species on a reference smectite. *Geochim. Cosmochim. Acta* submitted.

Morse, J. W., and Casey, W. H. (1988) Ostwald processes and mineral paragenesis in sediments. *Am. J. Sci.* **288,** 537-560.

Morse, J. W., Shanbhag, P. M., Saito, A., and Choppin, G. R. (1984) Interaction of uranyl ions in carbonate media. *Chem. Geol.* **42,** 85-99.

Mustre de Leon, J., Rehr, J. J., Zabinsky, S. I., and Albers, R. C. (1991) Ab initio curved-wave x-ray-absorption fine structure. *Phys. Rev. B* **44,** 4146-4156.

Muto, T., Kirono, S., and Kurata, H. (1965) Some aspects of fixation of uranium from natural waters. *Min. Geol. (Tokyo)* **15,** 287-298.

Nguyen, S. N., Silva, R. J., Weed, H. C., and Andrews, J. E., Jr. (1992) Standard Gibbs free energies of formation at the temperature 303.15 K of four uranyl silicates: soddyite, uranophane, sodium boltwoodite, and sodium weeksite. *J. Chem. Thermodyn.* **24,** 359-376.

O'Day, P. A. (1992) *Structure, bonding, and site preference of cobalt(II) sorption complexes on kaolinite and quartz from solution and spectroscopic studies.* Ph.D., Stanford Univ.

O'Day, P. A., Rehr, J. J., Zabinsky, S. I., and Brown, G. E., Jr. (1994) Extended x-ray absorption fine structure (EXAFS) analysis of multiple-scattering and disorder in mineral reference compounds. *J. Am. Chem. Soc.* in press.

Papelis, C., Hayes, K. F., and Leckie, J. O. (1988) *HYDRAQL: A program for the computation of chemical equilibrium composition of aqueous batch systems including surface-complexation modeling of ion adsorption at the oxide/solution interface.* Technical Report No. 306, Stanford University

Perrin, P. A. (1976) Structure cristalline du nitrate de dihydroxo diuranyle tetrahydrate. *Acta Crystallogr.* **B32,** 1658-1661.

Perry, D. L. (1982) Infrared and x-ray photoelectron evidence for a cation stabilized hydroxy-bridged uranyl species, $[(UO_2^{2+})_2(OH)_2]^{2+}$. *Inorg. Chim. Acta* **65,** L211-L213.

Petiau, J., Calas, G., and Petitmaire, D. (1986) Delocalized versus localized unoccupied 5f states and the uranium site structure in uranium oxides and glasses probed by x-ray-absorption near-edge structure. *Phys. Rev. B* **34,** 7350-7361.

Rehr, J. J., Mustre de Leon, J., Zabinsky, S. I., and Albers, R. C. (1991) Theoretical x-ray absorption fine structure standards. *J. Am. Chem. Soc.* **113,** 5135-5140.

Roof, R. B., Cromer, D. T., and Larson, A. C. (1964) The crystal structure of uranyl dihydroxide, UO2(OH)2. *Acta Crystallogr.* **17,** 701-705.

Sayers, D. E., and Bunker, B. A. (1988) Data Analysis. In *X-Ray Absorption Principles, Applications, Techniques of EXAFS, SEXAFS and XANES* (ed. D. C. Koningsberger and R. Prins); John Wiley & Sons, New York, 211-253 pp.

Schenck, C. V., Dillard, J. G., and Murray, J. W. (1983) Surface analysis and the adsorption of Co(II) on goethite. *J. Colloid Interface Sci.* **95,** 398-409.

Schindler, P. W., Liechti, P., and Westall, J. C. (1987) Adsorption of copper, cadmium, and lead from aqueous solution to the kaolinite/water interface. *Neth. J. Agric. Sci.* **35,** 219-230.

Scott, R. A. (1984) X-ray absorption spectroscopy. In *Structural and Resonance Techniques in Biological Research* (ed. D. L. Rousseau); Academic Press, Orlando, pp.

Sekine, K., Payne, T. E., Waite, T. D., and Davis, J. A. (1991) International Alligator Rivers analogue project (18): experimental study of uranium adsorption on kaolinite -pH dependence in air-equilibrated system, personal communication.

Shannon, R. D. (1976) Systematic Studies of Interatomic Distances in Oxides. In *The Physics and Chemistry of Minerals and Rocks* (ed. R. G. J. Strens); John Wiley & Sons, London, 403-431 pp.

Shannon, R. D., and Prewitt, C. T. (1969) Effective ionic radii in oxides and fluorides. *Acta Crystallogr.* **B25,** 925-946.

Sillen, L. G. (1954) On equilibria in systems with polynuclear complex formation. I. Methods for deducing the composition of the complexes from experimental data. "Core + Links" complexes. *Acta Chem. Scand.* **8,** 299-317.

Smith, D. K., Jr. (1984) Uranium mineralogy. In *Uranium geochemistry, mineralogy, geology, exploration and resources* (ed. B. DeVivo, et al.); The Institution of Mining and Metallurgy, 43-88 pp.

Sposito, G. (1984) *The surface chemistry of soils.* Oxford University Press, 234 p.

Stanton, J., and Maatman, R. W. (1963) The reaction between aqueous uranyl ion and the surface of silica gel. *J. Colloid Sci.* **18,** 132-146.

Stohl, F. V., and Smith, D. K. (1981) The crystal chemistry of the uranyl silicate minerals. *Am. Mineral.* **66,** 610-625.

Stumm, W., and Morgan, J. J. (1981) *Aquatic Chemistry.* John Wiley & Sons, 780 p.

Sylva, R. N., and Davidson, M. R. (1979) The hydrolysis of metal ions. Part 2. Dioxouranium (VI). *J. Chem. Soc. Dalton Trans.* 465-471.

Taylor, J. C., and Mueller, M. H. (1965) A neutron diffraction study of uranyl nitrate hexahydrate. *Acta Crystallogr.* **19,** 536-543.

Templeton, D. H., Zalkin, A., Ruben, H., and Templeton, L. K. (1985) Redetermination and absolute configuration of sodium uranyl (VI) triacetate. *Acta Crystallogr.* **C41,** 1439-1441.

Teo, B. K., and Lee, P. A. (1979) Ab initio calculations of amplitude and phase functions for extended x-ray absorption fine structure spectroscopy. *J. Am. Chem. Soc.* **101,** 2815-2829.

Triay, I. R. (1992) personal communication.

Tripathi, V. S. (1984) *Uranium(VI) transport modeling: geochemical data and submodels.* Ph.D. dissertation, Stanford Univ.

Tsunashima, A., Brindley, G. W., and Bastovanov, M. (1981) Adsorption of uranium from solutions by montmorillonite; compositions and properties of uranyl montmorillonites. *Clays Clay Miner.* **29,** 10-16.

Van Olphen, H., and Fripiat, J. J. (1979) *Data Handbook for Clay Materials and other Non-metallic Minerals.* Pergamon Press, 346 p.

Vaughan, D. (1986) *X-ray Data Booklet.* Lawrence Berkeley Laboratory.

Viswanathan, K., and Harneit, O. (1986) Refined crystal structure of β-uranophane, $Ca(UO_2)_2(SiO_3OH)_2{\cdot}5H_2O$. *Am. Mineral.* **71,** 1489-1493.

Weigel, F. (1986) Uranium. In *The Chemistry of the Actinide Elements* (ed. J. J. Katz, et al.); **1;** Chapman and Hall, New York, 169-442 pp.

Weigel, F., and Hoffmann, G. (1976) The phosphates and arsenates of hexavalent actinides. Part I. Uranium. *J. Less-Common Met.* **44,** 99-123.

Yamashita, H., Ozawa, Y., Nakajima, F., and Murata, T. (1980) The collection of uranium from sea water with hydrous metal oxide. II. The mechanism of uranium adsorption on hydrous titanium(IV) oxide. *Bull. Chem. Soc. Jpn.* **53,** 1-5.

Yvon, K., Jeitschko, W., and Parthe, E. (1977) LAZY PULVERIX, A computer program, for calculating x-ray and neutron diffraction powder patterns. *J. Appl. Crystallogr.* **10,** 73-74.

Zachariasen, W. H. (1954) Crystal chemical studies of the 5f-series of elements. XXIII. On the crystal chemistry of uranyl compounds and of related compounds of transuranic elements. *Acta Crystallogr.* **7,** 795-799.

Zalkin, A., Templeton, L. K., and Templeton, D. H. (1989) Structure of rubidium uranyl (VI) trinitrate. *Acta Crystallogr.* **C45,** 810-811.